Wittmann, H., von Blanckenburg, F. (2016): The geological significance of cosmogenic nuclides in large lowland river basins. - *Earth-Science Reviews*, *159*, pp. 118—141.

DOI: http://doi.org/10.1016/j.earscirev.2016.06.001

THE GEOLOGICAL SIGNIFICANCE OF COSMOGENIC NUCLIDES IN LARGE LOWLAND RIVER BASINS

H. Wittmann[1*] & F. von Blanckenburg[1,2]

[1]Helmholtz Centre Potsdam, GFZ German Research Centre for Geosciences, Telegrafenberg, 14473 Potsdam, Germany,

[2]Also at Institute of Geological Sciences, Freie Universität Berlin, Germany

*Corresponding author. E-mail address: wittmann@gfz-potsdam.de

ABSTRACT

Measured from a bag of sand taken in large rivers, the concentration of cosmogenic nuclides such as *in situ*-produced ^{10}Be, ^{26}Al, and ^{14}C can be used to constrain the mean sediment flux of the headwaters and assess the duration of sediment storage from source to sink. We revisit these principles, with examples from the Amazon and Ganga basins.

We identify two end member cases controlling the concentration of cosmogenic nuclides in lowland river sediment: 1) if the time scale of floodplain sediment storage is short compared to the half-life of the nuclide, *in situ* cosmogenic nuclide concentrations are not significantly altered in lowland basins. In this case the concentration of e.g. *in situ*-produced ^{10}Be in the sediment taken in the lowland

basin equals in most cases that exported from the sediment source area, but the variability in nuclide concentrations between headwater streams is significantly averaged-out. Thus to convert the measured river sediments' *in situ* cosmogenic nuclide concentration into a catchment-wide denudation rate, production rates are scaled to include those of the sediment-producing mountainous areas only, rather than the entire catchment area. Nuclide production in the lowlands, where no sediment is being produced, is hence excluded. This correction is termed "floodplain correction". 2) If sediment buried for periods of the order of the nuclides´ half-life is episodically re-entrained into the active river, paired nuclides, for example the ratio of $^{26}Al/^{10}Be$, through the differential decay of these isotopes, constrain the the storage duration and re-mixing of floodplain sediment.

As *in-situ* cosmogenic nuclides measure denudation rates over longer time scales, typically integrating between 10^3 and 10^5 yrs, their combination with modern estimates of sediment fluxes from river load gauging offers a rich potential of deciphering the controls of Earth surface fluxes across large basins. From this combination, we can assess how river systems react to external perturbations such as climate change or human interference, and how such signals are transmitted through the alluvial reaches of lowland basins. The most important results in both basins are that i) lowland Amazon and Ganga nuclide concentrations indeed broadly reflect the spatial average of Andean and Himalayan denudation, respectively, ii) the thus calculated sediment fluxes are within uncertainty of modern fluxes from sediment gauging, indicating complete sediment delivery to the sea without net loss into the basin, and iii) only the Amazon basin, given its size, contains a substantial fraction of sediment buried temporarily in the Quaternary.

Finally, we provide a short introduction to the use of meteoric cosmogenic nuclide ^{10}Be and its ratio to stable ^{9}Be, released by rock weathering, in lowlands. In the Amazon basin we show that ^{10}Be concentrations in fine-grained suspended loads, depth-integrated over the water column using Al/Si ratios, provide erosion rates whereas the $^{10}Be/^{9}Be$ ratio on Be adsorbed to particles provides the denudation rate. Both are similar to denudation rates from *in situ* ^{10}Be. We show that this system responds more sensitively to sediment storage than the *in situ* system, and both accumulation and decay of meteoric concentrations may thus be used to determine sediment residence time.

Keywords: Fluvial geomorphology, floodplains, denudation, erosion, *in situ* and meteoric cosmogenic nuclides, sediment budgets, Amazon, Ganga, Andes, Himalayas

1. INTRODUCTION

The role of lowland river basins in modifying source-specific sediment properties, for cycling of dissolved and particulate matter, and for setting the sensitivity of sediment transport to climate change and shifts in land use, has long been recognized. In the past years, cosmogenic nuclide methods have been developed for quantifying the mass transfer involved. Therefore, it is timely to highlight the recent methodological advances. These methods encompass *in situ* cosmogenic nuclides (produced within a mineral at the Earth's surface) or meteoric cosmogenic nuclides (produced within the atmosphere and bound to fine-grained material after precipitation). Cosmogenic nuclide methods are now well established as an integral

tool of Earth surface science. They serve to provide ages of Quaternary landforms and mass fluxes of eroding landscapes (see reviews of these applications by Gosse and Phillips (2001); Bierman and Nichols (2004); von Blanckenburg (2005); Granger and Riebe (2007); Ivy-Ochs and Kober (2008); Dunai (2010); Graly et al. (2010); Willenbring and von Blanckenburg (2010); Granger et al. (2013); von Blanckenburg and Willenbring (2014)).

Denudation rates from cosmogenic nuclides provide the sum of erosion and weathering in source areas that can be converted into sediment fluxes integrating over several kyr by multiplying with the sediment-supplying area. When compared with sediment gauging data, integrating over the past few decades, we can use the cosmogenic nuclide data to evaluate the temporal stability of sediment transport and thus source-sink connectivity. As recently reviewed by Romans et al. (2015) the stratigraphic record of source to sink sediment transfer records signals of external environmental forcings as well as internal sedimentary dynamics. To make use of this record it is of high importance to understand how rivers transmit signals of climate cycles and to estimate the fluvial preservation potential (Castelltort and Van Den Driessche, 2003; Phillips, 2003; Allen, 2008; Jerolmack and Paola, 2010; Armitage et al., 2011; Simpson and Castelltort, 2012; Armitage et al., 2013; Godard et al., 2013; Latrubesse, 2015).

But do lowland river cosmogenic nuclide concentrations, that during temporary storage in sedimentary deposits may both increase (by further irradiation) or decrease (by radioactive decay) indeed provide a new tool to quantitatively assess

these linkages? We show in this review how we can study the evolution of cosmogenic nuclide concentrations as sediment leaves the mountainous production zone and crosses large floodplain systems, by using both data and modeling approaches. We mainly review the principles of calculating denudation rates from *in situ* cosmogenic ^{10}Be in lowland settings, as compared to steady state equations used to calculate denudation rates in the high-relief sediment production zone. We illustrate the application of these principles by summarizing existing denudation rate data for the Amazon and Ganga basins and their source areas, namely the Andes and the Nepalese Himalayas. In these areas an exceptional wealth of cosmogenic nuclide and modern river flux data has been generated in past years. We include a short review of mass balance models of cosmogenic nuclides in floodplains (Wittmann and von Blanckenburg, 2009; Lauer and Willenbring, 2010).

We also provide a short account of the state-of-the-art of the meteoric ^{10}Be system and its ratio to stable ^{9}Be, released by weathering, for lowland settings. We finally compare *in situ*- with meteoric-cosmogenic nuclide derived denudation rates in the Amazon basin and discuss whether these two methods are expected to agree with each other, or whether they provide divergent but complementary information.

1.1 Dates and rates: principles of cosmogenic nuclides as Earth surface chronometers

Cosmogenic nuclides are used to determine ***dates*** (exposure or burial ages) and ***rates*** (erosion, the removal of solids; and denudation, the sum of total solid and dissolved material removal). A fundamental prerequisite is that none of these

nuclides existed before Earth surface material was exposed to cosmic radiation, or fallout of meteoric nuclides. This is the case for most of the radioactive nuclides, of which the half-life is much shorter than the age of most geologic materials. Three types of chronometric information can be obtained in Earth surface materials.

i) Exposure ages are determined through measuring the buildup of nuclides. The concentration is a function of the nuclide production or fallout rate and the duration of exposure.

ii) Burial ages are determined when a sample is buried deeply enough to stop new nuclide production (like in thick floodplain sediment). Then the measurement of a shorter-lived radionuclide (e.g., ^{14}C, ^{26}Al) relative to a longer-lived (e.g., ^{10}Be) or stable (e.g., ^{21}Ne) nuclide discloses the timing of burial from the radioactive decay of these coupled nuclides.

iii) Denudation rates, in contrast, can be determined if the build-up of cosmogenic nuclides at the surface is limited by the removal of mass from the surface that is continuously eroded, or dissolved, provided that such weathering occurs within the cosmic ray adsorption zone. In this case the concentration measured in a surface sample scales inversely with the rate of mass removal at the surface. If buried after erosion and shielded in sediment, decay-corrected concentrations provide a ***paleo-denudation rate***, i.e. the rate at which the source area was eroding at the time of deposition. If the mass loss of elements from the weathering zone relative to parent bedrock by mineral dissolution can be constrained, both physical **erosion** and chemical **weathering** rates can be obtained.

141 Two varieties of nuclides have commonly been used in Earth surface research (von
142 Blanckenburg and Willenbring (2014); see Fig. 1). Atmospherically produced
143 nuclides, such as meteoric ^{10}Be, were utilized for geomorphologic applications
144 already in the late 1980´s and early 1990's (Pavich et al., 1984; Brown et al., 1985;
145 Brown, 1987; You et al., 1988; Brown et al., 1992; Monaghan et al., 1992; McKean et
146 al., 1993). However, issues such as partial retentivity and the lack of accurate flux
147 estimates impaired its routine application (Willenbring and von Blanckenburg, 2010).
148 The meteoric ^{10}Be nuclide was initially sidelined by the success of the *in situ* variety,
149 produced in the uppermost layer of the Earth's surface (Lal, 1991; Gosse and Phillips,
150 2001; Dunai, 2010).
151
152 The first principle explained in this review is the determination of denudation rates
153 from the measurement of *in situ* cosmogenic nuclides in quartz from river sediment.
154 It is less known that meteoric ^{10}Be was first used to determine catchment-wide
155 erosion (Brown, 1987; Brown et al., 1988; You et al., 1988). The first studies
156 suggesting the *in situ*-produced nuclide variety as tool to determine catchment-wide
157 denudation rates followed D. Lals (Lal, 1991) comprehensive framework and were
158 published in the mid- to late 1990´s (Brown et al., 1995; Bierman and Steig, 1996;
159 Granger et al., 1996). The first systematic river basin scale studies appeared in 2001
160 (Kirchner et al., 2001; Schaller et al., 2001). *In situ*-produced ^{10}Be, measured in
161 quartz (Fig. 1) became the most commonly used nuclide. The reasons for this success
162 are that its half-life of 1.39 Myr (Chmeleff et al., 2010; Korschinek et al., 2010)
163 ensures zero initial concentration for most materials first exposed at the Earth's
164 surface, and it is in the range of many dating applications. Further, analytical efforts

and costs involved are manageable (Dunai, 2010), quartz is an abundant mineral that largely resists weathering (Kohl and Nishiizumi, 1992), and knowledge of production rates and their scaling for latitude and atmospheric scaling is constantly increasing (Lal, 1991; Masarik and Reedy, 1995; Stone, 2000; Balco et al., 2008; Lifton et al., 2014; Borchers et al., 2016; Phillips et al., 2016). Thus the nuclide can be used with high robustness and confidence for erosion studies in "sediment production" settings where the relief is such that sediment is readily exported from the catchment (see Fig. 1) (Bierman and Nichols, 2004; von Blanckenburg, 2005; Granger and Riebe, 2007).

The second principle explained in this review is the behavior of cosmogenic nuclides in sediment that has been stored in Quaternary deposits. Storage in sedimentary deposits may both increase (by further irradiation) and decrease (by radioactive decay), their cosmogenic nuclide concentrations thus depending on paleo-erosion rate, depositional age, and depositional depth (Granger and Muzikar, 2001; Schaller et al., 2004). Paleo-erosion rates were recently summarized in review articles (e.g. Granger and Schaller (2014); Dosseto and Schaller (2016)). Pairing cosmogenic ^{10}Be with stable noble gases such as ^{21}Ne measured in quartz (Niedermann, 2000; Niedermann, 2002), or the longer-lived ^{26}Al (half-life of 0.72 Myr; Samworth et al. (1972)), resulting in ^{21}Ne/^{10}Be and ^{26}Al/^{10}Be ratios (Granger and Muzikar, 2001; Granger, 2006; Balco and Shuster, 2009), is common to e.g. extend the time frame of investigation required for these applications (Granger and Muzikar, 2001; Schaller et al., 2002; Matmon et al., 2003; Partridge et al., 2003; Schaller et al., 2004; Balco and Stone, 2005; Stock et al., 2005; Haeuselmann et al., 2007; Kong et al., 2009; Hu et al.,

2011; Matmon et al., 2011; Wittmann et al., 2011b; Charreau et al., 2012; Bekaddour et al., 2014; McPhillips et al., 2016). Recently, the *in situ*-cosmogenic nuclide ^{14}C which has a much shorter half-life of 5730 yrs (Libby, 1955) was added to the family of cosmogenic isotopes measured in quartz (Lifton et al., 2001). When combined, $^{10}Be/^{14}C$ ratios can be used to constrain more recent Earth surface processes as this ratio is sensitive to kyr time scale variations in erosion rate, and sediment storage over kyrs (Hippe et al., 2012).

Studies exploring the transport and deposition zones of a river system (Fig. 1) with cosmogenic nuclides are still scarce. Granger et al. (1996) cautioned for the effect sediment storage can have on cosmogenic nuclide-derived denudation rates. These authors noted that "*during storage and transport, sediment can accumulate additional cosmogenic nuclides, or it can be shielded from cosmic ray exposure (…). However, the net effect on cosmogenic nuclide concentrations will be small as long as the mean residence time of storage and transport is much shorter than the erosional timescale*" (Granger et al., 1996). Wittmann and von Blanckenburg (2009) first explored this important prediction, by mapping-out the behavior and limitations of *in situ*-produced cosmogenic nuclides in global large lowland basins. In lowland settings, the mean residence time of storage is a function of the sediment accommodation space within the floodplain, and the rivers migration rate. We proceed to explain these systematics.

2. PRINCIPLES OF *IN SITU* COSMOGENIC NUCLIDES IN THE SEDIMENT SOURCE AREAS AND IN LOWLAND RIVER BASINS

2.1 Steady state denudation in the sediment production zone

Within the sediment production zone of a basin (Fig. 1), sediment is generated by weathering and erosion processes on the hillslope, leaves the zone by riverine transport, and moves down the sediment cascade (Burt and Allison, 2010; Hinderer, 2012). The concentration of an *in situ*-cosmogenic nuclide in the sediment leaving this zone is termed C_0 (in at/$g_{(Qtz)}$). A steady state C_0 is attained if export by erosion equals the rate of its production (Lal, 1991; von Blanckenburg, 2005). In that case, D_{insitu}, the denudation rate (in i.e. cm/yr) derived from *in situ*-produced ^{10}Be includes all mass losses from the surface by both physical erosion and chemical weathering reactions, where weathering loss is only accounted for if it occurs within the absorption depth scale (Lal, 1991; Riebe and Granger, 2013). The original equation derived to calculate steady state D_{insitu} (Lal, 1991) is as follows:

$$D_{insitu} = \left(\frac{P_0}{C_0} - \lambda\right)\frac{\Lambda}{\rho} \quad \text{(Eq. 1)}$$

However, since then the importance of additional nuclide production by slow and fast muons has been realized, such that the dependence of C_0 on D_{insitu} is more complex:

$$C_0 = \frac{\bar{P}_n}{\frac{\rho \times D_{insitu}}{\Lambda_n} + \lambda} + \frac{\bar{P}_{\mu s}}{\frac{\rho \times D_{insitu}}{\Lambda_{\mu s}} + \lambda} + \frac{\bar{P}_{\mu f}}{\frac{\rho \times D_{insitu}}{\Lambda_{\mu f}} + \lambda} \quad \text{(Eq. 2)}$$

where $\bar{P}_n$, $\bar{P}_{\mu s}$, $\bar{P}_{\mu f}$ are basin-wide ^{10}Be production rates (at/$g_{(Qtz)}$/yr) for neutrons, slow muons, and fast muons, respectively. The terms Λ_n, $\Lambda_{\mu s}$, $\Lambda_{\mu f}$ are effective attenuation lengths (g/cm^2) of neutrons, slow muons, and fast muons, respectively (Braucher et al., 2011, see supplement A; note that these terms are often deconvolved into further subfractions denoting different exponential absorption paths). The density of removed rock or soil is given by ρ (g/cm^3). The term ρ/Λ_n can be replaced by z*, the absorption depth scale (cm), which is the distance over which the cosmic-ray flux decreases by a factor of 1/*e*, or 63%. This vertical distance, divided by the denudation rate, gives the integration time scale of the method (von Blanckenburg, 2005). The time scale is a function of the denudation rate, and is the time required to erode a rock layer of a thickness of ca. 60 cm in rocks or ca. 100 cm in soils, representing the absorption depth scale of the cosmic rays producing these nuclides (Lal, 1991; von Blanckenburg, 2005). Note that for basin-scale studies, where denudation rates are not uniform, a requirement to solve equation (1) for D_{insitu} is that the integration time scale is smaller than the time scale for radioactive decay, or $D/z^* >> \lambda$. Therefore, the ^{10}Be method is applicable in those settings where D_{insitu} > 0.3 mm/kyr, while for ^{14}C D_{insitu} > 80mm/kyr (von Blanckenburg, 2005). If ρ is omitted from equation 1, a denudational mass flux (g/cm^2/yr) results. Denudation rates are typically reported in mm/yr or t/km^2/yr.

2.2 Modifications of in situ nuclide concentrations in lowlands

Equations 1 and 2 are only valid for a set of assumptions, the prime one being that steady state has been attained between cosmogenic nuclide production and their

258 removal by erosion. In the depositional zone of a river basin, however, there is no
259 continuous sediment removal from the surface layer that equals its production;
260 rather, sediment in the floodplain is locally and laterally eroded such as bank failure
261 and avulsions, and sediment storage may lead to additional production or decay of
262 nuclides. Thus sediment in the active channel comprises a mixture of fresh upstream
263 sediment (nuclide concentration C_0) with reworked floodplain material (C_{dep}). The
264 concentration of the active channel mixture C_{mix} depends on these concentrations
265 and the relative sediment fluxes. In keeping with the terminology introduced by
266 Wittmann and von Blanckenburg (2009), we define two floodplain end members
267 (Fig. 2) that lead to characteristic cosmogenic nuclide patterns once the previously
268 stored floodplain deposit is mixed with fresh river sediment from the source area.
269
270 The "***static floodplain***" is located away from the main stream. Reworking events by
271 an irregular avulsion or channel diversion of the river (Fig. 2) are considered to be
272 rare and episodic. As the main channel migrates away from the original sites of
273 deposition the distance to the main stream and thus the probability of preserving an
274 (increasingly older) deposit increase. These distal deposits are most likely of
275 Quaternary or older age. The nuclide concentration in modern stream sediment C_{mix}
276 will encounter a transient change following a remobilization event.
277
278 The "***dynamic floodplain***" in contrast is limited to the active channel belt, a zone
279 close to the main channel that is frequently reworked by the migrating river.
280 Relatively young, mostly Holocene deposits are continuously reworked and mixed
281 with fresh sediment. If at a given position within the main channel sediment storage

and sediment remobilization are balanced, the nuclide concentration at this site C_{mix} will not change with time.

During storage in both cases the initial *in situ* cosmogenic nuclide concentration C_0, established when the sediment was produced in the source area, is changed to a concentration in the lowland deposit C_{dep} (at/$g_{(Qtz)}$). At a given burial depth z (m) of a section of sediment stored in the floodplain, $C_{dep,z}$ depends on the density of sediment (ρ_{dep}; including pore water) in the floodplain, on the locally prevailing (most likely low) nuclide production rate at the sediment's surface P_{dep} (at/$g_{(Qtz)}$/yr) that contains all nucleogenic and muogenic production terms (for full equation including muonic production terms, we refer to equation 6 in Wittmann and von Blanckenburg (2009)), and the storage time *t* (yr) (Schaller et al., 2002):

$$C_{dep,z} = C_0 \times e^{-\lambda t} + \frac{P_{dep}}{\lambda} \times e^{\left(-\frac{\rho_{dep} \times z}{\Lambda}\right)}(1 - e^{-\lambda t}) \quad \text{(Eq. 3)}$$

C_{dep}, the nuclide concentration contained in an integrated sediment column to the maximum mobilization depth (z_{max}) is calculated by integrating $C_{dep,z}$ from the surface (z_0) over the depth of erodible floodplain sediment, providing a mean C_{dep}:

$$\mathrm{C_{dep}} = \frac{1}{\mathrm{z}_{max}} \int_{\mathrm{z}_0}^{\mathrm{z}_{max}} \mathrm{C_{dep,z}}\, \mathrm{dx} \quad \text{(Eq. 4)}$$

303 In the next two sections we illustrate how C_{dep} evolves in both the static and the
304 dynamic floodplain end members, and we provide examples from the Amazon and
305 the Ganga basin (see Fig. 3 for basin topography and sample locations).
306
307
308 ***2.3 Predicting nuclide concentrations in sediment re-entrained from static deposits***
309 We illustrate the effects of storage depth and time on C_{dep} for ^{10}Be ($^{10}Be_{dep}$), and the
310 $^{26}Al/^{10}Be_{dep}$ ratio for a static deposit. In Fig. 4A we see that at the surface ^{10}Be
311 concentrations almost always increase due to additional nuclide production, until
312 steady state between production and decay is attained at >3 Myr. We also see that if
313 stored very deeply at ca. 50 m, where even deep muonic production is low, ^{10}Be
314 concentrations decrease by radioactive decay. Fig. 4B shows that when measuring
315 both *in situ* ^{26}Al and *in situ* ^{10}Be the resulting $^{26}Al/^{10}Be$ ratio is sensitive to both
316 storage time and depth.
317
318 The re-entrainment of such static sediment having a nuclide concentration C_{dep} and
319 its mixing with fresh upstream sediment with C_0 results in mixed nuclide
320 concentrations C_{mix} ($at/g_{(Qtz)}$). In the Amazon basin, such entrainment of old,
321 formerly buried sediment has been traced in river sediment with paired *in situ* ^{26}Al
322 and *in situ* ^{10}Be in coarse-grained quartz (Wittmann et al., 2011b).
323
324 In an "erosion island" plot (Fig. 5), the $^{26}Al/^{10}Be$ ratio is linked to $^{10}Be_0$. $^{10}Be_0$ is a
325 measure of the denudation rate of the sediment during initial erosion, called
326 inheritance. Steadily eroding sediments with no pre-burial history plot on the steady

state erosion line (Fig. 5A). The ratio of ^{26}Al and ^{10}Be nuclide production rates at the surface is 6.5 to 7 (Balco et al., 2008; Goethals et al., 2009; Hidy et al., 2014). Samples that have been buried plot beneath the line, at lower $^{26}Al/^{10}Be$ ratios. Upon reactivation of buried sediment, the active channel will receive a fraction of buried material, such that ^{10}Be and ^{26}Al concentrations, called $^{10}Be_{mix}$ and $^{26}Al_{mix}$, and $(^{26}Al/^{10}Be)_{mix}$ emerge. In order to calculate the fraction of recycled material, f_{buried}, we must know $^{10}Be_0$ from ^{10}Be and $^{26}Al_0$ from ^{26}Al, such that the position on the constant steady state erosion line is constrained (see Fig. 5B):

$$\left(\frac{^{26}Al}{^{10}Be}\right)_{mix} = \frac{(^{26}Al_0 \times f_0 \; + ^{26}Al_{buried} \times f_{buried})}{(^{10}Be_0 \times f_0 \; + ^{10}Be_{buried} \times f_{buried})} \qquad \text{(Eq. 5)}$$

Since the sum of f_0 (the fraction of sediment containing $^{10}Be_0$ from steady state erosion in the source area) and f_{buried} equals 1, we can solve equation 5 for f_{buried} (Wittmann et al., 2011b). As we can constrain $^{10}Be_{dep}$ and $^{26}Al_{dep}$ only from the lowermost sample in the diagram, burial depths and ages are minimum estimates. The fractions of formerly buried end member incorporated into the non-buried channel material are thus maximum fractions.

At this stage it is important to point out that the “isochron method” was designed to determine depositional ages of buried sediment in which nuclides are being produced by cosmic rays not fully absorbed by the overlying sediment from linear regression of ^{26}Al versus ^{10}Be concentrations (Balco and Rovey, 2008). This method does not require assumptions on the inherited nuclide concentrations. However, the method cannot be applied to determine burial ages on river sediment that

351 comprises a mixture of such old sediment and fresh source area-derived river
352 sediment.
353
354 ***2.4 Amazon nuclide concentrations in sediment re-entrained from static deposits***
355 To our knowledge, the Amazon data shown in Fig. 5 is the only currently available
356 dataset suitable to estimate sediment reactivation by using the $(^{26}Al/^{10}Be)_{mix}$ ratio in
357 bedload sediment. $(^{26}Al/^{10}Be)_{mix}$ ratios well below ca. 6.5, indicating shielding from
358 cosmic ray production during deep burial (see Fig. 5), were detected in the
359 headwaters of cratonic rivers and also downstream in isolated floodplain deposits.
360 There, burial ages exceed 5 Myr. In contrast, Andean sediment evidently has not
361 experienced burial showing $^{26}Al/^{10}Be$ ratios of around 6.5 to 7 (see Fig. 5) (Wittmann
362 et al., 2011b). Such old craton-derived sediment is admixed to the Amazon by the
363 large Negro River, which joins the Amazon at Manaus, and the Madeira River, which
364 drains the Bolivian Andes and parts of the Brazilian Craton, and joins the Amazon
365 downstream of Manaus (Fig. 3).
366
367 ***2.5 Predicting the nuclide concentrations in the dynamic floodplains of the Amazon***
368 ***and Ganga basins***
369 We compiled sediment storage times *t* for dynamic floodplains (see supplement B ,
370 Table A1). These storage times are significantly shorter than the half lives of ^{10}Be and
371 ^{26}Al. This means that storage times are too short to allow for significant radioactive
372 decay of ^{10}Be or ^{26}Al even when shielded from cosmic irradiation (Fig. 4A). The
373 question is whether for ^{10}Be and ^{26}Al the nuclide concentration C_{mix} still increases

374 during the repeated storage cycles. However, *in situ* ^{14}C has a half-life exactly within
375 the range of storage times and should quantify storage duration.
376
377 The change of nuclide concentrations first depends on the floodplain configuration,
378 i.e. its width, depth (because the reservoir size governs the capacity of sediment
379 storage), and the upstream sediment flux (which together with the reservoir size
380 determines the storage duration). Nuclide concentrations secondly depend on
381 nuclide-specific characteristics, i.e. the initial upstream concentration C_0 (that
382 depends on source area erosion rate), the production rate in the lowlands, the
383 penetration depth of cosmic rays, and, mostly for ^{14}C, on the half-life of the nuclide.
384 Given this range in parameters, we need to revert to combined floodplain mass
385 balance and nuclide production models that evaluate the dependence of nuclide
386 accumulation and decay on floodplain parameters.
387
388 Two modeling studies have now mapped out the conditions under which nuclide
389 concentrations of *in situ*-produced ^{10}Be, ^{14}C, and ^{26}Al are modified as sediment
390 moves through dynamic floodplains. The "box" (compartment-based) model of
391 Wittmann and von Blanckenburg (2009) used *a priori* choices of floodplain exchange
392 parameters, sediment storage time, and sediment fluxes. These were explored for a
393 wide range of global lowland river settings. The numerical model by Lauer and
394 Willenbring (2010), later modified by Viparelli et al. (2013), uses numerically
395 determined gain or loss of floodplain mass depending on overbank deposition and
396 net bank erosion rates as input. The model was explored for the case of the local
397 Neuse river (mid-USA) and also addresses the clay flux passing through the reach.

398 This model makes predictions on the behavior of meteoric ^{10}Be in floodplains,
399 although the way the isotope migrates with the water flux through sediment, its
400 penetration depth, nor its adsorption behavior are specified. Both models have the
401 *in situ* nuclide production mechanisms (spallation and muonic) in common and
402 eventually derive the final steady state nuclide concentrations C_{mix} from mass
403 balance. Although their mathematical complexity differs considerably, the
404 predictions made by these two models are in good agreement. For comparison we
405 have employed both models to the Amazon and the Ganga basin using a single-
406 channel setup, i.e. assuming that the lowlands are fed by a single, source-area
407 draining river (see a description of the setup in Table 1 and Fig. 6). In contrast, the
408 numeric model as employed by Lupker et al. (2012a) for the Ganga basin uses a
409 setup where multiple headwater channels feed the lower Ganga.
410 Both models predict very low increases of only 1.8% for the box model and 1.7% for
411 the numerical model in long-lived (i.e. ^{10}Be) *in situ* nuclide concentrations relative to
412 C_0 along the lowland reach from the Andes to the Amazon mouth (Table 1, Fig. 6).
413 For the Ganga basin an increase of 1.5% is predicted by the box model and 6.5% by
414 the numerical model. Lupker et al., (2012a) predicted an increase of 13% relative to
415 $^{10}Be_0$ by notably more accurately addressing the variation in nuclide concentrations
416 of multiple headwater rivers. Evidently, this range in model results that depends on
417 each model configuration implies that a certain range in measured nuclide
418 concentrations can be expected in real settings, too. For short-lived nuclides, a
419 significant decrease in *in situ*-produced ^{14}C nuclide concentrations is predicted (Fig.
420 6, A-1,2).

421 The overall similar response of a few % increase despite differing sediment storage
422 times (14 kyr in the Amazon, 1.4 kyr in the Ganga) are due to the different
423 remobilization depths. For the much deeper Amazon channel, ^{10}Be that is produced
424 in the floodplain superficially is diluted by deeply sourced sediment that was
425 shielded from further production. The shallower channel of the Ganga, in contrast, is
426 more sensitive to irradiation, even at short storage times. In addition, the relatively
427 high Amazon $^{10}Be_0$ (stemming from the Andean erosion rate of ca. 0.2 mm/yr) is less
428 sensitive to additional surficial nuclide production in the lowlands than the three
429 times lower $^{10}Be_0$ of the Ganga (corresponding to high mean Himalayan erosion of
430 ca. 1.5 mm/yr; Fig. 5). Overall, however, changes in long-lived *in situ* nuclide
431 concentrations are predicted to be minor as most lowland settings are located at low
432 elevations, where production rates are much lower than those in the sediment-
433 producing highlands.
434
435 For ^{14}C, the significant predicted decrease from the headwaters to the floodplain
436 (Fig. 6) is due to the much shorter half-life, which makes this system sensitive to
437 storage times of a few thousand years. Due to this behavior, Wittmann and von
438 Blanckenburg (2009) proposed this nuclide to be a good proxy for sediment
439 residence time. Complicating factors for such use in floodplains however are: 1) The
440 initial *in situ*-^{14}C signal of the sediment eroded from the source area has to be stable
441 over time and representative of the erosion process. Even short burial and decay of
442 ^{14}C upstream of the floodplain might compromise this stability (Lupker et al., 2014).
443 2) Sediment cannot be considered as being well-mixed with respect to *in situ*-^{14}C in
444 floodplain sediment. Sediment mixing in floodplains takes place over time scale of a

445 few kyr, which is the same time scale as the ^{14}C half-life. Even small additions of
446 distal sediment anywhere along the floodplain reach may introduce high variability
447 into calculated residence times.
448
449 ***2.6 Identifying sediment sources from nuclide concentrations in lowland rivers***
450 To test the predictions made in the preceding section, namely that *in situ* nuclide
451 concentrations imprinted in the source area are hardly modified in transit through
452 the dynamic floodplain, requires tracing sediment from a single source. However,
453 the nuclide concentration of large lowland rivers is also controlled by the influx of
454 sediment from tributaries that drain source areas with different denudation rates.
455 These will contain distinct initial nuclide concentrations.
456
457 In the Amazon lowlands, Wittmann et al. (2011b) were able to separate the
458 entrained signature of the static craton-derived and other lowland deposits from
459 Andean-sourced sediment. This separation was done based on $^{26}Al/^{10}Be$ ratios,
460 indicating entrainment of previously buried sediment from the cratons, and on
461 different grain size distributions. A condition for use of grain size distributions as
462 source indicator is that these are not obscured through downstream fining.
463 Downstream fining occurs in larger sand-bed rivers through abrasion and selective
464 transport, whereas selective transport dominates over abrasion due to durable
465 lithologies, small grain sizes, and high degree of rounding (Frings, 2008). Evidence for
466 preservation of the grain size distribution was provided by Nordin et al. (1980) and
467 Mertes and Meade (1985) who showed that the particle size of the Amazon is
468 uniform from Iquitos to Óbidos. The area-weighed ^{10}Be nuclide concentration of

469 Andean sediment (comprising all grain sizes, n = 62, basins of >100 km^2) is ca.
470 5.6×10^4 $at/g_{(Qtz)}$ (Fig. 7). Note that we employed area-weighing of ^{10}Be
471 concentrations by adapting equation 7 for nuclide concentrations (see section 3.1).
472 An exception with respect to nuclide concentrations in the Andes is the Bolivian
473 Grande basin, where ^{10}Be nuclide concentrations are much higher at $40 \pm 56\times10^4$
474 $at/g_{(Qtz)}$ (± 1σ std. dev.) and also highly variable depending on physiographic region
475 (i.e. indicated by high std. dev.) (Kober et al., 2015). The ^{10}Be nuclide concentrations
476 of all other investigated regions are however very similar to the ^{10}Be nuclide
477 concentration detected downstream in fine-grained (125-500 µm) Amazon bedload
478 (5.3×10^4 $at/g_{(Qtz)}$, n = 18, see Fig. 7; Wittmann et al. (2011a)). This grain size fraction
479 is therefore derived from the Andes. Craton-derived sediment on the other hand
480 mainly contributes coarse-grained sandy sediment (Nordin et al., 1980; Franzinelli
481 and Potter, 1983) containing high nuclide concentrations (ca. 26.2×10^4 $at/g_{(Qtz)}$) from
482 slow erosion of the cratonic headwaters that was buried for Myr durations as shown
483 by $^{26}Al/^{10}Be$ ratios (section 2.3 and Wittmann et al. (2011b)).
484
485 In the lower Ganga basin Lupker et al. (2012a) measured mean ^{10}Be nuclide
486 concentrations in lowland sediment of 1.75×10^4 $at/g_{(Qtz)}$ (n = 14, area-weighed).
487 Notably, some variability in ^{10}Be concentrations exists for smaller lowland rivers (i.e.
488 Karnali, Kosi, Narayani, having between 17% and 37% lowland area at the sampled
489 locations), but the area-weighed lowland ^{10}Be nuclide concentration is very similar
490 to an area-weighed concentration of 1.5×10^4 $at/g_{(Qtz)}$ of the Himalayan source area
491 (Fig. 7, n = 65, >100 km^2). Lowland ^{10}Be concentrations were corrected by Lupker et
492 al. (2012a) for the sediment contribution from rivers draining the Indian craton (e.g.

493 the Chambal River, see Fig. 3), by using simple binary mixing equations. ^{10}Be nuclide
494 concentration there are very high with 43×10^4 at/$g_{(Qtz)}$ (Lupker et al., 2012a).
495 Although these areas are slowly eroding, the associated sediment flux leads to a ca.
496 three times elevated ^{10}Be nuclide concentration of the main stream below the
497 confluence with the Chambal River. These cratonic rivers also influence the grain size
498 of the lower Ganga. The overall grain size reduction is only 2% per 100 km of river
499 length, negligibly affecting Himalayan nuclide concentrations, but a slight coarsening
500 is observed downstream of Indian craton confluences (Singh et al., 2007). If similar
501 to the Amazon basin, these areas might also deliver old, deeply stored sediment to
502 the main Ganga. We cannot test this assumption because no ^{26}Al measurements are
503 available for the Ganga River.
504
505 These observations confirm that in both basins the erosion signal from the sediment
506 source area imprinted in the form of ^{10}Be nuclide concentrations is not significantly
507 changed, or, in other words, nuclide concentrations are conserved during transfer to
508 the sea. This is the case in both the Amazon and the Ganga Rivers. The models of
509 channel-floodplain interactions (section 2.5) predict this absence of change in the
510 concentration of long-lived *in situ* nuclides in lowland basins.
511
512

513 **3. CALCULATING DENUDATION RATES AND SEDIMENT FLUXES IN LOWLAND**
514 **BASINS**

515 ***3.1 Converting nuclide concentrations from lowland rivers into a denudation rate***
516 ***of the sediment-delivering mountains***

517 We have seen in the preceding section that the concentrations of long-lived *in situ*
518 nuclides that have been set in the eroding mountain hinterland are preserved in
519 lowland areas. They can be extracted by grain size-specific analysis and their
520 reduction by radioactive decay in re-entrained old sediment from static deposits can
521 be identified by paired nuclide analysis. This preservation leads to the opportunity to
522 determine the erosion signal of an entire mountain belt. If the denudation rate of
523 the entire basin including the lowlands is to be determined (using equation 2), a
524 floodplain-uncorrected denudation rate, termed "D_{insitu}" results. As this denudation
525 rate is based on the unreasonable assumption that the entire basin including the
526 floodplain provides sediment by erosion from the whole basins' surface, it is only an
527 "apparent" denudation rate. A "floodplain-corrected" denudation rate, termed
528 "$D_{insituFC}$", takes into account that the lowlands do not produce additional "primary"
529 sediment eroded under cosmogenic steady state conditions (equation 2), but merely
530 serve as a transfer route. Calculating a floodplain-corrected denudation rate is done
531 by using the production rate of the source area, termed P_{FC}, containing all
532 nucleogenic and muogenic production mechanisms, that is then scaled to the
533 altitude and latitude of the hinterland (Eq. 2).
534
535 As illustrated in Figure 8, this correction removes the decrease in apparent
536 denudation rates across lowland areas (see blue dashed curve in Fig. 8) that arises
537 when using the total production rate at the sampling point including the low-
538 elevation lowlands. Because all other areas that do not contribute sediment are not
539 considered, the resulting floodplain-corrected denudation rates $D_{insituFC}$ (mm/yr)
540 correspond to the sum of the hinterlands sediment production and weathering

rates. In practice, this calculation involves the digital delineation of the basin and clipping low-elevation floodplain areas by using a basin-specific cut-off elevation (using Digital Elevation Models, i.e. DEMs). From this floodplain-corrected denudation rate $D_{insituFC}$, we can calculate floodplain-corrected sediment and dissolved fluxes $QS_{insituFC}$ (t/yr) (that by definition also contain dissolved fluxes because we use denudation rates, i.e. the sum of erosion and weathering rates). We multiply $D_{insituFC}$ by the area of the production zone A_{source} and the source rock's density $\rho_{bedrock}$ (here a value of 2600 kg/m^3 is used, to relate the mass flux to bedrock lowering) and obtain:

$$QS_{insitu_{FC}} = D_{insitu_{FC}} \times A_{source} \times \rho_{bedrock} \quad \text{(Eq. 6)}$$

When considering regions, such as the entire Andes or the lowlands, an area-weighed denudation rate is calculated because smaller basins contribute less sediment than larger basins. This area-weighed denudation rate $\overline{D_{insituFC}}$ is calculated using equation (3) in Wittmann et al. (2009), in order to weigh each tributary according to tributaries' area relative to the summed area of individual subbasins *i*:

$$\overline{D_{insituFC}} = \frac{\sum_{i=1}^{n}(D_{insituFC} \times A_{source})}{\sum_{i=1}^{n} A_{source}} \quad \text{(Eq. 7)}$$

Equation 7 can also be used to calculate an area-weighed denudation rate of sub-basins of the Andes, in this case employing D_{insitu}.

564

565 ***3.2 Recent erosion rates from sediment gauging data and their correction in***
566 ***lowland basins***

567 The reconstruction of sediment dynamics over different temporal scales is
568 fundamental to understanding source-sink connectivity, because the time scale of
569 observation is crucial for signal analysis in sedimentary systems (Romans et al.,
570 2015). To provide such comparison of sediment fluxes over two entirely different
571 temporal scales we can compare cosmogenic nuclide-derived sediment fluxes
572 (integrating over millenia) with estimates of present-day mean sediment fluxes
573 resulting from instrumental monitoring of river loads (Wittmann et al., 2011a;
574 Covault et al., 2013).

575

576 A measure of present-day sediment flux can be calculated from measurements of
577 suspended sediment, QS_{gaug} (t/yr), derived from suspended sediment concentration
578 N_{susp} (mg/l) and water flux Q_{water} (m^3/sec) measurements. If Q_{water} can be identified
579 as the major control of N_{susp}, a sediment rating model can be established to calculate
580 the suspended sediment discharge from the usually long river discharge gauging
581 period and thus well-constrained Q_{water}. For the periods in which suspended
582 sediment concentration time series are lacking, this rating curve can then be used to
583 extrapolate QS_{gaug} by, e.g., using river discharge data alone (Asselman, 1999;
584 Horowitz, 2003). For a catchment of higher stream order that contains several sub-
585 catchments that all or partially have been gauged, a representative catchment-wide
586 QS_{gaug} can be calculated by normalizing the catchments' summed tributary QS_{gaug}
587 value to the entire catchments' area at the outlet (see Table 2).

588

589 Extrapolating gauging data, representing years to decades, to millennial time scales
590 has some shortcomings, as the period of observation necessary to capture the full
591 signal amplitude is required to cover the recurrence interval of high-magnitude, low-
592 frequency discharge events. In settings where sediment influx to river systems is
593 inherently stochastic and mostly driven by discrete events such as earthquakes and
594 rainstorms (Benda and Dunne, 1997), finding ways to predict recurrence intervals of
595 such extreme events is fundamental (e.g. Korup (2012)). However, after a large, e.g.,
596 earthquake-triggered mass wasting event decades of suspended sediment
597 measurements indicate that the increased erosion pulse may persist for several
598 years until all sediment has been evacuated from the catchment (Lin et al., 2008;
599 Hovius et al., 2011). Still the integration period of suspended sediment
600 measurements is, compared to the time scale usually covered by the *in situ*
601 cosmogenic method, relatively short, such that discrepancies related to different
602 integration time scales are expected (Kirchner et al., 2001; Schaller et al., 2001;
603 Dadson et al., 2003; Wittmann et al., 2009; Covault et al., 2013)

604

605 To make sediment gauging date comparable to *in situ* ^{10}Be-derived denudation rates,
606 one of two conversions is required. This need arises because sediment gauging
607 measures sediment flux QS_{gaug} (t/yr) whereas $D_{insituFC}$ is a measure of surface
608 lowering (mm/yr) or mass flux from a given area (t/km^2/yr). Thus either $D_{insituFC}$
609 needs to be converted into $QS_{insituFC}$ (t/yr) by equation 6 (see previous section), or we
610 need to convert measured sediment fluxes, termed QS_{gaug}, to erosion rates, termed
611 E_{gaug}. Note that unlike $D_{insituFC}$ these data do not incorporate a weathering fraction

unless suspended sediment data is supplemented by dissolved data. QS_{gaug} are divided by total basin area (km^2) to derive a specific sediment yield SSY_{gaug} ($t/km^2/yr$):

$$SSY_{gaug} = \frac{QS_{gaug}}{A_{total}} \quad \text{(Eq. 8)}$$

or by total basin area and bedrock density $\rho_{bedrock}$ (2600 kg/m^3) to obtain an erosion rate (mm/yr):

$$E_{gaug} = \frac{QS_{gaug}}{A_{total} \times \rho} \quad \text{(Eq. 9)}$$

For many basins, both gauging-derived erosion rates and specific sediment yields decrease with increasing basin area. This relationship can be described with a power law where the exponent globally varies between -0.06 and -0.85 and can even obtain positive values (Syvitski et al., 2005; de Vente et al., 2007). However the global mean exponent for basins world-wide is -0.5, which we attribute to reflect mostly the geometry-dictated increase in lowland area in equations 8 or 9 at a given upstream sediment flux QS_{gaug}. The variation around the global mean exponent arises as larger basins have proportionally more low relief area than do steep and rapidly eroding headwater basins (Milliman and Meade, 1983; Summerfield and Hulton, 1994; Hovius, 1998). Thus, sediment production decreases downstream, concurrently accompanied by an increase in deposition potential as accommodation space in larger valleys and floodplains increases (Hinderer, 2012). In order to be comparable

635 with the cosmogenic nuclide method and to provide meaningful erosion rates from
636 gauging data that do not merely decrease across lowlands because basin area
637 increases, we suggest a "floodplain correction" for lowland gauging data, too. A
638 floodplain-corrected erosion rate E_{gaugFP} is calculated by simply replacing A_{total} in
639 equation 9 with the area of the sediment-producing hinterland A_{source}. Similar to the
640 cosmogenic data, we calculated an area-weighed $\overline{E_{gaug}}$ for each sub-basin (Table 2)
641 by adapting equation 7 to gauging data, yielding:
642
643 $$\overline{E_{gaug}} = \frac{\sum_{i=1}^{n}(E_{gaugFC} \times A_{source})}{\sum_{i=1}^{n} A_{source}} \quad \text{(Eq. 10)}$$
644
645 The floodplain correction allows evaluation of whether sediment is being lost due to
646 deposition or added from erosion in lowland reaches. Thus, while long-lived *in situ*
647 cosmogenic nuclides record the sediment production rate in the source area,
648 suspended sediment data record sediment production *and* sediment transport,
649 thereby spatially integrating over all processes occurring in the production and the
650 deposition zones of a basin. For example, flooding caused by rainfall events in
651 lowland parts of the basin or anthropogenic erosion (Syvitski et al., 2005; de Vente
652 et al., 2007) may lead to erosion of temporarily stored floodplain sediment, resulting
653 in elevated sediment concentrations. At the same time, cosmogenic nuclide
654 concentrations will not vary, as long as no distal (old, partly shielded) sediment is
655 incorporated into the channel during the flood event.
656

3.3 Comparing fluxes from in situ cosmogenic nuclides with river loads in the Amazon and Ganga

We calculated *in situ*-cosmogenic nuclide-derived denudation rates from the ^{10}Be cosmogenic nuclide dataset shown in Figure 7 (using basins > 100 km^2 in order to be spatially representative). We summarized these source area and lowland datasets in Table 2 and Figure 9, and compared these to erosion rates calculated from measured suspended sediment fluxes (equations 8, 9). The full cosmogenic and gauging datasets are given in supplement C. Note that all rates summarized here were area-weighed according to equations 7 or 10. The area-weighed analytical uncertainties for the cosmogenic denudation rates are 15% for the entire Andes/Amazon and 24% for the Himalayan/Ganga datasets, respectively. Quantifying uncertainties for the suspended sediment dataset is more complex. Although the long observation periods of several decades and bedload contribution of only a few percent result in high confidence in the floodplain datasets of the Amazon and Ganga, estimates from multiple observation periods differ by 50% (see Wittmann et al., 2011a, Amazon and Lupker et al., 2011, Ganga). Therefore, to compare both methods, we decided to present the 1σ std. dev. of each dataset (Table 2) rather than uncertainties. The standard deviation gives a sense of natural variations present for each dataset and does not imply a precision that is inappropriate when comparing different methods.

For the lowlands of the Amazon basin at Óbidos (Fig. 3), we calculate an *in situ* cosmogenic nuclide-derived Amazon basin-wide denudation rate $\overline{D_{insitu}}$ of 0.11 mm/yr when no floodplain correction is employed. When the floodplain correction is employed, the $\overline{D_{insituFC}}$ is 0.18 mm/yr. This rate is similar to a $\overline{D_{insitu}}$ of the entire

681 Andes of 0.19 mm/yr (see section 4.1) and thus can be considered to represent the
682 combined sediment production and weathering rate of the source area. We
683 converted this Andean denudation rate to sediment and weathering fluxes QS_{insitu} by
684 using equation 6 and a sampled source area of 7.58×10^5 km^2 and obtained 380
685 Mt/yr; conversion of the $\overline{D_{insituFC}}$ of 0.18 mm/yr at Óbidos (using equation 6 and
686 the same sampled source area) leads to a sediment flux of 350 Mt/yr (Figs. 9, 10;
687 Table 2).
688
689 For the Ganga basin, a basin-wide $\overline{D_{insitu}}$ of 0.33 mm/yr is calculated at Harding
690 Bridge (see Table 2) when no floodplain correction is employed. A $\overline{D_{insituFC}}$ of 0.82
691 mm/yr (relating to $QS_{insituFP}$ of 390 Mt/yr when using a sampled source area of
692 1.84×10^5 km^2 in Eq. 6) compares to a $\overline{D_{insitu}}$ of 1.14 mm/yr for the Himalayan source
693 areas and an equivalent QS_{insitu} of 550 Mt/yr (see Figs. 9, 10).
694 The gauging-derived lowland dataset is similar to that measured in the source areas
695 (see lower part of Table 2). For the Amazon basin at Óbidos, a basin-wide $\overline{E_{gaug}}$ of
696 0.07 mm/yr is calculated. After removing the lowland area from this rate by
697 application of the floodplain correction (by using a sampled source area of 6×10^5 km^2
698 in Eq. 6), the $\overline{E_{gaugFC}}$ is 0.58 mm/yr, a value that compares to a source-area $\overline{E_{gaug}}$ of
699 0.47 mm/yr (see Table 2 and Fig. 9). In the Ganga basin, a non-floodplain corrected
700 $\overline{E_{gaug}}$ is 0.17 mm/yr, and a $\overline{E_{gaugFC}}$ denotes to 0.81 mm/yr (by using a sampled
701 source area of 1.85×10^5 km^2 in Eq. 6), a value that compares to a source-area $\overline{E_{gaug}}$
702 of 0.80 mm/yr (see Figs. 9, 10).
703
704 By comparison, dissolved fluxes are minor. There is independent evidence that

705 dissolved fluxes as recorded in the Amazon lowlands comprise only ca. 10% of the
706 suspended sediment flux (for summary on dissolved and suspended sediment fluxes
707 see Table 2 in Wittmann et al. (2011a)). Silicate weathering rates determined from
708 combined *in situ*- and gauging-derived estimates of D and W are similar for the
709 Andes and the Amazon lowlands and are generally low at ca. 100-200 t/km^2/yr
710 (corresponding to 0.04-0.08 mm/yr, or to ca. 10% of total D (Bouchez et al., 2014)).
711 Likewise, as explained in section 5, weathering intensities determined from the new
712 weathering and erosion ^{10}Be(meteoric)/^{9}Be proxy indicate similar weathering
713 intensities in the Andes and in the lowlands, respectively (Wittmann et al., 2015).
714 In the Himalayan source areas silicate weathering rates amount to only 17 t/km^2/yr
715 (corresponding to 0.007 mm/yr; Rai et al. (2010)). In such terrains, kinetically-limited
716 conditions prevail, meaning that minerals are eroded before they weather to
717 completeness (West et al., 2005; Gabet and Mudd, 2009; Dixon and von
718 Blanckenburg, 2012; Dixon and Riebe, 2014). However, Lupker et al. (2012b) found
719 that floodplain weathering dominated over mountain weathering in the Ganga
720 basin. Yet these floodplain processes are associated with considerable partitioning of
721 dissolved Si into the suspended load in clays that formed in the floodplain (Frings et
722 al., 2015) such that net silicate weathering fluxes even decrease along the floodplain
723 (Rai et al., 2010).
724

725 **4. THE GEOLOGICAL SIGNIFICANCE OF FLOODPLAIN DATA**

726 ***4.1 Across spatial scales: big brush or fine tip?***

727 Regarding the compiled denudation and erosion rate datasets we first discuss the

728 significance of denudation and erosion rates, their spatial averaging as catchment
729 area increases, and evaluate sediment fluxes from the headwaters to the lowlands to
730 the ocean. The following observations were made in the preceding section.
731 a) In the Amazon basin, D (from *in situ* ^{10}Be), differ by a factor of 2-3 to E (from
732 gauging), both in the source area ($\overline{D_{insitu}}$ = 0.19 $\pm$ 0.18 mm/yr; $\overline{E_{gaug}}$ = 0.47 $\pm$ 0.90
733 mm/yr) and in the lowlands ($\overline{D_{insituFC}}$ = 0.18 $\pm$ 0.03 mm/yr; $\overline{E_{gaugFC}}$ = 0.58 $\pm$ 0.20
734 mm/yr; see Fig. 10 and Table 2).
735 b) In the Ganga basin, D and E show a good agreement, both in the source area
736 ($\overline{D_{insitu}}$= 1.14 $\pm$ 0.82 mm/yr; $\overline{E_{gaug}}$= 0.80 $\pm$ 0.55 mm/yr; see Table 2) and in the
737 Ganga lowlands ($\overline{D_{insituFC}}$ = 0.82 $\pm$ 0.27 mm/yr; $\overline{E_{gaugFC}}$ = 0.81 $\pm$ 0.27 mm/yr).
738 c) In both the Andes-Amazon and the Himalaya-Ganga systems, cosmogenic nuclide-
739 derived D contains only a minor dissolved contribution. We can thus compare short-
740 term erosion rates directly to millennial time scale denudation rates and ignore the
741 weathering fluxes.
742
743 We summarize from our study the following first-order interpretations:
744 1) Anthropogenic perturbations, known to affect the Andean source areas by e.g.
745 gold mining and changes in land use (Maurice et al., 1999; Cleary, 2000; Vanacker et
746 al., 2007) can result in an increase in erosion towards modern times. The factor-of-2
747 difference between D_{insitu} and E_{gaug} in the Andes supports this interpretation. For
748 comparison, in the Highlands of Sri Lanka or the Paute basin in Ecuador, much higher
749 E_{gaug} than D_{insitu} are observed (see Fig. 11). For the Ganga data, where D_{insitu} and E_{gaug}
750 agree better, Lupker et al. (2012a) argued that human-impact in the Ganga basin
751 have not increased sediment mobilization.

752

753 2) $\overline{D_{insitu}}$ of the Himalayan source area might be overestimated due to several
754 potential causes. Non-steady state conditions, due to the occurrence of episodic
755 deep-seated (>5 m) landslides incorporating low ^{10}Be-concentrated material into
756 streams, may prevail. In catchments with frequent landslides, adequate spatial and
757 temporal mixing of sediment is established for catchments larger than 100 km^2
758 (Niemi et al., 2005; Yanites et al., 2009). In our compilation (Table 2, Fig. 9), we have
759 excluded catchments <100 km^2 for this reason. However, poor spatial mixing of
760 sediment has also been attributed to large precipitation events, that locally
761 remobilize large amounts of sediments (Lupker et al., 2012a). Further, in the
762 Himalaya, the more rapidly eroding areas tend to be the most quartz-rich lithologies.
763 Since the probability of non-ubiquitous quartz concentrations increases with
764 increasing catchment size, higher D_{insitu} than E_{gaug} may be caused by not correcting
765 for this effect.

766

767 3) We cannot exclude that E_{gaug} is underestimated if high magnitude, low-frequency
768 events are not captured in decades-spanning records (see section 3.2). Considering
769 the overall good agreement between cosmogenic nuclide-derived D and sediment
770 gauging-derived E, and the potential of floodplains to buffer variations in fluxes (see
771 next section), we attribute the gauging data a high likelihood to be representative.

772

773 4) The “sediment delivery ratio” (Walling, 1983; Syvitski et al., 2005; de Vente et al.,
774 2007), describing the ratio of sediment entering a basin to that transmitted through

775 a basin, is unity within uncertainty for these two river basins. Apparently, all
776 sediment is transmitted to the sea without intermittent loss.
777
778 5) We note that for both methods the variation contained in the data, estimated by
779 the coefficient of variation, C_v (Table 2), decreases from the source to the lowlands
780 in both basins. Source area-C_v are on average a factor 3 higher than in the lowlands.
781 Wittmann et al. (2009) showed for the Bolivian Beni basin that when sampling far
782 away from the mountain front, fluvial transport and mixing processes average-out
783 small-scale headwater variability, and a mean headwater denudation rate is
784 preserved. We find a similar decrease in variability from source to lowlands for the
785 Ganga basin. Thus a mean, representative orogenic denudation rate can be derived
786 from a bag of sediment sampled downstream. This decrease in variation is most
787 likely due to larger catchments being more representative of sediment transport
788 processes than smaller catchments, especially if a transfer zone is present in a basin
789 that is able to retain sediment for longer periods (Romans et al., 2015). Locally high
790 sediment inputs from stochastic mass wasting are diluted downstream. The lowland
791 floodplain has the ability to buffer changes in sediment supply and thus drives these
792 averaging effects (see next section).
793
794 6) Good agreement is observed between sedimentary lowland fluxes and sediment
795 volumes in offshore basins or deltas (Table 2): For the Amazon basin, Nittrouer and
796 Kuehl (1995) estimated a mean sediment flux of 550 - 1030 Mt/yr from ^{210}Pb activity
797 profiles (integration time scale of ca. 1 kyr), an estimation that is slightly higher than
798 the *in situ*-^{10}Be based lowland sediment flux (370 Mt/yr) and also encompasses the

799 gauging-based lowland flux (990 Mt/yr) (Table 2). For the Ganga basin, Métivier and
800 Gaudemer (1999) estimated a long-term deposition flux of ca. 510 Mt/yr for the
801 Bengal fan over the Quaternary from the Ganga River alone. This estimation from
802 the fan is at the higher end of gauging-derived estimates (ca. 200 - 550 Mt/yr, see
803 Table 2), but broadly agrees with *in situ* cosmogenic-derived sediment fluxes (ca. 400
804 Mt/yr).
805
806 ***4.2 Across temporal scales: Stability of lowland fluxes***
807 There are several potential causes for the major observations made in section 4.1,
808 i.e. that sediment fluxes in the mountain sources and across floodplains are similar,
809 that their variability decreases downstream, and that these sediment fluxes leaving
810 the large floodplains are again similar to sediment volumes stored offshore.
811 Constant source erosion rates over the time scales encompassed by the discussed
812 methods is one explanation for the observed similarity.
813
814 Buffering of sediment transport through the floodplain is another explanation for the
815 similarity over different time scales. Rivers react to external, high amplitude forcings
816 in the source area by either incising their alluvial reservoir or by aggrading it to
817 "buffer" against these changes. As a result sediment fluxes at the outlet are held
818 constant (Métivier and Gaudemer, 1999; Phillips, 2003). However, it is unclear over
819 which time scales these buffers act. Métivier and Gaudemer (1999) have calculated
820 4.7×10^5 yr as the time it takes to erode an alluvial reservoir of the size of the Ganga
821 floodplain, called "reaction time", and, based on their principles, Wittmann et al.
822 (2011a) have calculated a reaction time of 7×10^5 yr for the Amazon floodplain. These

823 time scales depend both on the size of the floodplain and on the sediment flux into
824 the floodplain, and only signals that are longer than the reaction time should be able
825 to pass the floodplain without alteration (Métivier and Gaudemer, 1999). The
826 relation between floodplain reaction time and period of the external forcing is
827 subject to an intense debate, and several models with differing outcomes have been
828 put forward (Allen, 2008; Jerolmack and Paola, 2010; Simpson and Castelltort, 2012;
829 Armitage et al., 2013; Godard et al., 2013). Romans et al. (2015) stress that signals
830 may be preserved in the stratigraphic record, and thus "survive" fluvial transport if
831 the period of signal forcing exceeds the reaction time of the alluvial reservoir and
832 also exceeds the magnitude of internal oscillations, such that signals are not
833 "shredded" by self-organized internal dynamics (Jerolmack and Paola, 2010).
834
835 In order to elucidate signal transmittance on an empirical basis, many authors use
836 the comparison of longer-term (e.g. cosmogenic or infill-derived fluxes) to shorter-
837 term (gauging) fluxes (Métivier and Gaudemer, 1999; Wittmann et al., 2011a;
838 Covault et al., 2013). For example, Covault et al. (2013) note from their global
839 compilation of modern gauging-based and longer-term cosmogenic nuclide-based
840 sediment fluxes that 28 sites agree within a factor of 2, and even 81 of 103 sites
841 exhibit a broad similarity by having within one order of magnitude similar fluxes.
842 Covault et al. (2013) note that these sites are predominantly from larger basins (see
843 Fig. 11). In Figure 11, we supplement Covault et al.´s (2013) compilation of longer-
844 term cosmogenic-derived versus modern gauging-derived sediment loads with data
845 from the European Alps (Wittmann et al., 2007; Norton et al., 2011; Hinderer et al.,
846 2013), the Ecuadorian Intermontane Andes (Vanacker et al., 2007), the Bolivian

847 Andes (Safran et al., 2005; Aalto et al., 2006; Insel et al., 2010), and the Nepalese
848 Himalayas (Andermann, 2011; Andermann et al., 2012). This added data supports
849 the observation that it is mostly the larger basins exhibiting broad similarity in
850 sediment discharge over time as recorded by the two methods. They show a broad
851 balance between modern and longer-term fluxes for many large rivers of the world.
852 If cosmogenic nuclides were added to the standard toolbox of methods applied to
853 the stratigraphic record, more insight into the fluvial transport system and the role it
854 is playing in transmitting source area and lowland signals could be gained.
855

856 # 5. Meteoric and ^{10}Be and the ^{10}Be/^{9}Be ratio in floodplains

857 ## *5.1 General principles*

858 Meteoric cosmogenic ^{10}Be atoms are produced in the atmosphere at high production
859 rates. Their global flux amounts to ca. 1×10^{6} atoms/cm^{2}/yr. After atmospheric
860 redistribution and precipitation they adsorb onto fine particles with high reactive
861 surface area (Willenbring and von Blanckenburg, 2010). Stable ^{9}Be, present in silicate
862 minerals in ppm concentrations, is released during weathering and mixes with ^{10}Be
863 in soil or river solutions to form a characteristic ^{10}Be/^{9}Be ratio. The potential of this
864 new isotope ratio tracer lies in the versatility of its applications. In floodplains, the
865 ^{10}Be concentration can be used to determine a) upland erosion rates and b)
866 floodplain sediment storage duration. The ^{10}Be/^{9}Be ratio provides c) denudation
867 rates while the fraction of ^{9}Be released during weathering from primary minerals
868 discloses d) the degree of rock weathering. The principle framework for these
869 applications is given in von Blanckenburg et al. (2012).

For the determination of erosion rates and exposure ages, sub-gram amounts of fine-grained samples can be measured, given the much higher meteoric ^{10}Be concentrations than *in situ* cosmogenic ^{10}Be. While for determination of *in situ* ^{10}Be in quartz meteoric ^{10}Be is removed by acid leaching (Kohl and Nishiizumi, 1992), the amounts of *in situ* ^{10}Be are negligible when meteoric ^{10}Be is measured. For the determination of denudation rates, reactive ^{10}Be/^{9}Be ratios (reac) are determined from phases such as Mn-Fe-(oxy)-hydroxides. This reactive Be is separated from samples by sequential chemical extractions (Tessier et al., 1979; Bourlès et al., 1989; Wittmann et al., 2012), the mineral-bound ^{9}Be retained in undissolved minerals is excluded, and the concentration is reported as $^{10}Be_{reac}$ and $^{9}Be_{reac}$ (in $at/g_{(solid)}$ or $g/g_{(solid)}$), respectively.

5.2 Atmospheric ^{10}Be deposition fluxes

A first prerequisite to use meteoric ^{10}Be for any quantitative information is knowledge of the ^{10}Be flux reaching Earth surface ^{10}Be flux $F_{met}^{^{10}Be}$, in units of $at/cm^2/yr$. This parameter is still associated with substantial uncertainties; one approach to obtain $F_{met}^{^{10}Be}$ that is most likely valid for large basin-wide studies (Wittmann et al., 2015) is by using a general atmospheric circulation model (GCM) coupled to an aerosol module (e.g. Heikkilä et al. (2013)) that also incorporates a physical model simulating processes of cosmic particle production and transport (Masarik and Beer, 1999) and variations in solar modulation and magnetic field strength. For smaller scales, measured inventories ^{10}Be in soil for given latitudes and

precipitation rates can be used to determine local $F_{met}^{^{10}Be}$ (Reusser et al., 2010; Willenbring and von Blanckenburg, 2010; Graly et al., 2011; Ouimet et al., 2015). As >95% of meteoric ^{10}Be production in the atmosphere takes place at elevations above 3 km altitude, scaling for altitude is not required for most locations (Willenbring and von Blanckenburg, 2010).

5.3 Meteoric ^{10}Be as tracer of erosion rates and sediment storage duration

The most simple application of meteoric ^{10}Be is the determination of erosion rates E_{met} (Willenbring and von Blanckenburg, 2010). To do so, we face two fundamental difficulties. First, only at near-neutral or higher pH is meteoric ^{10}Be fully retained. We can account for this loss by using solid/fluid partition coefficients and runoff (von Blanckenburg et al., 2012) (see below, Eq. 11). Second, ^{10}Be adsorption is grain size-dependent (Aldahan et al., 1999; Shen et al., 2004; Graly et al., 2010; Willenbring and von Blanckenburg, 2010) (Fig. 12). One means to remove this effect is to normalize over stable ^{9}Be, where the ^{10}Be/^{9}Be ratio does not depend on grain size (Figures 12B and 12D). If the ^{10}Be/^{9}Be ratio is used, we need to find means to extract an erosion or denudation rate from that ratio, however. This procedure is explained in section 5.4. Another way to obtain a representative ^{10}Be concentration from river sediment is to measure the Al/Si ratio in suspended sediment too, and correct the meteoric ^{10}Be concentration by using depth-integrated Al/Si ratios (Fig. 12C).

Once the grain size dependence has been addressed, the reactive (or bulk sediment) meteoric ^{10}Be concentration ($^{10}Be_{reac}$, in at/g_{solid}) can be converted into an erosion rate E_{met} (g/cm^2/yr, convertible into mm/yr by using rock density $\rho_{bedrock}$):

$$E_{met} = \frac{F_{met}^{^{10}Be}}{{}^{10}Be_{reac}} - \frac{q}{K_d} \quad \text{(Eq. 11)}$$

where q is water runoff ($cm^3/cm^2/yr$) and K_d is the solid/fluid partition coefficient for Be (ml/g). The q/K_d term takes into account the ^{10}Be lost in solution (von Blanckenburg et al., 2012) and can be ignored where Be is fully retentive (pH >6).

A second application of meteoric ^{10}Be is to evaluate the duration of static sediment storage in floodplains. This duration can be obtained by comparing the total mass export rate of meteoric ^{10}Be from a basin $J_{riv}^{^{10}Be}$ (at/yr) to the atmospheric deposition rate $J_{atm}^{^{10}Be}$. While $J_{atm}^{^{10}Be}$ is the meteoric flux (i.e. $F_{met}^{^{10}Be}$ multiplied by the basins area), $J_{riv}^{^{10}Be}$ is the sum of the riverine solid reactive and dissolved fractions transported by the river, called $J_{riv\_reac}^{^{10}Be}$ and $J_{riv\_diss}^{^{10}Be}$ respectively (all in at/yr):

$$J_{riv}^{^{10}Be} = (J_{riv\_reac}^{^{10}Be} + J_{riv\_diss}^{^{10}Be}) \times \left(1 - \exp^{(-\lambda t)}\right) \quad \text{(Eq. 12)}$$

These $J_{riv}^{^{10}Be}$ are calculated by area-normalizing the reactive or dissolved ^{10}Be concentrations with the solid export rate (from e.g. *in situ*-derived erosion rates, in $kg/m^2/yr$) or water discharge (in L/yr), respectively (Wittmann et al., 2015)).

If the ^{10}Be inventory of the basin is at steady state, $J_{riv}^{^{10}Be} / J_{atm}^{^{10}Be}$ equals 1 (Brown et al., 1988). If this ratio <1, the sediment storage duration can be calculated by solving

938 equation 12 for *t*. We illustrate this case for the riverine ^{10}Be flux deficit observed in
939 the Amazon basin in Figure 13A, i.e. the difference between $J_{riv}^{^{10}Be}$ and $J_{atm}^{^{10}Be}$. The
940 Amazon case provides a duration for storage of „static" sediment and the decay of
941 ^{10}Be contained in it of 3.7 Myr (Fig. 13A). An alternative explanation for the flux
942 deficit is that no stored sediment (and the ^{10}Be that is contained in it) reaches the
943 active channel. For the Amazon lowlands, this area would be 64% (Wittmann et al.,
944 2015).
945
946 A third application is the calculation of sediment transfer times for the case of
947 dynamic floodplains. Here we can make use of the fact that $F_{met}^{^{10}Be}$ does not change
948 from the mountainous source areas to the lowlands of a basin (see Fig. 14). In
949 contrast, *in situ* ^{10}Be production rates decrease over this distance. Hence, meteoric
950 ^{10}Be increases significantly during transfer along a floodplain, whereas *in situ* ^{10}Be
951 mainly does not increase. We illustrate this distinct behavior schematically in Fig. 14.
952
953 We can model the increase by a simple accumulation scenario where $^{10}Be_{reac}$
954 continuously accumulates in floodplain sediment during residence in the active
955 floodplain (Fig. 13B). When using equation 6 in Willenbring and von Blanckenburg
956 (2010) and assuming zero erosion of the stored lowland sediment, the sedimentary
957 ^{10}Be inventory *I* (at/cm^2) that is produced while the sediment is exposed to
958 continuous atmospheric deposition $F_{met}^{^{10}Be}$, can be calculated from equation 16 in
959 Wittmann et al. (2015):
960

$$I_{^{10}Be}(t) = \frac{F_{met}^{^{10}Be}}{\lambda}\left(1 - \exp^{-\lambda t}\right) + {}^{10}Be_{source} \times \rho \times z \times \exp^{-\lambda t}$$

(Eq. 13)

In this case is *t* the sediment transfer time and the right-hand term in equation 13 reflects the decay-affected contribution of source area-derived $^{10}Be_{reac}$ that is provided to the lowlands from the Andes ($^{10}Be_{source}$, in at/g_{solid}). As sediment density ρ we used a value of 2000 kg/m^3 for wet, silty sand (see Balco et al. (2005)) and *z* (m) is the remobilization depth of sediment. Note that the inventory of ^{10}Be does not depend on knowing the ^{10}Be penetration depth (Willenbring and von Blanckenburg, 2010), as long as the entire inventory is captured by sampling. However, to convert the ^{10}Be inventory into the ^{10}Be concentration contained in remobilized sediment, the remobilization depth needs to be known. In the example shown in Fig. 13B we use equation 13 with z = 1 m for the case of very shallow floodplain remobilization representing a topmost clay-rich layer ladden with meteoric ^{10}Be that is deposited during overbank spill and eroded during subsequent inundation. Using this depth, a sediment transfer time in the floodplain of only ca. 1.6 kyr is predicted to cause the additional accumulation of meteoric ^{10}Be across the Amazon floodplain. A deeper remobilization depth of several tens of meters down to the channel bottom (e.g. 20 m) would require longer sediment transfer times of ca. 29 kyr (not shown in Fig. 13B).

5.4 $^{10}Be/^{9}Be$ as denudation rate and weathering degree proxy

Within the mass balance framework of von Blanckenburg et al. (2012), meteoric ^{10}Be is the atmospheric flux tracer, and ^{9}Be is the tracer for the release of the trace metal by weathering, and thus their combination can be used to simultaneously determine denudation, erosion and weathering rates. In order to be able to calculate denudation rates from equation 14 we need to know the fraction of a parent rock's ^{9}Be that is released by weathering into the reactive and dissolved phases and the initial "parent" bedrock concentration of stable ^{9}Be ($^{9}Be_{parent}$, in µg/g). For large scale studies, a value of the average crustal composition of Be of 2.5 ± 0.5 µg/g (Rudnick and Gao, 2004) can be used (von Blanckenburg et al., 2012) to calculate D_{met}:

$$D_{met} = \frac{F_{met}^{^{10}Be}}{\left(\frac{^{10}Be}{^{9}Be}\right)_{reac} \times [\,^{9}Be]_{parent} \times (f_{reac}^{^{9}Be} + f_{diss}^{^{9}Be})} \quad \text{(Eq. 14)}$$

$(f_{reac}^{^{9}Be} + f_{diss}^{^{9}Be})$ can be determined in two ways (Wittmann et al., 2015): Either by knowing both the riverine reactive and dissolved ^{9}Be flux, or by sequential extractions of the reactive and the residual mineral-bound concentration from a given sediment sample. Then:

$$f_{reac}^{^{9}Be} + f_{diss}^{^{9}Be} = \left(\frac{^{9}Be_{min}}{^{9}Be_{reac}} + 1\right)^{-1} \quad \text{(Eq. 15)}$$

$(f_{reac}^{^{9}Be} + f_{diss}^{^{9}Be})$ describes the release of Be from primary minerals into the dissolved (diss) and particulate (reac) component and is thus a is a proxy for the degree of weathering. In the slow and complete weathering („supply-limited") case, this

fraction is close to 1, and all primary mineral-bound ^{9}Be is released. In fast and incomplete weathering („kinetically limited“) settings, this fraction is <1, and some ^{9}Be remains in undissolved primary minerals. Note that this fraction may be biased by grain size effects, as finer grains may yield higher $^{9}Be_{reac}$ than $^{9}Be_{min}$ inherited from sorting between coarse grain sizes and clays in the river (von Blanckenburg et al., 2012). This bias may then also affect denudation rates calculated from equation 14 where the weathering fraction is contained.

In the Amazon basin, $(f_{reac}^{^{9}Be} + f_{diss}^{^{9}Be})$ have been calculated from ^{9}Be data from suspended sediment depth profiles; this data was corrected for grain size bias during riverine sorting following the approach shown in Fig. 12C and is thus considered representative for the Amazon River where the majority of sediment flux is transported by suspended load (Wittmann et al., 2015). The $(f_{reac}^{^{9}Be} + f_{diss}^{^{9}Be})$ values are ca. 0.4 (i.e. 40% of Be mass has been released during weathering) for two Andean and the two lowland depth profiles and thus the weathering degree does not change from the Andes to the lowlands. One explanation for this stability in the two regimes is that sediments contained in the Amazon lowlands are pre-weathered in the Andes and potentially depleted of their ^{9}Be (Wittmann et al., 2015). Other studies (Bouchez et al., 2012; Bouchez et al., 2014) have found similar low weathering during transfer of sediments through the Amazon lowlands (compare section 3.3).

5.5 Meteoric $^{10}Be/^{9}Be$-derived denudation rates compared to *in situ*-derived

denudation rates in the Amazon

For a comparison between rates from *in situ* ^{10}Be with those from the meteoric ^{10}Be we first briefly repeat the types of rate information derived from both types, so that true geologic causes can be distinguished from differences introduced by possible methodological artefacts. Such comparison is possible for the Amazon basin, where both methods have been applied. All meteoric Be data is from Wittmann et al., (2015), and the *in situ* rates from source areas and lowland areas, respectively, are from Wittmann et al. (2009) and Wittmann et al. (2011a). We present

- E_{met*} that are meteoric-derived erosion rates from reactive ^{10}Be concentrations (eq. 11) of high confidence that have been corrected for grain size bias by means of depth integration using Al/Si in suspended loads (section 5.3, Fig. 12C).
- D_{met*} that are meteoric ^{10}Be/^{9}Be-derived denudation rates (Eq. 14) of high confidence where the parameter $f_{reac}^{^{9}Be} + f_{diss}^{^{9}Be}$ (Eq. 15) has been corrected for grain size bias by means of depth integration using Al/Si in suspended loads (section 5.4).
- D_{met} that are meteoric ^{10}Be/^{9}Be-derived denudation rates (Eq. 14) of lower confidence that have not been corrected for grain size bias potentially introduced by sorting that affects the $^{9}Be_{min}$/$^{9}Be_{reac}$ ratio used in equation 14.
- D_{insitu} that are *in situ* ^{10}Be-derived denudation rates of high confidence from source areas calculated from (Eq. 2) using the production rate scaling of the source area.
- $D_{insituFC}$ that are *in situ* ^{10}Be-derived denudation rates (Eq. 2) of high

confidence from floodplain areas where the floodplain correction (section 3.1, Fig. 8) has been applied to account for zero additional *in situ* nuclide production in the floodplain.

- We further note that in floodplain samples all meteoric erosion (E_{met*}) and denudation rates (D_{met*}, D_{met}) are likely biased as meteoric ^{10}Be concentrations are modified by both radioactive decay (Fig. 13A) or by accumulation (Fig. 13B) of meteoric ^{10}Be during floodplain storage.

We do not present E_{met} which are erosion rates (Eq. 11) based on reactive ^{10}Be concentrations from either bedload or suspended sediment samples that are of low confidence because they are not corrected for grain size bias introduced by particle sorting.

Figure 15 shows the comparison of highest confidence rates where available. E_{met*} and D_{met*} are available at four locations within the Amazon basin, where river depth profiles were sampled. At these sites, E_{met*} and D_{met*} are almost identical in three out of four locations, testifying to the low fraction of chemical weathering from dissolved loads in the basin that is discussed in section 3.3.

For the Andes we calculated an area-weighed D_{met} of 0.44 mm/yr. The corresponding $\overline{D_{insitu}}$ value is 0.19 mm/yr. Indeed, the same pattern, with D_{met} exceeding D_{insitu}, emerges for all large rivers draining the Andes (Upper Solimões, Madre de Dios, Upper Madeira, Beni, Upper Mamoré). We can speculate this difference to reflect true geologic causes: meteoric ^{10}Be likely samples more rapidly eroding lithologies such as shales that produce finer-grained sediment. Conversely, *in situ* denudation

rates from coarse quartz reflect more erosion-resistant granitoid lithologies (Wittmann et al, 2015).

Rivers from the cratons (Negro, Branco, Brazilian Craton) yield low denudation rates from both methods that are typical for slowly eroding cratonic landscapes. D_{met} range from 0.02 to 0.06 mm/yr. As in Andean rivers, D_{met} typically exceeds D_{insitu} by a factor of ca. 2. Too-high D_{met} for the cratonic rivers are most likely due to a grain size bias affecting the $^{9}Be_{min}/^{9}Be_{reac}$ ratio (Eq. 14). However, denudation rates of both methods are potentially compromised in these slowly eroding settings because sediment storage may introduce another bias through radioactive decay (section 2.4 for *in situ* ^{10}Be, Fig. 13A for meteoric ^{10}Be).

In the central Amazon lowlands, D_{met*} yields 0.17 mm/yr which compares to a $\overline{D_{insituFC}}$ value of 0.18 mm/yr. This agreement contrasts with the observations from the source areas, where D_{met} exceeds D_{insitu} by a factor of ca. 2. This shift in the difference might be apparent: In the floodplain, meteoric ^{10}Be concentrations can be modified by both accumulation and decay during sediment storage (Figs. 13A,B). Unlike $D_{insituFC}$ that in the floodplain records the mean sediment production rate of the source area, meteoric ^{10}Be is more sensitive to storage.

5.6 Meteoric ^{10}Be/^{9}Be: outlook

We are only beginning to understand the exact mechanisms of how meteoric ^{10}Be concentrations and ^{10}Be/^{9}Be ratios are modified by floodplain processes and how rivers transmit such signals to the sedimentary record. We have shown means to correct for incomplete retentivity (by means of the ^{9}Be normalization, Fig. 12B) and grain size-dependent ^{10}Be retention (by using depth-integrated Al/Si, Fig. 12C).

Resolving the uncertainties associated with ^{10}Be delivery from the atmosphere is paramount. Potentially, however, this system can be applied to deriving paleo-denudation rates in the terrestrial or marine sedimentary record, by using ^{10}Be/^{9}Be in clays or reactive Be adsorbed onto e.g. Fe-Mn oxides. The latter approach can be used to derive paleo-denudation rates from authigenic ocean sediments (von Blanckenburg and Bouchez, 2014; von Blanckenburg et al., 2015). The resolution with which changes in denudation as a function of climate change can be resolved depends critically on the transport path of ^{9}Be through basins in the dissolved and the particulate forms and on the release of the latter in seawater (von Blanckenburg and Bouchez, 2014; von Blanckenburg et al., 2015). Regardless, the entire, down to upper Miocene sedimentary record can now be accessed for studying Earth surface dynamics.

6. SUMMARY AND SAMPLING GUIDELINES

We have analyzed the effects that sediment storage and deposition can have on the *in situ* cosmogenic nuclide signal imprinted to sediment during erosion. When sediment transport through lowland basins is “dynamic”, which is the case when continuous exchange between channel sediment and sediment in the proximal floodplain during lateral river movement takes place, geologically short floodplain storage times (in the order of only several kyrs) result. These storage times are much shorter than the about Myr half-life of long-lived cosmogenic nuclides such as ^{10}Be and ^{26}Al, and they are shielded from cosmic rays. Consequently, additional nuclide production and also decay of *in situ*-produced nuclides during storage and

deposition are limited, and a modification of the initial *in situ*-cosmogenic nuclide signal inherited from the erosion process in the high-relief setting does not occur. We find that large-scale sediment transport effectively averages-out source area variability, and long-lived *in situ* nuclide concentrations, measured in lowland sediment and treated using the nuclides´ production rate in the source area, provide a representative mean denudation rate of the source area. We show this for the cases of the Amazon and Ganga basins. The conversion of these longer-term *in situ*-cosmogenic nuclide-derived denudation rates to sediment fluxes (by using the respective source areas and sediment density values) allows for the comparison to modern, gauging-derived fluxes and to those derived from deltaic and off-shore archives. From this comparison we find a remarkable temporal stability of sediment fluxes over Holocene times to the present in these two basins.

This simple picture of non-changing long-lived *in situ*-produced nuclide concentrations across floodplains is only challenged by 1) recycling of old, potentially buried floodplain sediment during distal channel-floodplain interaction which is coupled to 2) mixing of sediment with different provenance and grain sizes. For example in the Amazon basin, the fine sand grain size originates in the Andes and is not modified en route to the Amazon lowlands. Coarser sand, however, either originates in the cratonic areas, where the slow erosion imprints a much higher nuclide concentration, or is recycled from old lowland formations when the channel avulses into distal, inherently older floodplain deposits. In this case the ratio of $^{26}Al/^{10}Be$, from its differential decay, may trace this admixing of recycled versus "fresh" (in-channel source area-derived) material.

With the following *guidelines,* we aim to provide the reader with practical recommendations for deriving *in situ* ^{10}Be-based (or other long-lived cosmogenic nuclides) denudation rates or sediment fluxes from lowland river sediment. These guidelines summarize the findings from modeling approaches and field-based data:

1) In lowland rivers with deep (10´s of meters) actively migrating channels (e.g. >5 m/yr), the effect of nuclide production taking place at the floodplain surface is minor compared to the vast majority of sediment that is shielded at depth before remobilization, resulting in only small changes of the initial (source area-derived) nuclide concentration. Sampling bedload from deep, laterally active rivers should thus be preferred.
2) Nuclide production during lowland transfer of sediment in shallow migrating channels can be significant. But mostly such shallow floodplains are also characterized by short sediment storage duration. Sampling bedload from rivers with shallow floodplains is in order as long as sediment turnover is rapid. Thus, we suggest estimating the ratio of ingoing to exported sediment fluxes, e.g. from gauging data, before targeting specific areas for cosmogenic nuclide sampling.
3) Rivers fed by rapidly eroding source areas are potentially more affected by down-channel change as their initial source area-derived nuclide concentration is low and thus sensitive to additional production. Unless sediment storage duration is also short, more slowly eroding settings (0.1 to 0.5 mm/yr) should be preferred.
4) Entrainment of sediment from e.g. avulsions might reactivate old deeply stored sediment in which long-lived nuclides might have decayed. In rivers in which

lateral migration is limited to the active channel belt, modification of the source area signal by such incorporation of deeply stored old floodplain material is less likely.

5) In order to assess the influence of old, deeply stored sediment deposits, another long-lived nuclide, such as ^{26}Al, should be monitored along with ^{10}Be, as $^{26}Al/^{10}Be$ ratios are indicative of potential admixing of formerly buried floodplain material. If highly-weathered (i.e. cratonic) areas in the basin exist, a reconnaissance study for the distribution of nuclide concentrations in different grain sizes might be necessary.

Finally, we point at the opportunities arising from new nuclide systems. *In situ*-produced ^{14}C, measured in quartz, may have the potential to estimate sediment storage times over one to two of its half-life (ca. 5-10 kyrs). Meteoric ^{10}Be can be measured in fine-grained sediment where the presence of quartz is not a requirement. The meteoric ^{10}Be concentration alone yields an erosion rate, provided a representative concentration can be inferred from suspended sediment depth profiles and Al/Si. The flux balance of ^{10}Be and its increase in floodplains can be used to evaluate sediment residence times. Further, the adsorbed and reactive Be should be extracted chemically from reactive phases and the stable ^{9}Be measured, such that erosion rates, denudation rates, and the degree of weathering can be simultaneously determined from the meteoric $^{10}Be/^{9}Be$ system.

ACKNOWLEDGEMENTS

This research did not receive any specific grant from funding agencies in the public, commercial, or not-for-profit sectors, but gratefully acknowledges support from the Helmholtz Association. We thank M. Dziggel for help with crafting figures, R. Kapannusch for performing DEM basin delineations, and V. Godard for providing digital basin shapes. D. Scherler and C. Andermann are thanked for providing basin delineations and comments on earlier versions of this manuscript. M. Oelze is thanked for continuous support throughout all stages of this manuscript. Data used in this study was acquired with the help of J.-L. Guyot, L. Maurice, N. Dannhaus, J. Bouchez, J. Gaillardet, H. Roig, P. Kubik, M. Christl, S. Binnie, and S. Heinze. We thank an anonymous reviewer for constructive comments and M. Lupker for the detailed review and advice.

1208 TABLES

Table 1: Comparison of model input parameters and results for the Amazon and Ganga basins for long-lived *in situ* ^{10}Be

Model type[a] using each parameter		Parameters used for model calculation	Amazon basin[b]	Ganga basin[c]
Box	Numeric	Initial source-area derived ^{10}Be concentration	$^{10}Be_{(0)}$: 6.57x10^4 at/g$_{(Qtz)}$	$^{10}Be_{(0)}$: 2.21x10^4 at/g$_{(Qtz)}$
Box	Numeric	Initial sediment flux	QS_{insitu} = 380 Mt/yr (A_{source} = 8.5x10^5 km^2)	QS_{insitu} = 550 Mt/yr (A_{source} = 1.8x10^5 km^2)
Box	Numeric	Channel lateral migration rate	5 ± 2 m/yr	70 ± 35 m/yr
Box	Numeric	Active floodplain width	35 ± 15 km	40 ± 15 km
Box	Numeric	Active floodplain depth	23 ± 10 m	10 ± 5 m
Box	-	Sediment transfer time	14 kyr	1.4 kyr
Box	Numeric	Average transfer distance	3000 km	1000 km
-	Numeric	Floodplain density	1700 kg/m^3 (Dunne et al., 1998)	1500 kg/m^3
-	Numeric	Channel sinuosity	1.15 ± 0.2 (avg. from Mertes et al., 1996)	1.3 ± 0.2
-	Numeric	Fraction of QS in channel in sand-sized fraction	0.15 ± 0.05 (Dunne et al., 1998)	0.35 ± 0.15
-	Numeric	Fraction of QS in floodplain in sand-sized fraction	0.1 ± 0.05 (Dunne et al., 1998)	0.1 ± 0.05
-	Numeric	Floodplain aggradation	steady-state (Mertes et al., 1996; Bouchez et al., 2012)	0.5± 0.25 mm/yr
Increase in ^{10}Be concentration relative to $^{10}Be_{(0)}$ (%) (also see Fig. 6)		Box:	1.8	1.5
		Numeric:	1.7	6.3[d]

[a]The box model is based on Wittmann and von Blanckenburg (2009) and the numeric model is based on Lauer and Willenbring (2010).

[b]If no reference is given next to the parameter, the reference used is Wittmann and von Blanckenburg (2009).

[c]If no reference is given next to the parameter, the reference used is Lupker et al. (2012a).

[d]Note that our result is lower than that obtained by Lupker et al. (2012a), because we used a single channel setup, whereas Lupker used four tributary input streams.

1209

1210

1211

Table 2: Summary of measured *in situ*-derived denudation rates (upper part) and measured gauging-derived sediment fluxes (lower part).

			***In situ*-derived cosmogenic data[a]**				
AMAZON BASIN	Subbasin	Source or total basin area ($\times 10^5$ km^2)	n (>100 km^2)[b]	Area-weighed D_{insitu} ± 1σ SD (mm/yr)	Measured D_{insitu} at largest outlet (mm/yr)[c]	Area-weighed QS_{insitu} ± 1σ SD (Mt/yr)	C_v for denudation rates[d]
Andes: Subbasins or largest outlets at mountain front	Beni	0.68	38	0.37 ± 0.20	0.4 - 0.86	66 ± 35	
	Grande	0.60	17	0.38 ± 0.14	0.10 - 0.57[g]	59 ± 22	
	Solimões[e]	6.3	7	0.16 ± 0.11	0.27	257 ± 210	
entire sampled Andes draining to Amazon		7.58		**0.19 ± 0.18**		**380 ± 350**	**0.55**
Lowlands at Óbidos (using sampled source area for conversion from D to QS)[f]		7.58	17		**0.18 ± 0.03**	**350 ± 70**	**0.19**
Lowlands at Óbidos (no floodpl. corr., using total basin area for conversion from D to QS)[f]		*50.9*	*17*		***0.11 ± 0.03***	***1480 ± 370***	
GANGA BASIN							
Himalayas: Subbasin or largest outlets at mountain front	Upper Ganga	0.32	3	1.22 ± 0.60	1.9	100 ± 50	
	Yamuna	0.096	18	0.76 ± 0.56	0.56	20 ± 14	
	Karnali	0.46	3	1.19 ± 0.75	0.8 - 1.9	140 ± 90	
	Narayani	0.34	25	1.54 ± 0.96	1.0 - 1.7	140 ± 70	
	Kosi	0.62	8	0.69 ± 0.78	0.4 - 0.8	110 ± 125	
entire sampled Himalayas draining to Ganga		1.84		**1.14 ± 0.82**		**550 ± 390**	**0.82**
Lowlands at Harding Bridge (using sampled source area for conversion from D to QS)[h]		1.84	8		**0.82 ± 0.27**	**390 ± 130**	**0.31**
Lowlands at Harding Bridge (no floodpl. corr.; using total basin area for conversion from D to QS)[h]		*8.73*	*8*		***0.33 ± 0.50***	***760 ± 1140***	

			Gauging-derived suspended sediment data[j]			
AMAZON BASIN	Subbasin	Source or total basin area ($\times 10^5$ km^2)	n (>100 km^2)[b]	Catchment-wide QS_{gaug} (Mt/yr)[j]	Measured QS_{gaug} at largest outlet (Mt/yr)	Area-weighed E_{gaug} (mm/yr)	C_v for erosion rates[d]
Andes: Subbasins or largest outlets at mountain front	Beni	0.68	13	210 ± 185	160 - 300	1.20 ± 1.06	
	Grande	0.60	15	210 ± 150	125 - 180	1.33 ± 0.97	
	Solimões[e]	4.7	14	630 ± 480	553	0.33 ± 0.25	
entire Andes draining to Amazon		6.0		**1050 ± 820**	**840 - 890**	**0.47 ± 0.90**	**0.98**
Lowlands at Óbidos (using sampled source area for conversion from QS to E)[f]		6.0	6	**900 ± 310**	**560 - 1320**	**0.58 ± 0.20**	**0.34**
Lowlands at Óbidos (no floodplain corr.; using total area for conversion from QS to E)[f]		*50.9*	*6*			**0.07 ± 0.02**	
Amazon Delta: 550 - 1030 Mt/yr measured from ^{210}Pb activity profiles (Nittrouer and Kuehl, 1995).							
GANGA BASIN							
Himalayas: Subbasin or largest outlets at mountain front	Upper Ganga	0.32	3	12 ± 13	10.1	0.14 ± 0.15	
	Yamuna	0.096	2	18	18	0.73 ± 0.73	
	Karnali	0.46	8	110 ± 80	76 - 210	0.89 ± 0.66	
	Narayani	0.34	13	100 ± 50	97 - 120	1.09 ± 0.60	
	Kosi	0.62	8	130 ± 65	170 - 180	0.81 ± 0.40	
entire Himalayas draining to Ganga		1.84		**370 ± 230**		**0.80 ± 0.55**	**0.75**
Lowlands at Harding Bridge (using sampled source area for conversion from QS to E)[k]		1.84	8	**390 ± 130**	**200 - 550**	**0.81 ± 0.27**	**0.33**
Lowlands at Harding Bridge (no floodplain corr.; using total area for conversion from QS to E)[k]		*8.73*	*8*			**0.17 ± 0.06**	

Bengal Delta: 320 - 920 Mt/yr measured from stratigraphic profiles (Wasson, 2003; Goodbred and Kuehl, 2000)[l].

Bengal Fan: 510 Mt/yr from Métivier and Gaudemer (1999)[l].

Note that uncertainty given gives the data spread (1σ std. dev. of the dataset). We chose to present standard deviations and not analytical uncertainties because the latter is not available for QS_{gaug} , they would not represent natural variations and would imply a precision that is not appropriate when comparing different methods. In situ-derived denudation rates were calculated using a total SLHL production rate of 3.75 at/$g_{(Qtz)}$/yr and the scaling model of Dunai (2000) (see supplement A for details).

[a]All values are area-weighed ± 1σ std. dev., calculated according to Eq. 7. All lowland data is floodplain corrected (i.e. using the sampled source area for calculations), except where indicated. When no floodplain-correction was applied, the total basin area was used in Eq. 6 for conversion between D and QS.

[b]References for datasets used are displayed in Fig. 3. Grande dataset by Kober et al. (2015) not included (see text).

[c]A range is given if more than one measurement for the largest outlet is available to display variability.

[d]C_v gives the coeeficient of variation and is the ratio of the standard deviation to the mean of each dataset.

[e]*In situ* tributaries contained: Napo, Maranon, Ucayali; Gauging tributaries: also Huallaga (see Fig. 3).

[f]Comprises lowland data at Manacapuru, Iracema, Parintins, lower Madeira, Obidos, and Varzea data; for entire dataset see Tables 2,3 in Wittmann et al. (2011a).

[g]Two values measured for the Grande at Abapo deviate strongly (Wittmann et al., 2009; Kober et al., 2015). Note that a area-weighed D_{insitu} of the Grande basin is 0.11 ± 0.27 mm/yr (n=71).

[h]Comprises lowland data of lower Karnali, Kosi and Narayani and all data from lower Ganga below Varanasi to Harding Bridge; c.f. Table 1 in Lupker et al. (2012a).

[i]For measured QS_{gaug}, the range is given (for largest outlets) to display variability in data; E_{gaug} are area-weighed ± 1σ std. dev. All lowland data is floodplain corrected (i.e. using the sampled source area for calculations), except where indicated (see Eqs. 8,9 for calculation of E_{gaug}). No dissolved loads were added.

[j]Calculated using upscaling, i.e. the sum of all measured QS values was multiplied by the largest drainage area and then divided by the sum of all areas.

[k]Comprises measured QS data at Harding Bridge (cf. Lupker et al. (2012a)).

[l]Values are for Ganga only. Brahmaputra contribution was removed by assuming a 40% sediment flux contribution of the Ganga relative to the Brahmaputra.

1212

1213

FIGURE CAPTIONS

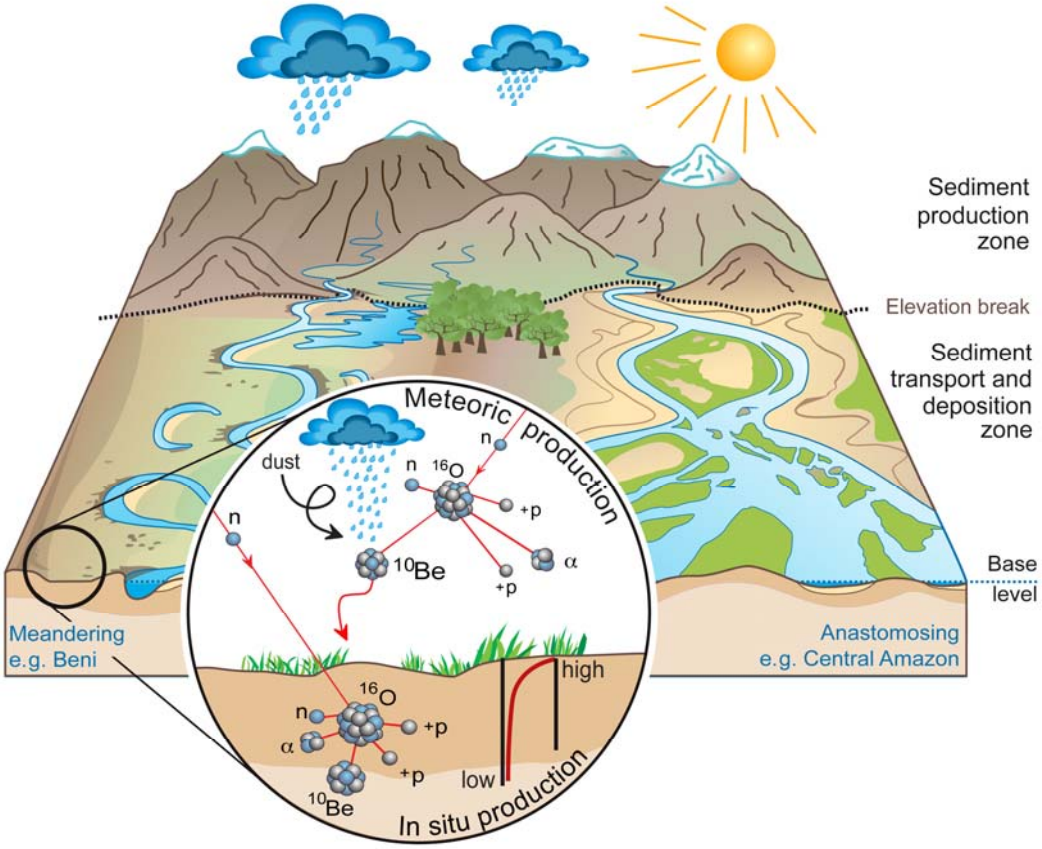

Fig. 1: Sediment routing from the zone of sediment production (in high mountain settings) to transport and storage in low-relief floodplain regions. The left-hand system is a lowland river that is migrating (e.g. the large Beni River in Bolivia), and the right-hand system is anastomosing (e.g. the Amazon River). Both types store and permanently release sediment that mixes the cosmogenic nuclides it carries with those contained in the main stream. The main production pathways of "meteoric" (i.e. within the atmosphere) and "*in situ*" (i.e. within the mineral grain) cosmogenic ^{10}Be are shown in the inset. Both varieties of ^{10}Be are mainly produced from spallation reactions of target atoms (e.g. ^{16}O) that are hit by high-energy cosmic rays (neutrons, protons). Secondary cosmic rays (protons, neutrons, and very light particles, such as muons) and cosmogenic nuclides are the result. *In situ* production is high at Earth´s surface and decreases with increasing depth through cosmic ray attenuation.

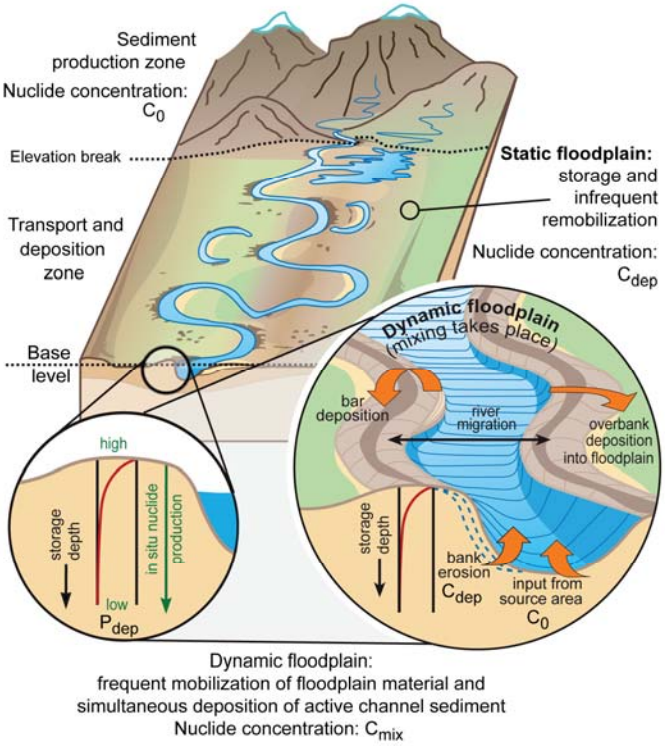

Fig. 2: Illustration of “dynamic floodplain” and “static” cases, and the nuclide concentrations in the participating compartments. In the static case, sediment is stored (nuclide concentration: C_{dep}) and eventually eroded and re-incorporated into the main channel (C_{mix}). In the case of the dynamic floodplain, channel- floodplain interaction leads to permanent remobilization and deposition due to the proximity to the main channel. The right-hand blow up shows parameters that influence the mixing between sediment in the channel and floodplain material. In the main channel, source area-derived material from close to the mountain front (C_0) is mixed (C_{mix}) with floodplain sediment eroded from bank deposits (C_{dep}). At the same time, sediment is deposited in the floodplain by bar- and overbank deposition (C_{mix}).

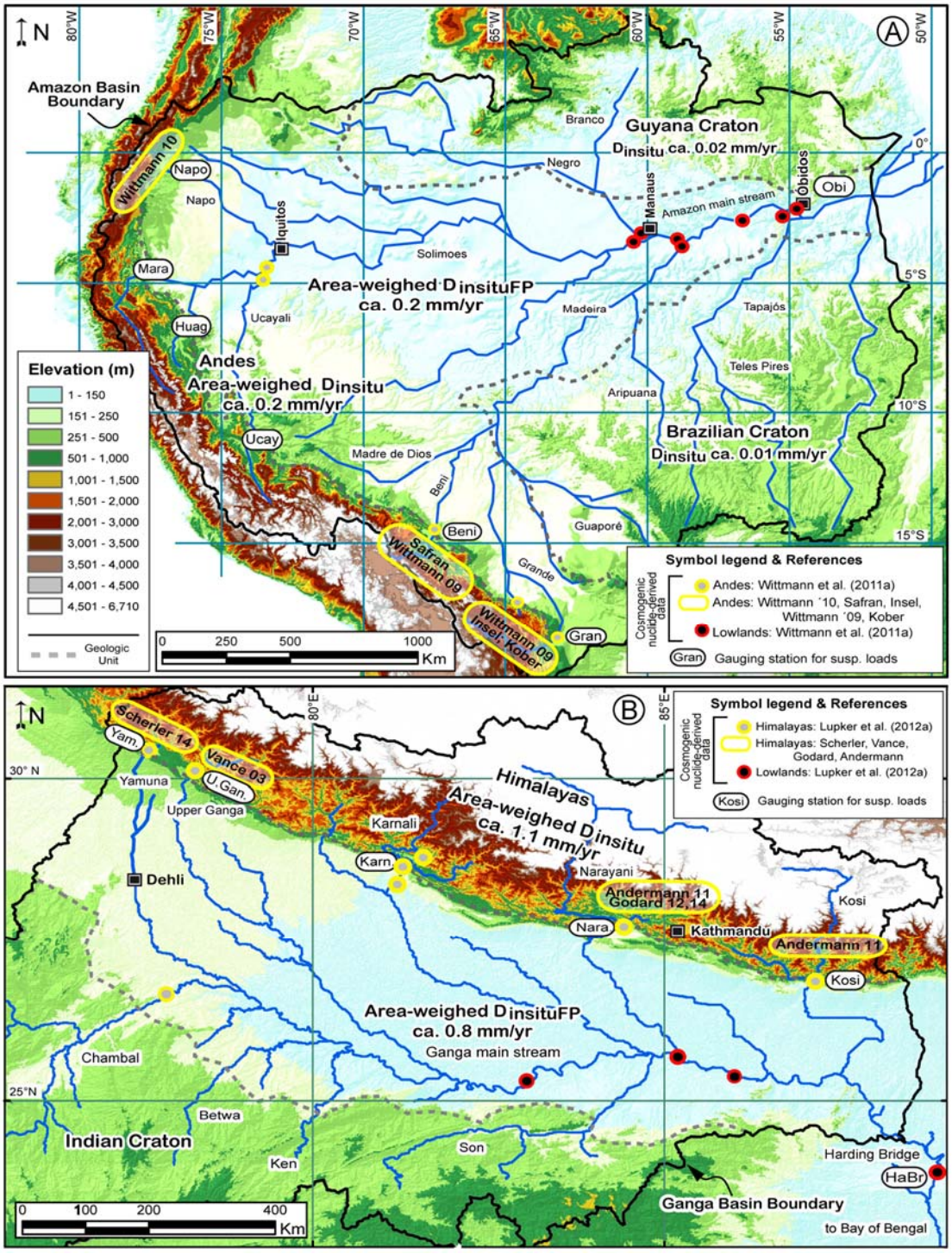

Fig. 3: Topographic and fluvial drainage map of the Amazon (A) and Ganga (B) basins. Elevation is scaled using identical color schemes in both basins. Yellow-rimmed symbols denote cosmogenic-nuclide sampling locations (only basins > 100 km^2 are shown) and first author´s name of studies (or first authors name and year for ambiguous studies) that were used for compilation (Table 2). Mean source area D_{insitu} and floodplain-corrected (see section 3.1) lowland $D_{insituFP}$ are given. White ellipses denote gauging station for suspended sediment (only basins >100 km^2 are shown; for compilation see Table 2). *Refs. for gauging data in*

Amazon basin are: Napo- Armijos et al. (2013); Mara = Maranon at Borja and Huag = Huallage at Chazuta- Pepin et al. (2013); Ucay = Ucayali at Pucallpa- Santini et al. (2014); Beni = Beni at Rurrenabaque and larger stations within upper Beni basin- Aalto et al. (2006); Pepin et al. (2013); Gran = Grande at Abapo and larger stations within upper Grande basin- Guyot et al. (1996); Aalto et al. (2006); Pepin et al. (2013). In the Amazon lowlands at Obi = Óbidos, we compiled data from Meade (1985); Dunne et al. (1998); Guyot et al. (2005); Filizola and Guyot (2009); Martinez et al. (2009). *Refs. for gauging data in Ganga basin are*: Yam. = Yamuna- Jha et al. (1988); U. Gan. = Upper Ganga- Abbas and Subramanian (1984); Karn. = Karnali - Andermann et al. (2012); Lupker et al. (2012a); Nara. = Narayani- Sinha and Friend (1994); Gabet et al. (2008); Andermann et al. (2012); Lupker et al. (2012a); Kosi- Sinha and Friend (1994); Andermann et al. (2012); Lupker et al. (2012a). Note that the work by Lupker et al. (2012a) comprises a secondary data source for several gauging stations, including HaBr = Harding Bridge station that is located downstream of the Hooghly diversion.

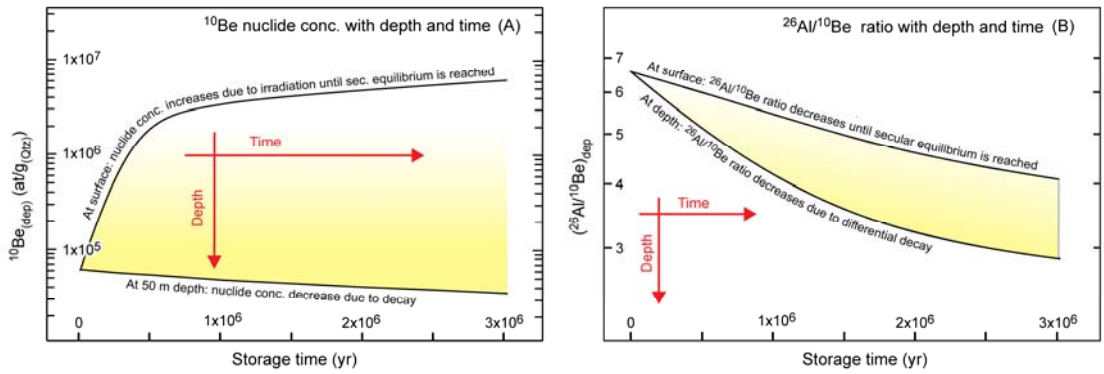

Fig. 4 A): Example of time- and depth dependent evolution of lowland *in situ* ^{10}Be concentrations with storage time in a static deposit. The examples are calculated for an initial ^{10}Be concentration $^{10}Be_0$ of 6×10^4 at/$g_{(Qtz)}$ and further irradiation at a total production rate of 3.75 at/$g_{(Qtz)}$/yr and simultaneous decay. At the surface of the floodplain, ingrowth of the nuclide will occur with time, until a secular equilibrium between production and decay is attained. When stored deeply, decay becomes significant (lower curve calculated for a storage depth of 50 m, where further irradiation is virtually absent due to complete shielding). B): Example of the time- and depth-dependent evolution of the ^{26}Al/^{10}Be ratio in this static case, from an initial ^{26}Al/^{10}Be ratio of 6.5, which is the surface production ratio between the two nuclides. Due to the faster decay of ^{26}Al, the ratio of the nuclides is more sensitive to storage than single nuclide concentrations.

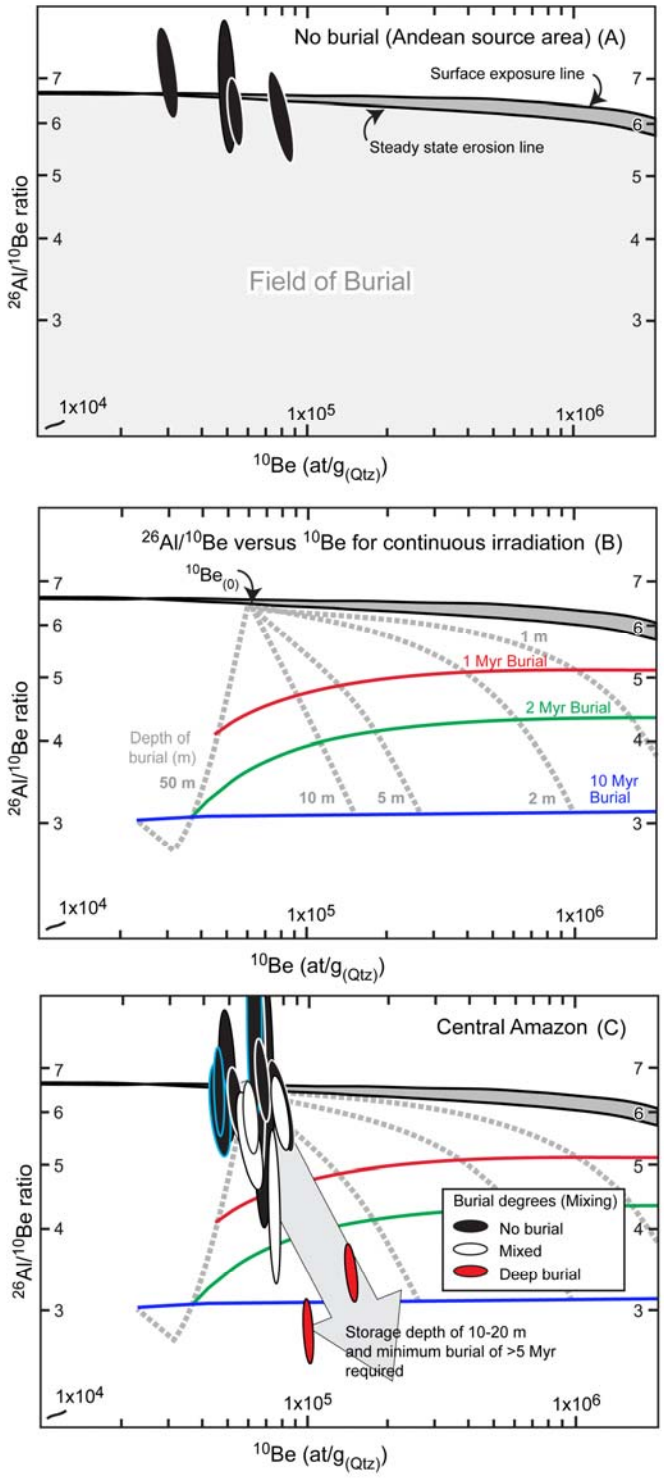

Fig. 5: The change in ^{26}Al/^{10}Be ratio versus the ^{10}Be concentration in quartz with duration and depth of burial (the "erosion island" plot, Lal (1991); showing the constant exposure and steady state erosion lines), with examples from the Amazon basin. A): Samples from the Andean source areas (black ellipses) have ^{26}Al/^{10}Be ratios of around 6.5 and plot onto the steady state erosion line. These samples have never been buried. Samples that plot below the line would have been buried. B): When the overburden is not entirely shielding the sample from cosmic irradiation (e.g. in a shallow floodplain), the erosion island plot is calculated assuming simultaneous nuclide production and decay. A given ^{26}Al/^{10}Be ratio then represents a burial age at a given depth. Contour lines of storage depth (stippled grey lines) are shown starting from a ^{10}Be$_0$ (representative for a given family of samples). C): Burial-exposure history for the lower Amazon River (modified from Wittmann et al., 2011b). In the lower Amazon River, samples comprise mixtures of sediment with no previous burial (from Andean sources given in black or black with blue rim for visibility) and deeply buried sediment (red ellipses), resulting in mixed samples (open ellipses). If the initial ^{10}Be concentration of ^{10}Be$_0$ is known or can be inferred, minimum storage depths and burial durations can be inferred.

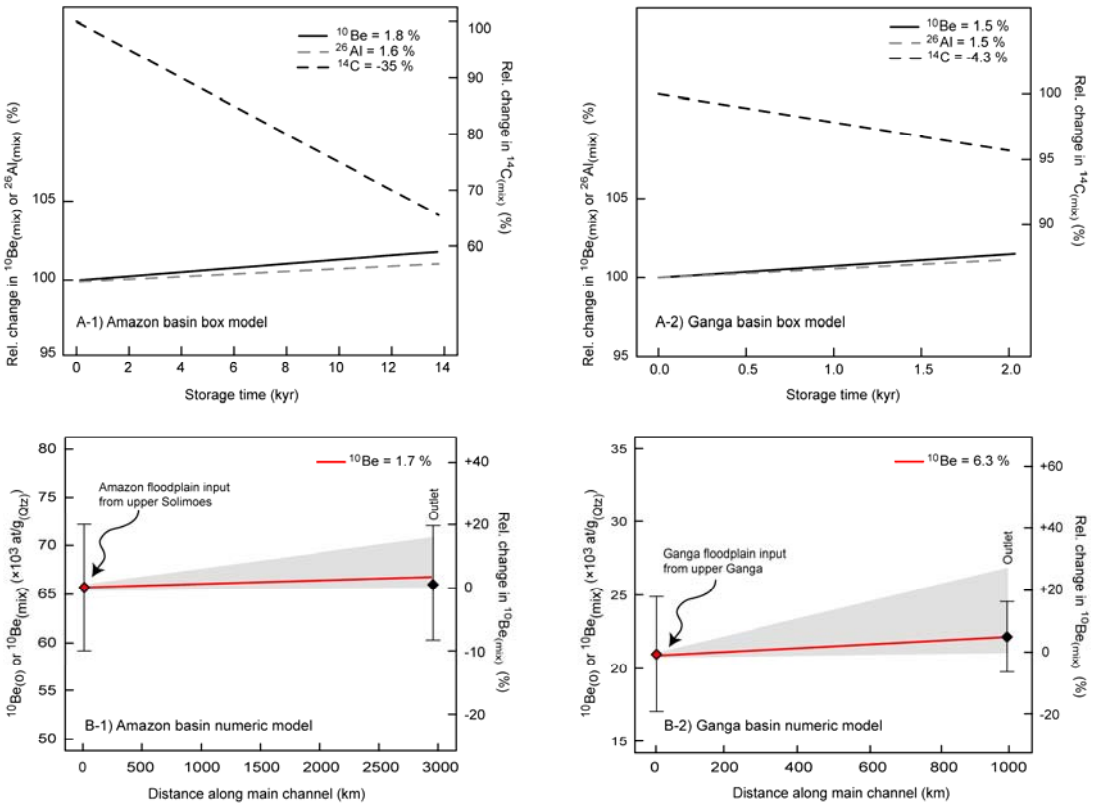

Fig. 6, Box (upper panels) and numeric (lower panels) models of relative changes in lowland river sediment nuclide concentrations C_{mix}. A-1,2): Results of the model of Wittmann and von Blanckenburg (2009) for the Amazon (A-1) and Ganga (A-2) rivers (using their eqs. 2-4). Long-lived *in situ* (^{10}Be, ^{26}Al) nuclide concentration changes are shown on the left Y-axis, and *in situ* ^{14}C nuclide concentration changes are shown on the right Y-axis. Relative changes in nuclide concentrations as a function of total storage time (kyr) in a dynamic floodplain were calculated for all three nuclides relative to the upstream concentration $^{10}Be_0$ (see Table 1). The differences in the change of nuclide accumulation are mainly due to the different half-lives of the three nuclides. B-1,2): Results of the model by Lauer and Willenbring (2010), using their eq. 17, as a function of total distance along the main channel (km). Red line indicates change of ^{10}Be signal along the floodplain within grey 1σ uncertainty space, and red and black diamonds give the real measured $^{10}Be_0$ and $^{10}Be_{mix}$ (at/$g_{(Qtz)}$) with their analytical uncertainties, respectively. Note that we used the same input parameters as Lupker et al. (2012) for the Ganga (Table 1), but using a single-channel system (i.e. having only one major tributary draining the source area). The Amazon system was also modeled as being a single channel from the Andes to the mouth. Note that both model types were (re-)calculated using the same total SLHL production rate of 3.75 at/g/yr for ^{10}Be and muonic parametrization (Braucher et al., 2011) (for details see supplement A).

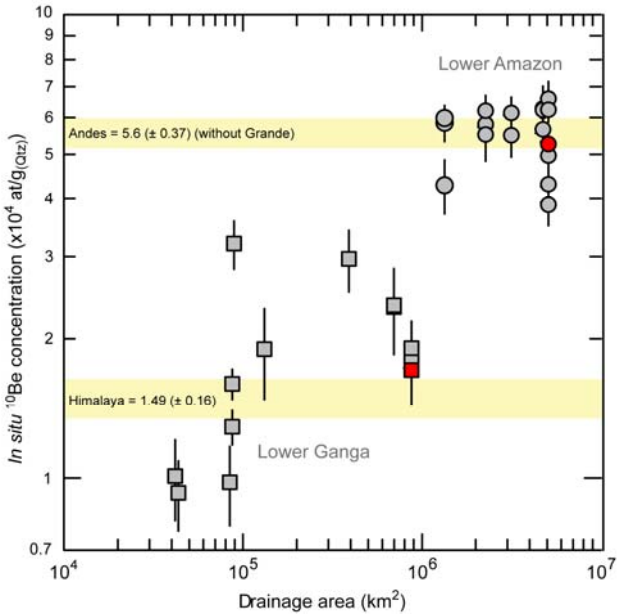

Fig. 7: *In situ* ^{10}Be nuclide concentrations (×10^4 at/$g_{(Qtz)}$) and associated analytical 1σ uncertainties measured in lowland river sediment of the Ganga and Amazon Rivers. The Amazon lowland dataset comprises only fine-grained sediment (n=18) and the Ganga lowland dataset (including all floodplain data, i.e. also data from lower Karnali, Narayani, and Kosi rivers, n = 14) is corrected for Indian craton input. Red symbols give area-weighed nuclide concentrations for the lowland areas; yellow bars give area-weighed (± 1σ analytical uncertainty) Andean and Himalayan source area data of catchments > 100 km^2. Andean data is from Safran et al. (2005); Wittmann et al. (2009); Insel et al. (2010); Wittmann et al. (2010); Wittmann et al. (2011a); the Grande dataset by Kober et al. (2015) is not shown (average is ca. 40×10^4 at/$g_{(Qtz)}$); upper Nepalese Himalaya data is from Vance et al. (2003); Wobus et al. (2005); Andermann (2011); Godard et al. (2012); Lupker et al. (2012a); Godard et al. (2014); Scherler et al. (2014).

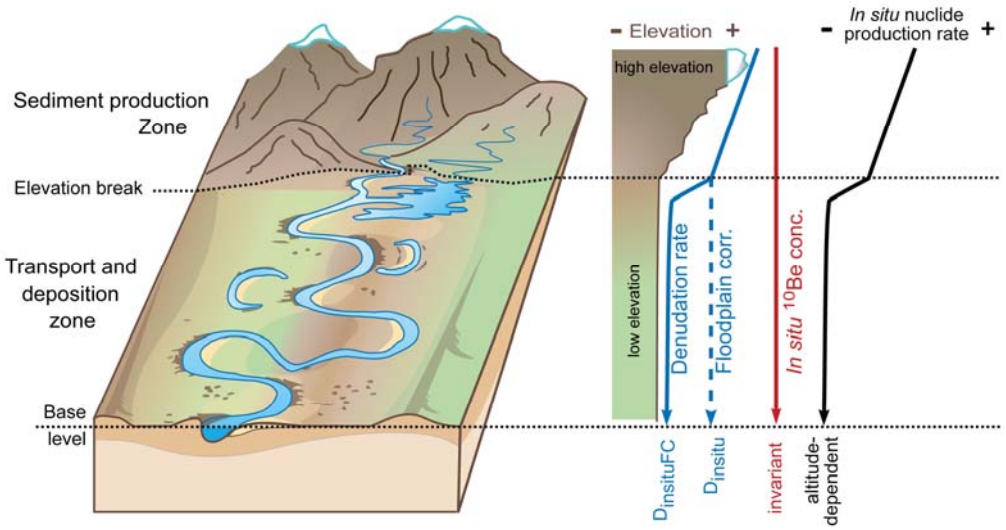

Fig. 8: Concept of the "floodplain correction" of denudation rates. The *in situ* nuclide production rate (black curve) is high in high-altitude mountain regions, and low in low-altitude floodplain regions. Long-lived *in situ* nuclide (e.g. ^{10}Be) concentrations of sediment transported along these domains are shown here as invariant (red curve). If the production rates P_{FC} of the source area are used, the denudation rate of the source area results ($D_{insituFC}$; blue dashed curve), whereas if the production rate of the whole basin above the sampling point is used, denudation rates integrate over the entire basin area and are thus apparent rates.

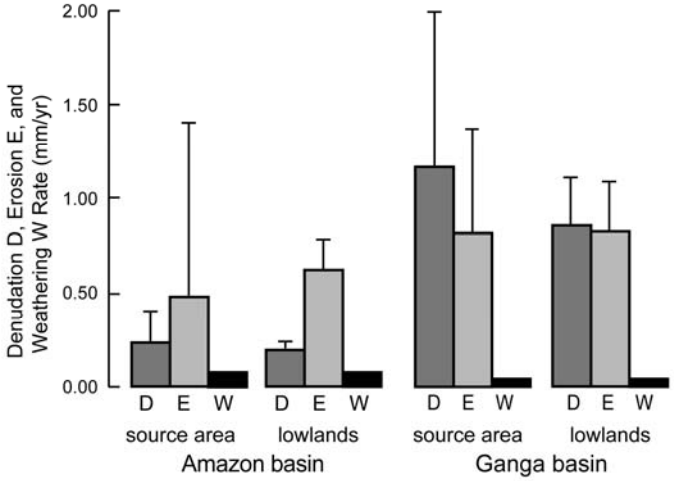

Fig. 9: Longer-term area-weighed denudation rates D from *in situ* ^{10}Be, area-weighed modern erosion rates E from gauging, and published silicate weathering rates W (in mm/yr) across the Amazon and Ganga basins from source area to the lowlands. For references see text. Uncertainties denote the 1σ std. dev. for the D and E datasets, and a 10% uncertainty was assumed for the W dataset.

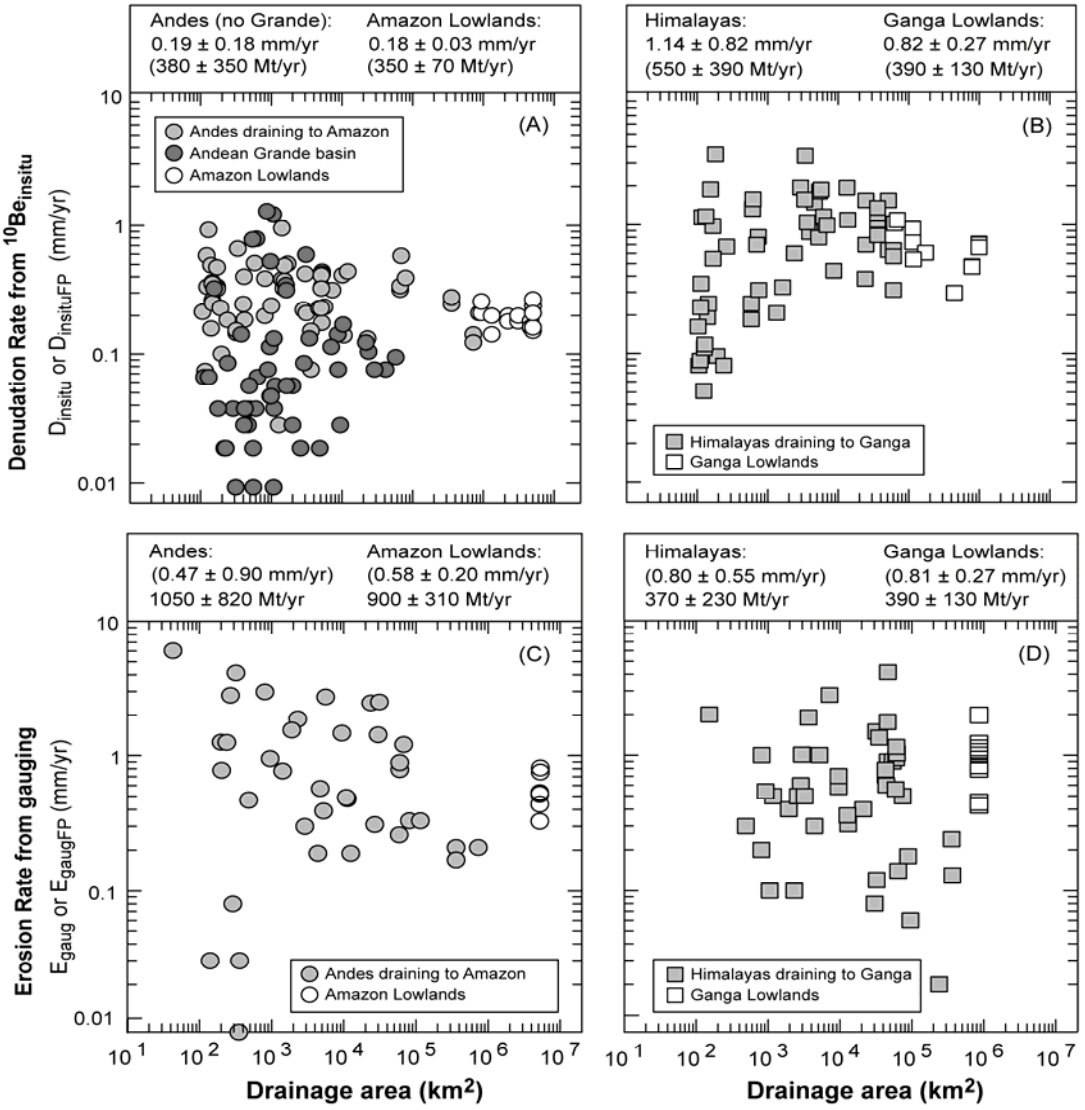

Fig. 10: Denudation from *in situ* cosmogenic ^{10}Be (A, B) and erosion rates from gauging (C, D) (all in mm/yr) from the source areas to the lowlands for the Amazon and the Ganga basins versus drainage area (km^2, note that we omitted basins <100 km^2 to exclude small-scale effects). All lowland denudation and erosion rates are floodplain-corrected according to equations 6 and 10, respectively. Area-weighed denudation/erosion rates/sediment fluxes and the 1σ std. dev. of each dataset are shown above each panel. Converted values are shown in brackets, using the surface areas given in Table 2. For references see Fig. 3 and for details see Table 2.

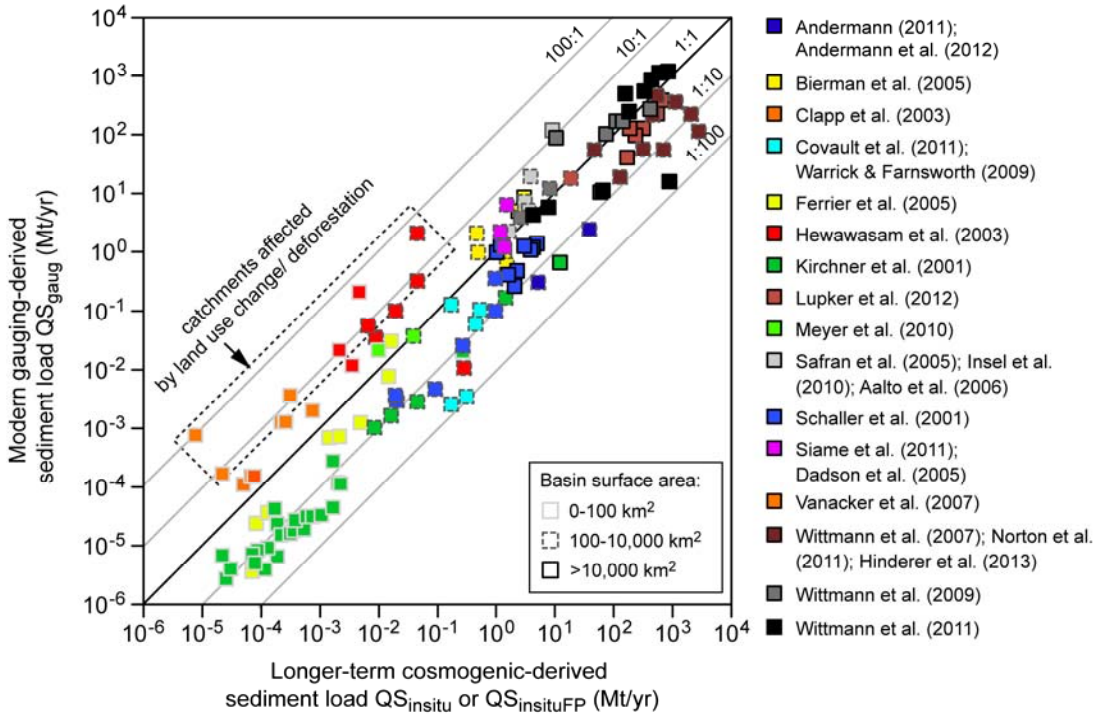

Fig. 11: Modern gauging-derived versus longer-term cosmogenic nuclide-derived sediment load data from approximately the same locations (n=129), color-coded according to publication source (last author is always the reference for gauging dataset where applicable, i.e. if no second reference for gauging data is given, we rely on the compilation or measurement for gauging data in the given reference). Basin surface area (km^2) is coded by rim color for small (0-100 km^2), medium (100-10000 km^2), and large catchments (>10000 km^2). For references on gauging data in Amazon and Ganga basins see Fig. 3. The datasets from the highly anthropogenized settings (Sri Lanka and Paute basin from Hewawasam et al. (2003); Vanacker et al. (2007), respectively) are highlighted by the dashed box. Note that the smaller Alpine basins, although having high sediment flux, display larger disagreement between QS_{gaug} and QS_{insitu}, whereas all other larger rivers agree reasonably well.

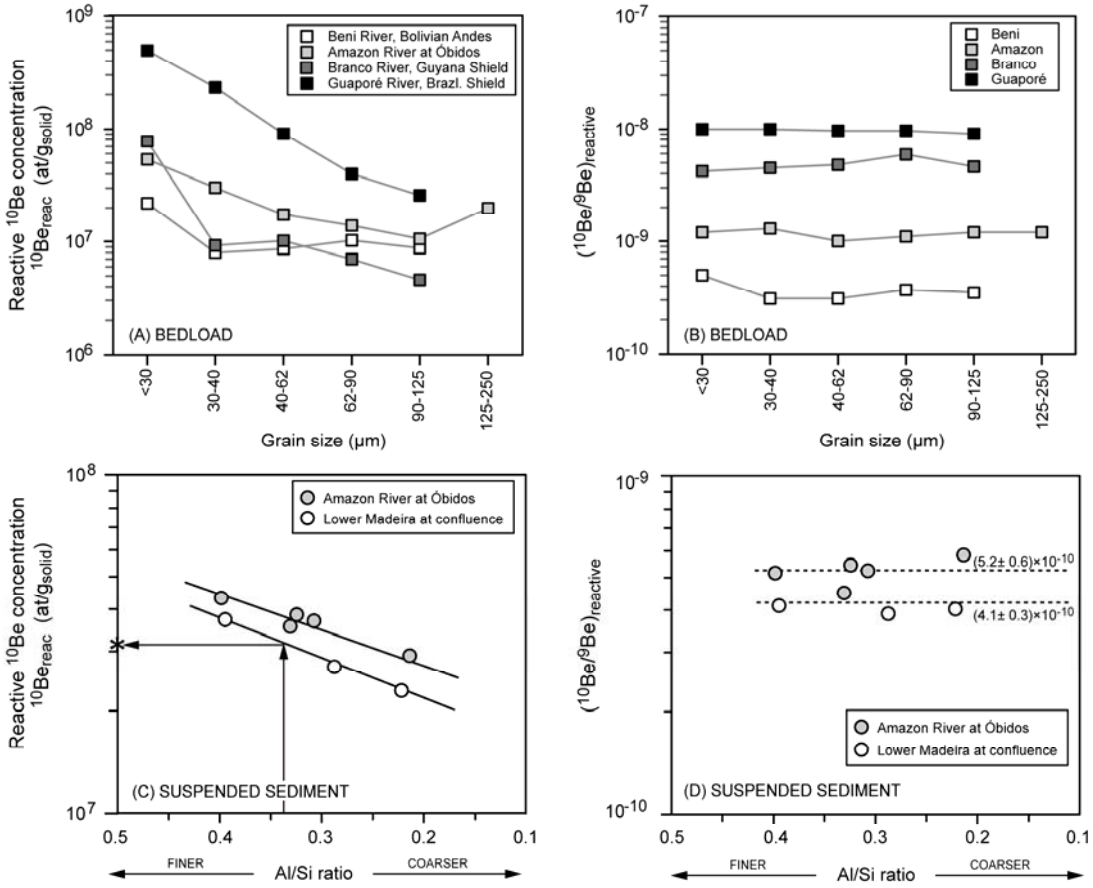

Fig. 12: The grain size-dependence of reactive (adsorbed and precipitated) meteoric ^{10}Be concentrations on grain size (A, C) and the removal of this dependence by normalizing over reactive ^{9}Be (B) or by linear regression using a representative Al/Si ratio as grain size indicator (C). A) $^{10}Be_{reac}$ (at/g_{solid}) and B) $^{10}Be/^{9}Be$ ratio from bedload of different Amazon rivers (both modified from von Blanckenburg et al. (2012); data from Wittmann et al. (2012)), C) $^{10}Be_{reac}$ (at/g_{solid}) and D) $^{10}Be/^{9}Be$ ratios (with mean and 1σ std. dev. of each dataset) from suspended sediment in the lower Madeira and the Amazon at Óbidos, sampled at various depths in the river, versus Al/Si ratio (cosmogenic data from Wittmann et al. (2015) and Al/Si data from Bouchez et al. (2011b); both quantities measured on splits of the same sample). The Al/Si ratio is a proxy for grain size (Galy et al., 2008; Bouchez et al., 2011a). Note that when knowing a depth-integrated Al/Si ratio representative for the river´s sediment flux, a representative ^{10}Be concentration (black star) can be derived from linear regression (example shown in C), with arrows showing a depth-integrated Al/Si ratio of the Madeira of 0.34 from Bouchez et al. (2011b) in this example. From this ^{10}Be concentration, an erosion rate can be calculated that is not affected by bias from riverine particle sorting. The same correction can be done with ^{9}Be data in order to calculate a representative weathering fraction. Most uncertainties are within symbol size.

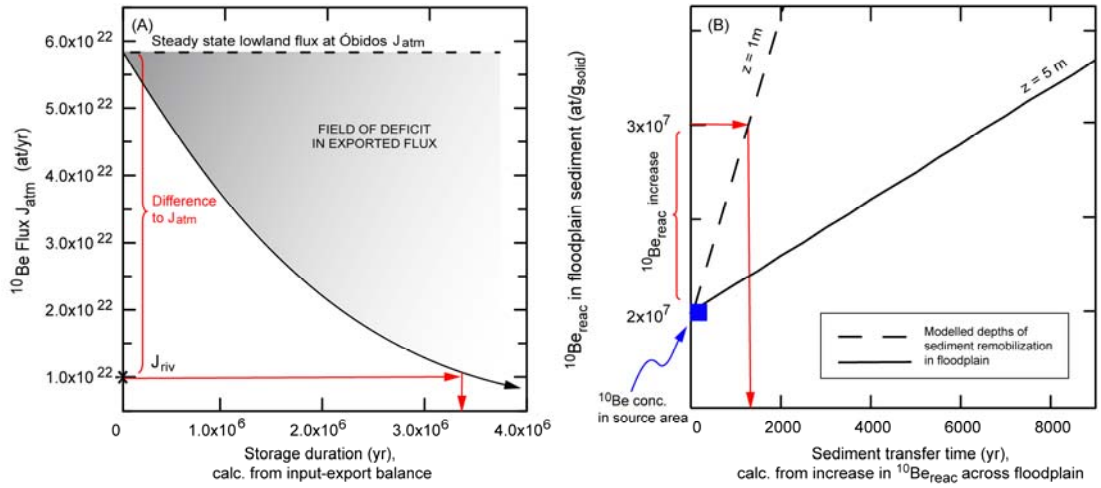

Fig. 13: A) The duration (in Myr) of static storage required to reduce the riverine flux of ^{10}Be in the Amazon lowlands at Óbidos (J_{riv}) relative to the depositional flux onto the floodplain upstream of Óbidos (J_{atm}, dotted black line). Here $J_{riv}^{^{10}Be}$ was calculated by using an *in situ*-derived sediment flux (Wittmann et al., 2015). The red horizontal arrow corresponds to the effective lowland riverine flux and shows potential ^{10}Be radioactive decay during static storage the field of deficit representing 3.7 Myr of storage. B) Model of ^{10}Be accumulation over time scales typical of dynamic floodplain-channel interaction in the Amazon basin. Note that for these short time scales, decay of ^{10}Be is negligible. The observed increase in floodplain-derived $^{10}Be_{reac}$ (ca. 1×10^7 at/g) was added to the $^{10}Be_{reac}$ of ca. 2×10^7 at/g contained in Andean source area sediment (blue square). The predicted ^{10}Be inventory was calculated using equation 12 and converted into $^{10}Be_{reac}$ by assuming two different remobilization depths (z = 1, 5 m). For a mean remobilization depth of ca. 1 m, which would correspond to the case where a clay layer deposited on top of the floodplain binds all meteoric ^{10}Be deposited from the atmosphere, the observed increase in ^{10}Be across the floodplain would correspond to a transfer time of ca. 1.6 kyr. Both Figures modified from Wittmann et al. (2015).

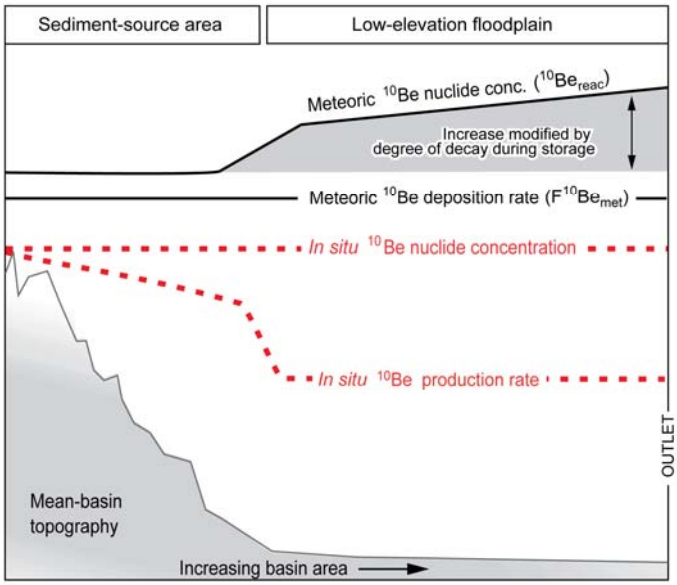

Fig. 14: Schematic illustration of the different behavior of meteoric versus *in situ*-cosmogenic nuclides in large lowland basins; principle is adapted from Wittmann et al. (2011a). *In situ* nuclide production decreases significantly across lowland areas, whereas meteoric depositional fluxes are not dependent on elevation (at elevations below 3 km). In dynamic floodplains, long-lived *in situ* nuclide concentrations are not modified during storage and reworking. Meteoric cosmogenic nuclide concentrations are thus much more sensitive to storage.

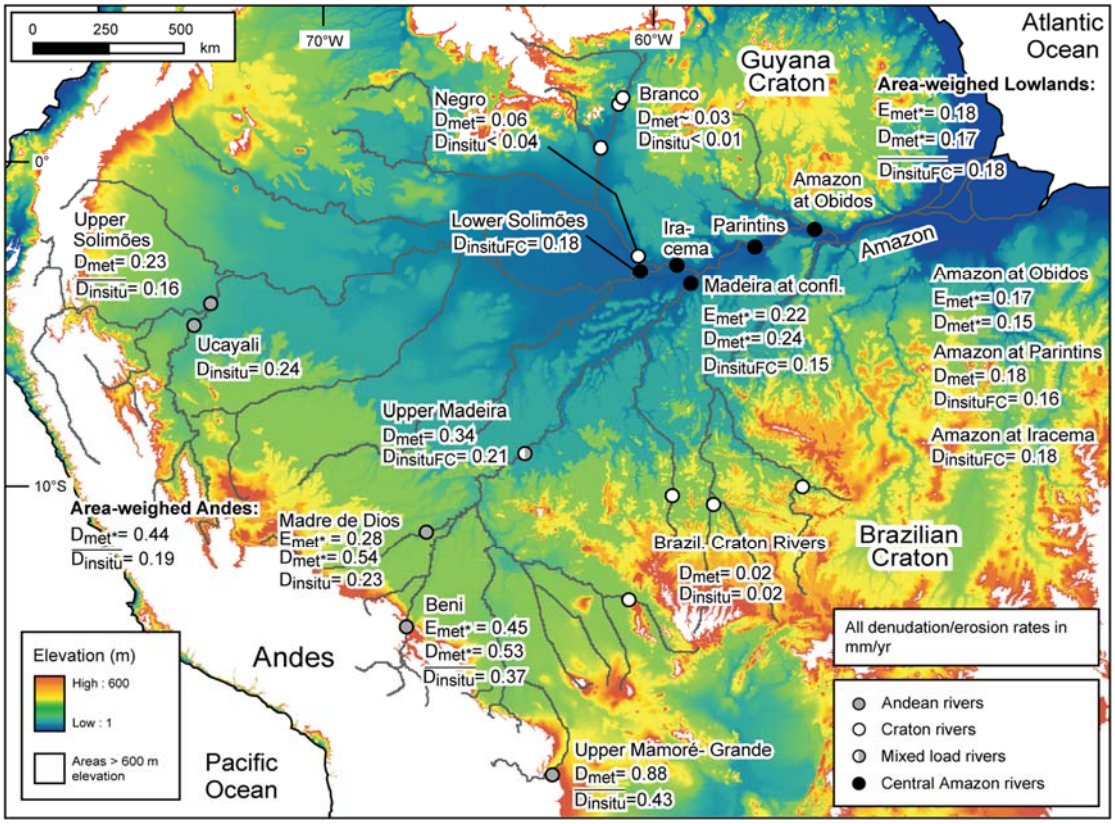

Fig. 15: Elevation map of the Amazon basin with comparison of denudation rates (D_{met}; D_{met*}) and high-confidence erosion rates E_{met*} with D_{insitu} and $D_{insituFC}$ (from *in situ* ^{10}Be concentrations in sand-sized quartz from bedload; Wittmann et al., 2009; 2011a; $\overline{D_{insitu}}$ or $\overline{D_{insituFC}}$ are area-weighed values from Table 2). E_{met*} and D_{met*} are from depth-integrated suspended sediment measured at four locations where depth profiles were available. Lower confidence rates are denudation rates from $^{10}Be/^{9}Be$ from bedload (D_{met}) where the ^{9}Be fractions are potentially affected by grain size bias. We show area-weighed meteoric rates for the source areas (Andes) and the Amazon outlet; the area-weighed Andean rate was calculated using both D_{met} from bedload and D_{met*}; the area-weighed lowland rate was calculated using D_{met*} from the two lowland depth profiles (Madeira and Amazon at Óbidos).

REFERENCES

Aalto, R., Dunne, T. and Guyot, J.L., 2006. Geomorphic controls on Andean denudation rates. Journal of Geology, 114(1): 85-99.

Abbas, N. and Subramanian, V., 1984. Erosion and sediment transport in the Ganges river basin (India). Journal of Hydrology, 69(1-4): 173-182.

Aldahan, A., Ye, H.P. and Possnert, G., 1999. Distribution of beryllium between solution and minerals (biotite and albite) under atmospheric conditions and variable pH. Chemical Geology, 156(1-4): 209-229.

Allen, P.A., 2008. From landscapes into geological history. Nature, 451(7176): 274-276.

Andermann, C., 2011. Climate, topography and erosion in the Nepal Himalayas. Ph.D. Thesis, Université de Rennes 1, Rennes, 173 pp.

Andermann, C., Crave, A., Gloaguen, R., Davy, P. and Bonnet, S., 2012. Connecting source and transport: Suspended sediments in the Nepal Himalayas. Earth and Planetary Science Letters, 351-352(0): 158-170.

Armijos, E., Laraque, A., Barba, S., Bourrel, L., Ceron, C., Lagane, C., Magat, P., Moquet, J.S., Pombosa, R., Sondag, F., Vauchel, P., Vera, A. and Guyot, J.L., 2013. Yields of suspended sediment and dissolved solids from the Andean basins of Ecuador. Hydrological Sciences Journal, 58(7): 1478-1494.

Armitage, J.J., Duller, R.A., Whittaker, A.C. and Allen, P.A., 2011. Transformation of tectonic and climatic signals from source to sedimentary archive. Nature Geoscience, 4(4): 231-235.

Armitage, J.J., Dunkley Jones, T., Duller, R.A., Whittaker, A.C. and Allen, P.A., 2013. Temporal buffering of climate-driven sediment flux cycles by transient catchment response. Earth and Planetary Science Letters, 369-370(0): 200-210.

Asselman, N.E.M., 1999. Suspended sediment dynamics in a large drainage basin: the River Rhine. Hydrological Processes, 13(10): 1437-1450.

Balco, G. and Rovey, C.W., II, 2008. An isochron method for cosmogenic-nuclide dating of buried soils and sediments. American Journal of Science, 308(10): 1083-1114.

Balco, G. and Shuster, D.L., 2009. ^{26}Al-^{10}Be-^{21}Ne burial dating. Earth and Planetary Science Letters, 286(3-4): 570-575.

Balco, G. and Stone, J.O., 2005. Measuring middle Pleistocene erosion rates with cosmic-ray-produced nuclides in buried alluvial sediment, Fisher Valley, southeastern Utah. Earth Surface Processes and Landforms, 30: 1051-1067.

Balco, G., Stone, J.O., Lifton, N.A. and Dunai, T.J., 2008. A complete and easily accessible means of calculating surface exposure ages or erosion rates from Be-10 and Al-26 measurements. Quaternary Geochronology, 3(3): 174-195.

Balco, G., Stone, J.O.H. and Jennings, C., 2005. Dating Plio-Pleistocene glacial sediments using the cosmic-ray-produced radionuclides ^{10}Be and ^{26}Al. American Journal of Science, 305(1): 1-41.

Bekaddour, T., Schlunegger, F., Vogel, H., Delunel, R., Norton, K.P., Akçar, N. and Kubik, P., 2014. Paleo erosion rates and climate shifts recorded by Quaternary cut-and-fill sequences in the Pisco valley, central Peru. Earth and Planetary Science Letters, 390(0): 103-115.

Benda, L. and Dunne, T., 1997. Stochastic forcing of sediment supply to channel networks from landsliding and debris flow. Water Resources Research, 33(12): 2849-2863.

Bierman, P. and Steig, E.J., 1996. Estimating rates of denudation using cosmogenic isotope abundances in sediment. Earth Surface Processes and Landforms, 21(2): 125-139.

Bierman, P.R. and Nichols, K.K., 2004. Rock to sediment - Slope to sea with Be-10 - Rates of landscape change. Annual Review of Earth and Planetary Sciences, 32: 215-255.

Borchers, B., Marrero, S., Balco, G., Caffee, M., Goehring, B., Lifton, N., Nishiizumi, K., Phillips, F., Schaefer, J. and Stone, J., 2016. Geological calibration of spallation production rates in the CRONUS-Earth project. Quaternary Geochronology, 31: 188-198.

Bouchez, J., Gaillardet, J., France-Lanord, C., Maurice, L. and Dutra-Maia, P., 2011a. Grain size control of river suspended sediment geochemistry: Clues from Amazon River depth profiles. Geochemistry Geophysics Geosystems, 12(3): Q03008.

Bouchez, J., Gaillardet, J., Lupker, M., Louvat, P., France-Lanord, C., Maurice, L., Armijos, E. and Moquet, J.-S., 2012. Floodplains of large rivers: Weathering reactors or simple silos? Chemical Geology, 332-333(0): 166-184.

Bouchez, J., Gaillardet, J. and von Blanckenburg, F., 2014. Weathering Intensity in Lowland River Basins: From the Andes to the Amazon Mouth. Procedia Earth and Planetary Science, 10(0): 280-286.

Bouchez, J., Lupker, M., Gaillardet, J., France-Lanord, C. and Maurice, L., 2011b. How important is it to integrate riverine suspended sediment chemical composition with depth? Clues from Amazon River depth-profiles. Geochimica Et Cosmochimica Acta, 75(22): 6955-6970.

Bourlès, D., Raisbeck, G.M. and Yiou, F., 1989. ^{10}Be and ^{9}Be in marine sediments and their potential for dating. Geochimica Et Cosmochimica Acta, 53(2): 443-452.

Braucher, R., Merchel, S., Borgomano, J. and Bourlès, D.L., 2011. Production of cosmogenic radionuclides at great depth: A multi element approach. Earth and Planetary Science Letters, 309(1-2): 1-9.

Brown, E.T., Edmond, J.M., Raisbeck, G.M., Bourlès, D., Yiou, F. and Measures, C.I., 1992. Beryllium isotope geochemistry in tropical river basins. Geochimica Et Cosmochimica Acta, 56: 1607-1624.

Brown, E.T., Stallard, R.F., Larsen, M.C., Raisbeck, G.M. and Yiou, F., 1995. Denudation rates determined from the accumulation of in situ-produced ^{10}Be in the Luquillo experimental forest, Puerto Rico. Earth and Planetary Science Letters, 129(1-4): 193-202.

Brown, L., 1987. 10Be as a tracer of erosion and sediment transport. Chemical Geology, 65(3-4): 189-196.

Brown, L., Klein, J. and Middleton, R., 1985. Anomalous isotopic concentrations in the sea off Southern California. Geochimica Et Cosmochimica Acta, 49(1): 153-157.

Brown, L., Pavich, M.J., Hickman, R.E., Klein, J. and Middleton, R., 1988. Erosion of the eastern United States observed with ^{10}Be. Earth Surface Processes and Landforms, 13(5): 441-457.

Burt, T. and Allison, R. (Editors), 2010. Sediment cascades- An integrated approach. Wiley-Blackwell, Oxford, UK.

Castelltort, S. and Van Den Driessche, J., 2003. How plausible are high-frequency sediment supply-driven cycles in the stratigraphic record? Sedimentary Geology, 157(1-2): 3-13.

Charreau, J., Kent-Corson, M.L., Barrier, L., Augier, R., Ritts, B.D., Chen, Y., France-Lannord, C. and Guilmette, C., 2012. A high-resolution stable isotopic record from the Junggar Basin (NW China): Implications for the paleotopographic evolution of the Tianshan Mountains. Earth and Planetary Science Letters, 341,Äì344(0): 158-169.

Chmeleff, J., von Blanckenburg, F., Kossert, K. and Jakob, D., 2010. Determination of the ^{10}Be half-life by multicollector ICP-MS and liquid scintillation counting. Nuclear Instruments & Methods in Physics Research Section B- Beam Interactions with Materials and Atoms, 268(2): 192-199.

Cleary, D. (Editor), 2000. Small scale gold-mining in Brazilian Amazonia. Amazonia at the Crossroads. Institute of Latin America Studies, London, UK, 58-72 pp.

Covault, J.A., Craddock, W.H., Romans, B.W., Fildani, A. and Gosai, M., 2013. Spatial and Temporal Variations in Landscape Evolution: Historic and Longer-Term Sediment Flux through Global Catchments. The Journal of Geology, 121(1): 35-56.

Dadson, S.J., Hovius, N., Chen, H.G., Dade, W.B., Hsieh, M.L., Willett, S.D., Hu, J.C., Horng, M.J., Chen, M.C., Stark, C.P., Lague, D. and Lin, J.C., 2003. Links between erosion, runoff variability and seismicity in the Taiwan orogen. Nature, 426(6967): 648-651.

de Vente, J., Poesen, J., Arabkhedri, M. and Verstraeten, G., 2007. The sediment delivery problem revisited. Progress in Physical Geography, 31(2): 155-178.

Dixon, J.L. and Riebe, C.S., 2014. Tracing and Pacing Soil Across Slopes. Elements, 10(5): 363-368.

Dixon, J.L. and von Blanckenburg, F., 2012. Soils as pacemakers and limiters of global silicate weathering. Comptes Rendus Geoscience, 344(11–12): 597-609.

Dosseto, A. and Schaller, M., 2016. The erosion response to Quaternary climate change quantified using uranium isotopes and in situ-produced cosmogenic nuclides. Earth-Science Reviews, 155: 60-81.

Dunai, T.J., 2000. Scaling factors for production rates of in situ produced cosmogenic nuclides: a critical reevaluation. Earth and Planetary Science Letters, 176(1): 157-169.

Dunai, T.J., 2010. Cosmogenic nuclides: Principles, Concepts, and Applications in Earth Surface Sciences. Cambridge University Press, New York.

Dunne, T., Mertes, L.A.K., Meade, R.H., Richey, J.E. and Forsberg, B.R., 1998. Exchanges of sediment between the flood plain and channel of the Amazon River in Brazil. Geological Society of America Bulletin, 110(4): 450-467.

Filizola, N. and Guyot, J.L., 2009. Suspended sediment yields in the Amazon basin: an assessment using the Brazilian national data set. Hydrological Processes, 23: 3207-3215.

Franzinelli, E. and Potter, P.E., 1983. Petrology, chemistry, and texture of modern river sands, Amazon river system. Journal of Geology, 91(1): 23-39.

Frings, P.J., Clymans, W., Fontorbe, G., Gray, W., Chakrapani, G., Conley, D.J. and De La Rocha, C., 2015. Silicate weathering in the Ganges alluvial plain. Earth and Planetary Science Letters, 427: 136-148.

Frings, R.M., 2008. Downstream fining in large sand-bed rivers. Earth-Science Reviews, 87(1-2): 39-60.

Gabet, E.J., Burbank, D.W., Pratt-Sitaula, B., Putkonen, J. and Bookhagen, B., 2008. Modern erosion rates in the High Himalayas of Nepal. Earth and Planetary Science Letters, 267(3-4): 482-494.

Gabet, E.J. and Mudd, S.M., 2009. A theoretical model coupling chemical weathering rates with denudation rates. Geology, 37(2): 151-154.

Galy, V., France-Lanord, C. and Lartiges, B., 2008. Loading and fate of particulate organic carbon from the Himalaya to the Ganga-Brahmaputra delta. Geochimica Et Cosmochimica Acta, 72(7): 1767-1787.

Godard, V., Bourlès, D.L., Spinabella, F., Burbank, D.W., Bookhagen, B., Fisher, G.B., Moulin, A. and Léanni, L., 2014. Dominance of tectonics over climate in Himalayan denudation. Geology.

Godard, V., Burbank, D.W., Bourlès, D.L., Bookhagen, B., Braucher, R. and Fisher, G.B., 2012. Impact of glacial erosion on 10Be concentrations in fluvial sediments of the Marsyandi catchment, central Nepal. Journal of Geophysical Research: Earth Surface, 117(F3): F03013.

Godard, V., Tucker, G.E., Burch Fisher, G., Burbank, D.W. and Bookhagen, B., 2013. Frequency-dependent landscape response to climatic forcing. Geophysical Research Letters, 40(5): 859-863.

Goethals, M.M., Hetzel, R., Niedermann, S., Wittmann, H., Fenton, C.R., Kubik, P., Christl, M. and Von Blanckenburg, F., 2009. An improved experimental determination of cosmogenic $^{10}Be/^{21}Ne$ and $^{26}Al/^{21}Ne$ production ratios in quartz. Earth and Planetary Science Letters, 284: 187-198.

Gosse, J.C. and Phillips, F.M., 2001. Terrestrial in situ cosmogenic nuclides: theory and application. Quaternary Science Reviews, 20(14): 1475-1560.

Graly, J.A., Bierman, P.R., Reusser, L.J. and Pavich, M.J., 2010. Meteoric 10Be in soil profiles: A global meta-analysis. Geochimica Et Cosmochimica Acta, 74(23): 6814-6829.

Graly, J.A., Reusser, L.J. and Bierman, P.R., 2011. Short and long-term delivery rates of meteoric 10Be to terrestrial soils. Earth and Planetary Science Letters, 302(3-4): 329-336.

Granger, D.E., 2006. A review of burial dating methods using ^{26}Al and ^{10}Be. Special Paper 415: In Situ-Produced Cosmogenic Nuclides and Quantification of Geological Processes, 415(0): 1-16.

Granger, D.E., Kirchner, J.W. and Finkel, R., 1996. Spatially averaged long-term erosion rates measured from in situ-produced cosmogenic nuclides in alluvial sediment. Journal of Geology, 104(3): 249-257.

Granger, D.E., Lifton, N.A. and Willenbring, J.K., 2013. A cosmic trip: 25 years of cosmogenic nuclides in geology. Geological Society of America Bulletin, 125(9-10): 1379-1402.

Granger, D.E. and Muzikar, P.F., 2001. Dating sediment burial with in situ-produced cosmogenic nuclides: theory, techniques, and limitations. Earth and Planetary Science Letters, 188(1-2): 269-281.

Granger, D.E. and Riebe, C.S., 2007. Cosmogenic nuclides in weathering and erosion. In: J.I. Drever (Editor), Treatise on Geochemistry. Surface and Ground Water, Weathering, and Soils. Elsevier, London.

Granger, D.E. and Schaller, M., 2014. Cosmogenic Nuclides and Erosion at the Watershed Scale. Elements, 10(5): 369-373.

Guyot, J.L., Filizola, N. and Laraque, A., 2005. The suspended sediment flux of the River Amazon at Obidos, Brazil, 1995-2003. In: D.E. Walling and A.J. Horowitz (Editors), Proceedings of symposium S1 held during the Seventh IAHS Scientific Assembly. IAHS Publication, Foz do Iguaco, BRAZIL, pp. 347-354.

Guyot, J.L., Filizola, N., Quintanilla, J. and Cortez, J., 1996. Dissolved solids and suspended sediment yields in the Rio Madeira basin, from the Bolivian Andes to the Amazon, Proceedings of the Exeter Symposium. IAHS Publication, Exeter, UK, pp. 55-63.

Haeuselmann, P., Granger, D.E., Jeannin, P.Y. and Lauritzen, S.E., 2007. Abrupt glacial valley incision at 0.8 Ma dated from cave deposits in Switzerland. Geology, 35(2): 143-146.

Heikkilä, U., Beer, J., Abreu, J.A. and Steinhilber, F., 2013. On the Atmospheric Transport and Deposition of the Cosmogenic Radionuclides (10Be): A Review. Space Science Reviews, 176(1-4): 321-332.

Hewawasam, T., von Blanckenburg, F., Schaller, M. and Kubik, P., 2003. Increase of human over natural erosion rates in tropical highlands constrained by cosmogenic nuclides. Geology, 31(7): 597-600.

Hidy, A.J., Gosse, J.C., Blum, M.D. and Gibling, M.R., 2014. Glacial-interglacial variation in denudation rates from interior Texas, USA, established with cosmogenic nuclides. Earth and Planetary Science Letters, 390(0): 209-221.

Hinderer, M., 2012. From gullies to mountain belts: A review of sediment budgets at various scales. Sedimentary Geology, 280(0): 21-59.

Hinderer, M., Kastowski, M., Kamelger, A., Bartolini, C. and Schlunegger, F., 2013. River loads and modern denudation of the Alps- A review. Earth-Science Reviews, 118(0): 11-44.

Hippe, K., Kober, F., Zeilinger, G., Ivy-Ochs, S., Maden, C., Wacker, L., Kubik, P.W. and Wieler, R., 2012. Quantifying denudation rates and sediment storage on the eastern Altiplano, Bolivia, using cosmogenic 10Be, 26Al, and in situ 14C. Geomorphology, 179(0): 58-70.

Horowitz, A.J., 2003. An evaluation of sediment rating curves for estimating suspended sediment concentrations for subsequent flux calculations. Hydrological Processes, 17: 3387-3409.

Hovius, N. (Editor), 1998. Controls on sediment supply by large rivers. Relative role of eustasy, climate, and tectonism in continental rocks, 59. Society for Sedimentary Geology Special Publication (SEPM), Tulsa, Oklahoma, 3-16 pp.

Hovius, N., Meunier, P., Lin, C.-W., Chen, H., Chen, Y.-G., Dadson, S., Horng, M.-J. and Lines, M., 2011. Prolonged seismically induced erosion and the mass balance of a large earthquake. Earth and Planetary Science Letters, 304(3–4): 347-355.

Hu, X., Kirby, E., Pan, B., Granger, D.E. and Su, H., 2011. Cosmogenic burial ages reveal sediment reservoir dynamics along the Yellow River, China. Geology, 39(9): 839-842.

Insel, N., Ehlers, T.A., Schaller, M., Barnes, J.B., Tawackoli, S. and Poulsen, C.J., 2010. Spatial and temporal variability in denudation across the Bolivian Andes from multiple geochronometers. Geomorphology, 122(1-2): 65-77.

Ivy-Ochs, S. and Kober, F., 2008. Surface exposure dating with cosmogenic nuclides. Quaternary Science Journal, 57(1-2): 179-209.

Jerolmack, D.J. and Paola, C., 2010. Shredding of environmental signals by sediment transport. Geophysical Research Letters, 37(19): L19401.

Jha, P.K., Subramanian, V. and Sitasawad, R., 1988. Chemical and sediment mass transfer in the Yamuna River — A tributary of the Ganges system. Journal of Hydrology, 104(1–4): 237-246.

Kirchner, J.W., Finkel, R.C., Riebe, C.S., Granger, D.E., Clayton, J.L., King, J.G. and Megahan, W.F., 2001. Mountain erosion over 10 yr, 10 k.y., and 10 m.y. time scales. Geology, 29(7): 591-594.

Kober, F., Zeilinger, G., Hippe, K., Marc, O., Lendzioch, T., Grischott, R., Christl, M., Kubik, P.W. and Zola, R., 2015. Tectonic and lithological controls on denudation rates in the central Bolivian Andes. Tectonophysics, 657: 230-244.

Kohl, C.P. and Nishiizumi, K., 1992. Chemical isolation of quartz for measurement of in-situ -produced cosmogenic nuclides. Geochimica Et Cosmochimica Acta, 56(9): 3583-3587.

Kong, P., Granger, D.E., Wu, F.-Y., Caffee, M.W., Wang, Y.-J., Zhao, X.-T. and Zheng, Y., 2009. Cosmogenic nuclide burial ages and provenance of the Xigeda paleo-lake: Implications for evolution of the Middle Yangtze River. Earth and Planetary Science Letters, 278(1-2): 131-141.

Korschinek, G., Bergmaier, A., Faestermann, T., Gerstmann, U.C., Knie, K., Rugel, G., Wallner, A., Dillmann, I., Dollinger, G., von Gostomski, C.L., Kossert, K., Maiti, M., Poutivtsev, M. and Remmert, A., 2010. A new value for the half-life of ^{10}Be by heavy-ion elastic recoil detection and liquid scintillation counting. Nuclear Instruments & Methods in Physics Research Section B- Beam Interactions with Materials and Atoms, 268(2): 187-191.

Korup, O., 2012. Earth's portfolio of extreme sediment transport events. Earth-Science Reviews, 112(3-4): 115-125.

Lal, D., 1991. Cosmic ray labeling of erosion surfaces: in situ nuclide production rates and erosion models. Earth and Planetary Science Letters, 104(2-4): 424-439.

Latrubesse, E.M., 2015. Large rivers, megafans and other Quaternary avulsive fluvial systems: A potential “who's who” in the geological record. Earth-Science Reviews, 146(0): 1-30.

Lauer, J.W. and Willenbring, J.K., 2010. Steady-state reach-scale theory for radioactive tracer concentration in a simple channel/floodplain system. J. Geophys. Res. Earth Surface, 115: F04018.

Libby, W., 1955. Radiocarbon Dating. University of Chicago Press, Chicago.

Lifton, N., Sato, T. and Dunai, T.J., 2014. Scaling in situ cosmogenic nuclide production rates using analytical approximations to atmospheric cosmic-ray fluxes. Earth and Planetary Science Letters, 386(0): 149-160.

Lifton, N.A., Jull, A.J.T. and Quade, J., 2001. A new extraction technique and production rate estimate for in situ cosmogenic C-14 in quartz. Geochimica Et Cosmochimica Acta, 65(12): 1953-1969.

Lin, G.-W., Chen, H., Hovius, N., Horng, M.-J., Dadson, S., Meunier, P. and Lines, M., 2008. Effects of earthquake and cyclone sequencing on landsliding and fluvial sediment transfer in a mountain catchment. Earth Surface Processes and Landforms, 33(9): 1354-1373.

Lupker, M., France-Lanord, C., Lavè, J., Bouchez, J., Galy, V., Mètivier, F., Gaillardet, J., Lartiges, B. and Mugnier, J.-L., 2011. A Rouse-based method to integrate the chemical composition of river sediments: Application to the Ganga basin. J. Geophys. Res., 116(F4): F04012.

Lupker, M., Blard, P.-H., Lavé, J., France-Lanord, C., Leanni, L., Puchol, N., Charreau, J. and Bourlès, D., 2012a. ^{10}Be-derived Himalayan denudation rates and sediment budgets in the Ganga basin. Earth and Planetary Science Letters, 333-334(0): 146-156.

Lupker, M., France-Lanord, C., Galy, V., Lavé, J., Gaillardet, J., Gajurel, A.P., Guilmette, C., Rahman, M., Singh, S.K. and Sinha, R., 2012b. Predominant floodplain over mountain weathering of Himalayan sediments (Ganga basin). Geochimica Et Cosmochimica Acta, 84(0): 410-432.

Lupker, M., Hippe, K., Wacker, L., Christl, M. and Wieler, R., 2014. Sediment transfer in a Himalayan catchment, ETH Zuerich, Zuerich, Switzerland.

Martinez, J.M., Guyot, J.L., Filizola, N. and Sondag, F., 2009. Increase in suspended sediment discharge of the Amazon River assessed by monitoring network and satellite data. Catena, 79(3): 257-264.

Masarik, J. and Beer, J., 1999. Simulation of particle fluxes and cosmogenic nuclide production in the Earth's atmosphere. Journal of Geophysical Research: Atmospheres, 104(D10): 12099-12111.

Masarik, J. and Reedy, R.C., 1995. Terrestrial cosmogenic-nuclide production systematics calculated from numerical simulations. Earth and Planetary Science Letters, 136(3-4): 381-395.

Matmon, A., Crouvi, O., Enzel, Y., Bierman, P., Larsen, J., Porat, N., Amit, R. and Caffee, M., 2003. Complex exposure histories of chert clasts in the late Pleistocene shorelines of Lake Lisan, southern Israel. Earth Surface Processes and Landforms, 28(5): 493-506.

Matmon, A., Stock, G.M., Granger, D.E. and Howard, K.A., 2011. Dating of Pliocene Colorado River sediments: Implications for cosmogenic burial dating and the evolution of the lower Colorado River. Geological Society of America Bulletin: B30453.1.

Maurice, L., Quiroga, I., Guyot, J.L. and Malm, O., 1999. Mercury pollution in the Upper Beni River, Amazonian Basin: Bolivia. Ambio, 28(4): 302-306.

McKean, J.A., Dietrich, W.E., Finkel, R.C., Southon , J.R. and Caffee, M.W., 1993. Quantification of soil production and downslope creep rates from cosmogenic 10Be accumulations on a hillslope profile. Geology, 21(4): 343-346.

McPhillips, D., Hoke, G.D., Liu-Zeng, J., Bierman, P.R., Rood, D.H. and Niedermann, S., 2016. Dating the incision of the Yangtze River gorge at the First Bend using three-nuclide burial ages. Geophysical Research Letters: n/a-n/a.

Meade, R.H., 1985. Suspended Sediment in the Amazon River and its tributaries in Brazil during 1982-1984, U.S. Geological Survey, Washington, D.C.

Mertes, L.A.K., Dunne, T. and Martinelli, L.A., 1996. Channel-floodplain geomorphology along the Solimoes-Amazon River, Brazil. Geological Society of America Bulletin, 108(9): 1089-1107.

Mertes, L.A.K. and Meade, R.H., 1985. Particle sizes of sands collected from the bed of the Amazon River and its tributaries during 1982–1984, U.S. Geological Survey, Washington, D.C.

Métivier, F. and Gaudemer, Y., 1999. Stability of output fluxes of large rivers in South and East Asia during the last 2 million years: implications on floodplain processes. Basin Research, 11(4): 293-303.

Milliman, J. and Meade, R.H., 1983. World-wide delivery of river sediment to the oceans. Journal of Geology, 91: 1-21.

Monaghan, M.C., McKean, J., Dietrich, W. and Klein, J., 1992. ^{10}Be chronometry of bedrock-to-soil conversion rates. Earth and Planetary Science Letters, 111(2-4): 483-492.

Niedermann, S., 2000. The 21Ne production rate in quartz revisited. Earth and Planetary Science Letters, 183(3,Äì4): 361-364.

Niedermann, S., 2002. Cosmic-Ray-Produced Noble Gases in Terrestrial Rocks: Dating Tools for Surface Processes. Reviews in Mineralogy and Geochemistry, 47(1): 731-784.

Niemi, N.A., Oskin, M., Burbank, D.W., Heimsath, A.M. and Gabet, E.J., 2005. Effects of bedrock landslides on cosmogenically determined erosion rates. Earth and Planetary Science Letters, 237(3-4): 480-498.

Nittrouer, C.A. and Kuehl, S.A., 1995. Geological significance of sediment transport and accumulation on the Amazon continental shelf- Preface. Marine Geology, 125(3-4): 175-176.

Nordin, C.F., Meade, R.H., Curtis, W.F., Bosio, N.J. and Landim, P.M.B., 1980. Size distribution of Amazon River bed sediment. Nature, 286(5768): 52-53.

Norton, K., von Blanckenburg, F., DiBiase, R., Schlunegger, F. and Kubik, P., 2011. Cosmogenic ^{10}Be-derived denudation rates of the Eastern and Southern European Alps. International Journal of Earth Sciences, online first: 1-17.

Ouimet, W., Dethier, D., Bierman, P., Wyshnytzky, C., Shea, N. and Rood, D.H., 2015. Spatial and temporal variations in meteoric 10Be inventories and long-term deposition rates, Colorado Front Range. Quaternary Science Reviews, 109: 1-12.

Partridge, T.C., Granger, D.E., Caffee, M.W. and Clarke, R.J., 2003. Lower Pliocene Hominid Remains from Sterkfontein. Science, 300(5619): 607-612.

Pavich, M.J., Brown, L., Klein, J. and Middleton, R., 1984. ^{10}Be accumulation in a soil chronosequence. Earth and Planetary Science Letters, 68(2): 198-204.

Pepin, E., Guyot, J.L., Armijos, E., Bazan, H., Fraizy, P., Moquet, J.S., Noriega, L., Lavado, W., Pombosa, R. and Vauchel, P., 2013. Climatic control on eastern Andean denudation rates (Central Cordillera from Ecuador to Bolivia). Journal of South American Earth Sciences, 44(0): 85-93.

Phillips, F.M., Argento, D.C., Balco, G., Caffee, M.W., Clem, J., Dunai, T.J., Finkel, R., Goehring, B., Gosse, J.C., Hudson, A.M., Jull, A.J.T., Kelly, M.A., Kurz, M., Lal, D., Lifton, N., Marrero, S.M., Nishiizumi, K., Reedy, R.C., Schaefer, J., Stone, J.O.H., Swanson, T. and Zreda, M.G., 2016. The CRONUS-Earth Project: A synthesis. Quaternary Geochronology, 31: 119-154.

Phillips, J.D., 2003. Alluvial storage and the long-term stability of sediment yields. Basin Research, 15(2): 153-163.

Rai, S.K., Singh, S.K. and Krishnaswami, S., 2010. Chemical weathering in the Plain and Peninsular sub-basins of the Ganga: Impact on Major ion chemistry and Elemental Fluxes. Geochimica Et Cosmochimica Acta, 74(8): 2340-2355.

Reusser, L., Graly, J., Bierman, P. and Rood, D., 2010. Calibrating a long-term meteoric ^{10}Be accumulation rate in soil. Geophysical Research Letters, 37(19): L19403.

Riebe, C.S. and Granger, D.E., 2013. Quantifying effects of deep and near-surface chemical erosion on cosmogenic nuclides in soils, saprolite, and sediment. Earth Surface Processes and Landforms, 38(5): 523-533.

Romans, B.W., Castelltort, S., Covault, J.A., Fildani, A. and Walsh, J.P., 2015. Environmental signal propagation in sedimentary systems across timescales. Earth-Science Reviews, 153: 7-29.

Rudnick, R.L. and Gao, S., 2004. Composition of the Continental Crust. In: D.H. Heinrich and K.T. Karl (Editors), Treatise on Geochemistry. Elsevier, Amsterdam, pp. 1-64.

Safran, E.B., Bierman, P., Aalto, R., Dunne, T., Whipple, K.X. and Caffee, M., 2005. Erosion rates driven by channel network incision in the Bolivian Andes. Earth Surface Processes and Landforms, 30: 1007-1024.

Samworth, E., Warburton, E. and Engelbertink, G., 1972. Beta decay of the 26Al ground state. Physical Review C, 5(1): 138-142.

Santini, W., Martinez, J.M., Espinoza Villar, R., Cochonneau, G., Vauchel, P., Moquet , J.S., Baby, P., Espinoza Villar, J.C., Lavado Casimiro, W.S., Carranza Valle, J.L. and Guyot, J.L., 2014. Sediment budget in the Ucayali River basin, an Andean tributary of the Amazon River, Sediment Dynamics from the Summit to the Sea. IAHS Publication, New Orleans, USA, pp. 320-325.

Schaller, M., von Blanckenburg, F., Hovius, N. and Kubik, P.W., 2001. Large-scale erosion rates from in situ-produced cosmogenic nuclides in European river sediments. Earth and Planetary Science Letters, 188(3-4): 441-458.

Schaller, M., von Blanckenburg, F., Hovius, N., Veldkamp, A., van den Berg, M.W. and Kubik, P.W., 2004. Paleoerosion rates from cosmogenic Be-10 in a 1.3 Ma terrace sequence: Response of the river meuse to changes in climate and rock uplift. Journal of Geology, 112(2): 127-144.

Schaller, M., von Blanckenburg, F., Veldkamp, A., Tebbens, L.A., Hovius, N. and Kubik, P.W., 2002. A 30 000 yr record of erosion rates from cosmogenic Be-10 in Middle European river terraces. Earth and Planetary Science Letters, 204(1-2): 307-320.

Scherler, D., Bookhagen, B. and Strecker, M.R., 2014. Tectonic control on 10Be-derived erosion rates in the Garhwal Himalaya, India. Journal of Geophysical Research: Earth Surface, 119: 1-23.

Shen, C., Beer, J., Kubik, P.W., Suter, M., Borkovec, M. and Liu, T.S., 2004. Grain size distribution, ^{10}Be content and magnetic susceptibility of micrometer-nanometer loess materials. Nuclear Instruments and Methods in Physics Research Section B: Beam Interactions with Materials and Atoms, 223-224: 613-617.

Simpson, G. and Castelltort, S., 2012. Model shows that rivers transmit high-frequency climate cycles to the sedimentary record. Geology, 40(12): 1131-1134.

Singh, M., Singh, I.B. and Müller, G., 2007. Sediment characteristics and transportation dynamics of the Ganga River. Geomorphology, 86(1–2): 144-175.

Sinha, R. and Friend, P.F., 1994. River systems and their sediment flux, Indo-Gangetic plains, Northern Bihar, India. Sedimentology, 41(4): 825-845.

Stock, G.M., Anderson, R.S. and Finkel, R.C., 2005. Rates of erosion and topographic evolution of the Sierra Nevada, California, inferred from cosmogenic 26Al and 10Be concentrations. Earth Surface Processes and Landforms, 30(8): 985-1006.

Stone, J.O., 2000. Air pressure and cosmogenic isotope production. Journal of Geophysical Research- Solid Earth, 105(B10): 23753-23759.

Summerfield, M.A. and Hulton, N.J., 1994. Natural controls of fluvial denudation rates in major world drainage basin. Journal of Geophysical Research-Solid Earth, 99(B7): 13871-13883.

Syvitski, J.P.M., Vorosmarty, C.J., Kettner, A.J. and Green, P., 2005. Impact of humans on the flux of terrestrial sediment to the global coastal ocean. Science, 308(5720): 376-380.

Tessier, A., Campbell, P.G.C. and Bisson, M., 1979. Sequential extraction procedure for the speciation of particulate trace metals. Analytical Chemistry, 51(7): 844-851.

Vanacker, V., von Blanckenburg, F., Govers, G., Molina, A., Poesen, J., Deckers, J. and Kubik, P., 2007. Restoring dense vegetation can slow mountain erosion to near natural benchmark levels. Geology, 35(4): 303-306.

Vance, D., Bickle, M., IvyOchs, S. and Kubik, P., 2003. Erosion and exhumation in the Himalaya from cosmogenic isotope inventories of river sediments. Earth and Planetary Science Letters, 206: 273-288.

Viparelli, E., Wesley Lauer, J., Belmont, P. and Parker, G., 2013. A numerical model to develop long-term sediment budgets using isotopic sediment fingerprints. Computers & Geosciences, 53(0): 114-122.

von Blanckenburg, F., 2005. The control mechanisms of erosion and weathering at basin scale from cosmogenic nuclides in river sediment. Earth and Planetary Science Letters, 237(3-4): 462-479.

von Blanckenburg, F. and Bouchez, J., 2014. River fluxes to the sea from the oceans 10Be/9Be ratio. Earth and Planetary Science Letters, 387(0): 34-43.

von Blanckenburg, F., Bouchez, J., Ibarra, D.E. and Maher, K., 2015. Stable runoff and weathering fluxes into the oceans over Quaternary climate cycles. Nature Geoscience, 8(7): 538-542.

von Blanckenburg, F., Bouchez, J. and Wittmann, H., 2012. Earth surface erosion and weathering from the ^{10}Be (meteoric)/^{9}Be ratio. Earth and Planetary Science Letters, 351-352: 295-305.

von Blanckenburg, F. and Willenbring, J.K., 2014. Cosmogenic Nuclides: Dates and Rates of Earth-Surface Change. Elements, 10(5): 341-346.

Walling, D.E., 1983. The sediment delivery problem. Journal of Hydrology, 65(1-3): 209-237.

West, A.J., Galy, A. and Bickle, M., 2005. Tectonic and climatic controls on silicate weathering. Earth and Planetary Science Letters, 235(1-2): 211-228.

Willenbring, J.K. and von Blanckenburg, F., 2010. Meteoric cosmogenic Beryllium-10 adsorbed to river sediment and soil: Applications for Earth-surface dynamics. Earth-Science Reviews, 98(1-2): 105-122.

Wittmann, H. and von Blanckenburg, F., 2009. Cosmogenic nuclide budgeting of floodplain sediment transfer. Geomorphology, 109(3-4): 246-256.

Wittmann, H., von Blanckenburg, F., Bouchez, J., Dannhaus, N., Naumann, R., Christl, M. and Gaillardet, J., 2012. The dependence of meteoric ^{10}Be concentrations on particle size in Amazon River bed sediment and the extraction of reactive ^{10}Be/^{9}Be ratios. Chemical Geology, 318-319(0): 126-138.

Wittmann, H., von Blanckenburg, F., Dannhaus, N., Bouchez, J., Guyot, J.L., Maurice, L., Roig, H., Filizola, N., Gaillardet, J. and Christl, M., 2015. A test of the new cosmogenic ^{10}Be(meteoric)/^{9}Be proxy for simultaneously determing basin-wide erosion rates, denudation rates, and the degree of weathering in the Amazon basin. Journal of Geophysical Research- Earth Surface, 120(12): 2498-2528.

Wittmann, H., von Blanckenburg, F., Guyot, J.-L., Laraque, A., Bernal, C. and Kubik, P., 2010. Sediment production and transport from in-situ produced cosmogenic ^{10}Be and river loads in the Napo River basin, an upper Amazon tributary of Ecuador and Peru. Journal of South American Earth Sciences, 31: 45-53.

Wittmann, H., von Blanckenburg, F., Guyot, J.L., Maurice, L. and Kubik, P.W., 2009. From source to sink: Preserving the cosmogenic 10Be-derived denudation rate signal of the Bolivian Andes in sediment of the Beni and Mamoré foreland basins. Earth and Planetary Science Letters, 288(3-4): 463-474.

Wittmann, H., von Blanckenburg, F., Kruesmann, T., Norton, K.P. and Kubik, P.W., 2007. Relation between rock uplift and denudation from cosmogenic nuclides in river sediment in the Central Alps of Switzerland. Journal of Geophysical Research-Earth Surface, 112(F4).

Wittmann, H., von Blanckenburg, F., Maurice, L., Guyot, J.L., Filizola, N. and Kubik, P.W., 2011a. Sediment production and delivery in the Amazon River basin quantified by in situ-produced cosmogenic nuclides and recent river loads. Geological Society of America Bulletin, 123(5-6): 934-950.

Wittmann, H., von Blanckenburg, F., Maurice, L., Guyot, J.-L. and Kubik, P., 2011b. Recycling of Amazon floodplain sediment quantified by cosmogenic Al-26 and Be-10. Geology, 39(5): 467-470.

Wobus, C., Heimsath, A., Whipple, K. and Hodges, K., 2005. Active out-of-sequence thrust faulting in the central Nepalese Himalaya. Nature, 434(7036): 1008-1011.

Yanites, B.J., Tucker, G.E. and Anderson, R.S., 2009. Numerical and analytical models of cosmogenic radionuclide dynamics in landslide-dominated drainage basins. Journal of Geophysical Research, 114.

You, C.F., Lee, T., Brown, L., Shen, J.J. and Chen, J.C., 1988. 10Be study of rapid erosion in Taiwan. Geochimica Et Cosmochimica Acta, 52(11): 2687-2691.

Supplemantary Information

Part A- TREATMENT OF COSMOGENIC NUCLIDE DATA

Please note that where necessary, we have recalculated published cosmogenic nuclide concentration data mentioned below relative to the secondary AMS standard "07KNSTD" ((Nishiizumi et al., 2007); measured relative to a half life of 1.39 ± 0.012x10^6 yrs by Chmeleff et al. (2010); Korschinek et al. (2010)) to make the data comparable. We then re-calculated all denudation rates relative to Dunai (2000) time-independent scaling scheme and a corresponding SLHL nucleogenic production rate (Borchers et al., 2016; Phillips et al., 2016) of 3.7 at/$g_{(Qtz)}$/yr. Muonic contributions are ca. 1% at SLHL, yielding a total SLHL production rates of 3.75 at/$g_{(Qtz)}$/yr used, where muonic coefficients were calculated following Braucher et al. (2011), using values of 157 g/cm^2 for neutrons, 1500 g/cm^2 for slow muons, and 4320 g/cm^2 for fast muons, respectively (Braucher et al., 2011). Note that the procedure for re-calculation of production rates and nuclide concentrations is summarized in the supplement table A1 of Wittmann et al. (2011). Production rates were calculated on a pixel-by-pixel basis using a 90 m SRTM DEM (except for large basins from Andermann (2011), and those by Lupker et al. (2012)which were

calculated using a 1 km-resolution DEM). Topographic shielding was carried out following Norton and Vanacker (2009) and the nucleogenic production rate was set to zero for pixels covered by ice using a digital glacier map for the Himalayas (National Snow and Ice Data Center, 1999). A snow shielding correction factor as well as a correction due to changes in Earth´s magnetic field were not applied.

Part B- COMPILATION OF SEDIMENT STORAGE TIMES IN FLOODPLAINS OF THE AMAZON AND GANGA BASINS

Supplement Table A1: Estimates of storage times in the Amazon and Ganga basins

Basin & position in sediment cascade		Method	Estimated *t* ($x10^3$ yr)	Mode of estimation	Reference
Amazon	Headwaters	U-Series disequilibria	3	"lag time"	Dosseto et al., 2006
	Lowlands	Channel belt width and river migration rates	4	Beni tributary only	Wittmann and von Blanckenburg, 2009
		U-Series disequilibria	14	transfer time for reach Beni - Madeira confl.	Dosseto et al., 2006
		Size of entire floodplain reservoir and river migration rates	200	"floodplain response time" to remove entire floodplain reservoir during e.g. sea level drop[a]	Castelltort and Van Den Driessche, 2003
		Size of entire floodplain reservoir and river migration rates	700	"floodplain response time" to remove entire floodplain reservoir during e.g. sea level drop[a]	Wittmann et al., 2011 (based on Métivier & Gaudemer, 1999)
Ganga	Headwaters	Dating of valley fills	3-32; up to 100	"lag time"	Blöthe & Korup, 2013
	Lowlands	Channel belt width and river migration rates	1.4	time to remove sand reservoir in floodplain	Lupker et al., 2012a (based on Lauer & Willenbring, 2010)
		U-Series disequilibria	20-25	transfer time for susp. sediment	Granet et al., 2010
		U-Series disequilibria	<100	transfer time for bedload	Granet et al., 2007
		Size of entire floodplain reservoir and river migration rates	100	"floodplain response time" to remove entire floodplain reservoir during e.g. sea level drop[a]	Castelltort and Van Den Driessche, 2003
		Size of entire floodplain reservoir and river migration rates	470	"floodplain response time" to remove entire floodplain reservoir during e.g. sea level drop[a]	Métivier & Gaudemer, 1999

[a]Note that the "response times" estimated by Métivier and Gaudemer (1999) and Castelltort and Van Den Driessche (2003) are theoretical storage times. These denote the maximum time that would be needed to remove the entire floodplain reservoir (i.e. floodplain volumes are calculated from estimated storage depths and the width from entire fluvial valleys, by assuming continuous channel migration rates).

Part C- COMPILED COSMOGENIC NUCLIDE AND RIVER-LOAD GAUGING DATA

Cosmogenic nuclide data:

	Reference	Sample ID	Basin/River	Denudation Rate (mm/yr)	Total area (> ca.100 km2)	Source area (km2) (> 300m elevation)	Area-weighted value (mm/yr)	±	1σ SD of dataset	Sediment flux (Mt/yr)	±	1σ SD of dataset
AMAZON BASIN	Safran et al., 2005	BOL-31	Beni	0.21	111							
	Safran et al., 2005	BOL-16	Beni	0.073	120							
	Safran et al., 2005	BOL-28	Beni	0.57	127							
	Safran et al., 2005	BOL-01	Beni	0.90	134							
	Safran et al., 2005	BOL-25	Beni	0.16	146							
	Safran et al., 2005	BOL-27	Beni	0.48	146							
	Safran et al., 2005	BOL-40	Beni	0.26	152							
	Safran et al., 2005	BOL-24	Beni	0.25	154							
	Safran et al., 2005	BOL-34a	Beni	0.33	177							
	Safran et al., 2005	BOL-34b	Beni	0.46	177							
	Safran et al., 2005	BOL-34c	Beni	0.32	177							
	Safran et al., 2005	BOL-08	Beni	0.23	198							
	Safran et al., 2005	BOL-17	Beni	0.18	248							
	Safran et al., 2005	BOL-45	Beni	0.64	348							
	Safran et al., 2005	BOL-43	Beni	0.24	416							
	Safran et al., 2005	BOL-30	Beni	0.39	425							
	Safran et al., 2005	BOL-14	Beni	0.18	432							
	Safran et al., 2005	BOL-44	Beni	0.50	601							
	Safran et al., 2005	BOL-32	Beni	0.20	834							
	Safran et al., 2005	BOL-37	Beni	0.38	841							
	Safran et al., 2005	BOL-22	Beni	0.38	1460							
	Safran et al., 2005	BOL-41	Beni	0.93	1460							
	Safran et al., 2005	BOL-19	Beni	0.32	1540							
	Safran et al., 2005	BOL-20	Beni	0.49	1760							
	Safran et al., 2005	BOL-07	Beni	0.22	2930							
	Safran et al., 2005	BOL-13	Beni	0.21	3230							
	Safran et al., 2005	BOL-21	Beni	0.17	5360							
	Safran et al., 2005	BOL-38a	Beni	0.43	5410							
	Safran et al., 2005	BOL-38b	Beni	0.41	5410							
	Safran et al., 2005	BOL-15	Beni	0.23	5830							
	Safran et al., 2005	BOL-42	Beni	0.40	10400							
	Safran et al., 2005	BOL-18	Beni	0.14	10900							
	Safran et al., 2005	BOL-50	Beni	0.57	70200							
	Insel et al., 2010	N04	Beni	0.14	332							
	Insel et al., 2010	N04-2	Beni	0.15	332							
	Insel et al., 2010	N05	Beni	0.10	205							
	Wittmann et al., 2009	BE 1a	Beni	0.29	68000							
	Wittmann et al., 2009	BE 1b	Beni	0.31	68000		0.37	±	0.20	66	±	35
										(using 68000 km2 for conversion)		
	Insel et al., 2010	S08	Grande	0.33	129							
	Insel et al., 2010	S09	Grande	0.35	152							
	Insel et al., 2010	S09-2	Grande	0.35	152							
	Insel et al., 2010	S12	Grande	0.24	1036							
	Insel et al., 2010	S06	Grande	0.028	1318							
	Wittmann et al., 2009	PIR 18b	Grande	0.36	1590							
	Wittmann et al., 2009	PIR 18c	Grande	0.48	1590							
	Insel et al., 2010	S15	Grande	0.42	3127							
	Insel et al., 2010	S04	Grande	0.08	3763							
	Insel et al., 2010	S04-2	Grande	0.15	3763							
	Wittmann et al., 2009	CHA 23a	Grande	0.22	4862							
	Insel et al., 2010	S10	Grande	0.23	5194							
	Wittmann et al., 2009	MAN 15b	Grande	0.33	5298							
	Wittmann et al., 2009	ICH 21a	Grande	0.31	7580							
	Wittmann et al., 2009	GR 25a	Grande	0.13	23500							
	Wittmann et al., 2009	GR 17b-Mts only	Grande	0.39	59800							
	Wittmann et al., 2009	GR 19b	Grande	0.54	59800		0.38	±	0.14	60	±	22
										(using 59800 km2 for conversion)		
	Wittmann et al., 2010	Na 0a-1	Solimoes	0.37	5270							
	Wittmann et al., 2010	Na 0a-2	Solimoes	0.30	5270							
	Wittmann et al., 2010	Na 1b	Solimoes	0.40	12400							
	Wittmann et al., 2011	Pe 107a-1	Solimoes	0.23	238000							
	Wittmann et al., 2011	Pe 107a-2	Solimoes	0.25	238000							
	Wittmann et al., 2011	Pe 101a-1	Solimoes	0.13	630000							
	Wittmann et al., 2011	Pe 101a-2	Solimoes	0.12	630000		0.16	±	0.11	260	±	180
										(using 630000 km2 for conversion)		
							Entire Andes draining to Amazon: **0.19**	±	**0.18**			
			total area used for conversion:		**757800**					**380**	±	**350**

	Reference	Sample ID	Basin/River	Denudation Rate (mm/yr)	Total area (> ca.100 km2)	Source area (km2) (> 300m elevation)	FC-corr D (mm/yr)	±	1σ SD of dataset	Sediment flux (Mt/yr)	±	1σ SD of dataset
FLOODPLAIN	Wittmann et al., 2009	MAR 18a-1	Marmoré	0.12	599400	282214	0.15					
	Wittmann et al., 2009	MAR 18a-2	Marmoré	0.10	599400	282214	0.13					
	Wittmann et al., 2009	MAD 19a	Madeira	0.16	881900	282214	0.19					
	Wittmann et al., 2009	MAD 20a-1	Madeira	0.16	954300	282214	0.19					
	Wittmann et al., 2009	MAD 20a-2	Madeira	0.20	954300	282214	0.24					
	Wittmann et al., 2011	(3)-Napo lower	Lower Napo	0.12	93171	17715	0.20					
	Wittmann et al., 2011	(4)-Man 0.2a	Manacapuru	0.13	2270010	500272	0.18					
	Wittmann et al., 2011	(4)-Man 1.1a	Manacapuru	0.13	2270010	500272	0.19					
	Wittmann et al., 2011	(4)-Man 2.85a	Manacapuru	0.12	2270010	500272	0.17					
	Wittmann et al., 2011	(7)-Ir 1.75a	Iracema	0.11	3154060	628165	0.17					
	Wittmann et al., 2011	(7)-Ir 1.75b	Iracema	0.12	3154060	628165	0.19					
	Wittmann et al., 2011	(8)-Mad 0.5a	Madeira	0.09	1336000	282214	0.14					
	Wittmann et al., 2011	(8)-Mad 1.8a	Madeira	0.13	1336000	282214	0.19					
	Wittmann et al., 2011	(8)-Mad 1.8b	Madeira	0.09	1336000	282214	0.13					
	Wittmann et al., 2011	Par 0.9a	Parintins	0.11	4736250	947182	0.17					
	Wittmann et al., 2011	Par 2.2a	Parintins	0.10	4736250	947182	0.15					
	Wittmann et al., 2011	Par 2.2b	Parintins	0.10	4736250	947182	0.15					
	Wittmann et al., 2011	(16)-Ama-a	Obidos	0.09	5087830	947182	0.14					
	Wittmann et al., 2011	Soc-b	Varzea	0.11	5087830	947182	0.22					
	Wittmann et al., 2011	Soc-c1	Varzea	0.11	5087830	947182	0.22					
	Wittmann et al., 2011	Soc-c2	Varzea	0.12	5087830	947182	0.25					
	Wittmann et al., 2011	Gran-b	Varzea	0.07	5087830	947182	0.15					
	Wittmann et al., 2011	Gran-c	Varzea	0.09	5087830	947182	0.19					
			total area used for conversion:		757800		0.18	±	0.03	350	±	65

	Reference	Sample ID	Basin/River	Denudation Rate (mm/yr)	Area (> ca.100 km2)	Area-weighted value (mm/yr)	±	1σ SD of dataset	Sediment flux (Mt/yr)	±	1σ SD of dataset
GANGA	Vance et al., 2003	AK43	Upper Ganga	0.87	21690						
BASIN	Vance et al., 2003	AK36	Upper Ganga	0.87	21690						
	Lupker et al., 2012	BR924-Mts only	Upper Ganga	1.91	21690	1.22	±	0.60	100 (using 32400 km2 for conversion)	±	50
	Scherler et al., 2014	DS7-048/1	Yamuna	0.44	100						
	Scherler et al., 2014	DS6-080A/14	Yamuna	1.41	103						
	Scherler et al., 2014	DS7-088/16	Yamuna	0.25	123						
	Scherler et al., 2014	DS7-077/9	Yamuna	0.31	128						
	Scherler et al., 2014	DS7-049/2	Yamuna	0.13	168						
	Scherler et al., 2014	DS7-061/4	Yamuna	0.10	210						
	Scherler et al., 2014	DS6-088/18	Yamuna	0.84	231						
	Scherler et al., 2014	DS7-072/10	Yamuna	0.23	514						
	Scherler et al., 2014	DS6-094/P1	Yamuna	0.31	516						
	Scherler et al., 2014	DS6-081/13	Yamuna	1.63	536						
	Scherler et al., 2014	DS6-023C/15	Yamuna	1.94	548						
	Scherler et al., 2014	DS7-055/Y1	Yamuna	1.00	647						
	Scherler et al., 2014	DS6-018/Y2	Yamuna	0.26	1179						
	Scherler et al., 2014	DS6-085/P2	Yamuna	0.41	1440						
	Scherler et al., 2014	DS7-071/T1	Yamuna	1.09	3477						
	Scherler et al., 2014	DS7-076/T2	Yamuna	0.99	4670						
	Lupker et al., 2012	YAM Q3-Mts only	Yamuna	0.56	7620	0.76	±	0.56	20 (using 9570 km2 for conversion)	±	14
	Lupker et al., 2012	CA10-5-Mts only	Karnali	0.48	21260						
	Lupker et al., 2012	PB80-Mts only	Karnali	1.91	45430						
	Lupker et al., 2012	LO743-Mts only	Karnali	0.79	45430	1.19	±	0.75	140 (using 45970 km2 for conversion)	±	90
	Godard et al., 2012	NEP030	Narayani	0.06	110						
	Godard et al., 2012	NIB-975-02	Narayani	2.32	136						
	Andermann-2011 PhD	NP-A5s	Narayani	0.69	148						
	Godard et al., 2012	NEP003	Narayani	0.87	614						
	Andermann-2011 PhD	NP-A1s	Narayani	0.39	657						
	Andermann-2011 PhD	NP081016A	Narayani	4.17	3000						
	Andermann-2011 PhD	CAJ-7	Narayani	1.30	3207						
	Andermann-2011 PhD	NP-A39s	Narayani	1.67	3981						
	Andermann-2011 PhD	NP-A10s	Narayani	1.83	4086						
	Andermann-2011 PhD	NP-A18s	Narayani	2.23	4798						
	Andermann-2011 PhD	Arr-3A	Narayani	2.31	5048						
	Andermann-2011 PhD	NP-A20s	Narayani	1.43	5469						
	Andermann-2011 PhD	Arr-2	Narayani	1.23	6091						
	Andermann-2011 PhD	Arr-3B	Narayani	2.38	11716						
	Andermann-2011 PhD	Arr-4	Narayani	1.35	11997						
	Lupker et al., 2012	LO741-Mts only	Narayani	1.03	31770						
	Lupker et al., 2012	CA10-10-Mts only	Narayani	1.35	31770						
	Lupker et al., 2012	LO1001-Mts only	Narayani	1.51	31770						
	Lupker et al., 2012	LO1001-Mts only	Narayani	1.67	31770						
	Godard et al., 2014	PO-150311-05	Narayani	0.21	91						
	Godard et al., 2014	KP-160311-09	Narayani	0.10	93						
	Godard et al., 2014	KP-160311-10	Narayani	0.11	97						
	Godard et al., 2014	KP-090311-05	Narayani	0.29	99						
	Godard et al., 2014	KP-090311-01	Narayani	0.14	111						
	Godard et al., 2014	TR-170311-03	Narayani	1.21	147	1.54	±	0.96	140 (using 34450 km2 for conversion)	±	70
	Godard et al., 2014	EK-180311-05	Kosi	1.43	116.5						
	Andermann-2011 PhD	NP080912A	Kosi	0.75	2105						
	Andermann-2011 PhD	NP080913A	Kosi	2.39	2572						
	Andermann-2011 PhD	NP080913B	Kosi	1.94	2962						
	Andermann-2011 PhD	NP080924A	Kosi	0.15	113						
	Lupker et al., 2012	LO763-Mts only	Kosi	0.79	53610						
	Lupker et al., 2012	CA987-Mts only	Kosi	0.40	53610						
	Lupker et al., 2012	CA987-Mts only	Kosi	0.72	53610	0.69	±	0.78	110 (using 62000 km2 for conversion)	±	125
						Entire Himalayas draining to Ganga: **1.14**	±	**0.82**			
			total area used for conversion:		**184389**				**550**	±	**390**

	Reference	Sample ID	Basin/River	Denudation Rate (mm/yr)	Total area (> ca.100 km2)	Source area (km2) (> 300m elevation)	FC-corr D (mm/yr)	±	1σ SD of dataset	Sediment flux (Mt/yr)	±	1σ SD of dataset
FLOODPLAIN	Lupker, 2012	BR355-1 Fc	Karnali	1.10	87040	64940	1.15					
	Lupker, 2012	BR355-2 Fc	Karnali	0.88	87040	64940	0.91					
	Lupker, 2012	BR343 Fc	Karnali	0.45	131840	72010	0.76					
	Lupker, 2012	BR336 Fc	Narayani	1.50	41800	34450	1.27					
	Lupker, 2012	BR310 Fc	Narayani	1.49	43500	34450	1.35					
	Lupker, 2012	BR330 Fc	Kosi	0.51	89110	56210	0.68					
	Lupker, 2012	BR8135 Sc	Ganga	0.04	390410	45540	0.37					
	Lupker, 2012	BR315 Sc	Ganga	0.15	697540	153270	0.60					
	Lupker, 2012	BR8138 Sc	Ganga	0.15	697540	153270	0.59					
	Lupker, 2012	BR418 Sc	Ganga	0.23	873240	220150	0.84					
	Lupker, 2012	BR717 Sc	Ganga	0.23	873240	220150	0.89					
	Lupker, 2012	BR8221 Sc	Ganga	0.23	873240	220150	0.84					
	Lupker, 2012	BR8252-1 Sc	Ganga	0.23	873240	220150	0.88					
	Lupker, 2012	BR8252-2 Sc	Ganga	0.23	873240	220150	0.84					
			total area used for conversion:		**184389**		0.821	±	0.27	390	±	130

Gauging data:

		River	Station Code	Total area (> ca.100 km2)	Sampled source area (km2)		Gauging-derived Load (Mt/yr)	Calculated erosion rate (mm/yr)	Area-weighted erosion value (mm/yr)	±	1σ SD of dataset
AMAZON	Pepin et al, 2013	Beni	AB	67500			161.8	0.92			
BASIN	Aalto et al., 2006	Beni	AIN	29900			115.0	1.48			
	Aalto et al., 2006	Beni	AQM	9400			36.8	1.51			
	Aalto et al., 2006	Beni	COT	5600			40.6	2.79			
	Aalto et al., 2006	Beni	LUR	810			6.4	3.04			
	Aalto et al., 2006	Beni	MIG	360			0.047	0.050			
	Aalto et al., 2006	Beni	MIS	350			0.012	0.013			
	Aalto et al., 2006	Beni	POR	240			0.80	1.28			
	Aalto et al., 2006	Beni	SIR	270			2.0	2.85			
	Aalto et al., 2006	Beni	SRC	4700			7.1	0.58			
	Aalto et al., 2006	Beni	TAM	950			2.4	0.97			
	Aalto et al., 2006	Beni	VBA	1900			7.8	1.58			
	Aalto et al., 2006	Beni	VER	140			0.011	0.030			
			sum area =	**122120**		**sum load =**	**380.8**		**1.20**	**±**	**1.06**
			largest basin=	**67500**		**"Upscaled load"=**	**210.5**				
	Aalto et al., 2006	Grande	ARC	23700			154.3	2.50			
	Aalto et al., 2006	Grande	HUR	11200			14.1	0.48			
	Aalto et al., 2006	Grande	MIZ	10800			14.1	0.50			
	Aalto et al., 2006	Grande	PAZ	4360			2.2	0.19			
	Aalto et al., 2006	Grande	PNA	31200			296.9	3.66			
	Aalto et al., 2006	Grande	AP	59800			125.0	0.80			
	Aalto et al., 2006	Pirai	ANG	1420			2.9	0.79			
	Aalto et al., 2006	Pirai	BER	480			0.60	0.48			
	Aalto et al., 2006	Pirai	EPS	203			0.42	0.80			
	Aalto et al., 2006	Pirai	LBE	2880			2.3	0.31			
	Aalto et al., 2006	Pirai	PEI	4160			1.0	0.09			
	Aalto et al., 2006	Mamoré	ICO	2300			11.4	1.91			
	Aalto et al., 2006	Mamoré	LOC	200			0.67	1.29			
	Wittmann et al., 2009	Grande	AP	59800			138.0	0.89			
	Pepin et al, 2013	Grande	ABA	59480			178.2	1.15			
			sum area =	**271983**		**sum load =**	**942.1**		**1.33**	**±**	**0.97**
			largest basin=	**59480**		**"Upscaled load"=**	**206.0**				
	Pepin et al, 2013	upper Maranon	BOR	115410			136.6	0.46			
	Pepin et al, 2013	upper Ucayali	CHA	70270			70.3	0.38			
	Pepin et al, 2013	middle Ucayali	ATA	191020			200.0	0.40			
	Santini et al., 2014	middle Ucayali	LAG	191180			445.0	0.90			
	Santini et al., 2014	middle Ucayali	PIN	22300			60.0	1.03			
	Santini et al., 2014	middle Ucayali	PUC	261070			300.0	0.44			
	Armijos et al., 2013	Napo	SEB	5272			6.2	0.46			
	Armijos et al., 2013	Napo	FDO	12443			8.2	0.25			
	Armijos et al., 2013	Napo	ROC	26861			20.8	0.30			
	Armijos et al., 2013	Pastaza	PAS	12700			8.7	0.26			
	Armijos et al., 2013	Santiago River	SAN	23880			17.3	0.28			
	Santini et al., 2014	lower Ucayali	REQ	360490			205.0	0.22			
	Guyot et al., 96	lower Maranon	SRE	360550			168.0	0.18			
	Wittmann et al., 2011	upper Solimoes	TAM	733470			413.0	0.22			
			sum area =	**2386916**		**sum load =**	**2059.1**		**0.33**	**±**	**0.25**
			largest basin=	**733470**		**"Upscaled load"=**	**632.7**				
									Area weighted total erosion rate:		
						sum upscaled=	**1050.0**		**0.47**	**±**	**0.9**
					(used this value for conversion)						
Floodplain	Filizola & Guyot 2009	Amazon	OBI	5087830	600000		556.0	0.36			
	Dunne et al, 1998	Amazon	OBI	5087830	600000		1239.0	0.79			
	Guyot et al, 2005	Amazon	OBI	5087830	600000		810.0	0.52			
	Meade, 1985 (USGS)	Amazon	OBI	5087830	600000		1321.5	0.85			
	Martinez et al., 09	Amazon	OBI	5087830	600000		688.0	0.44			
	Martinez et al., 09	Amazon	OBI	5087830	600000		801.0	0.51			
									Area weighted total erosion rate:		
						total measured load=	**902.6**		**0.58**	**±**	**0.2**

		River	Station Code	Total area (> ca.100 km2)	Sampled source area (km2)		Gauging-derived Load (Mt/yr)	Calculated erosion rate (mm/yr)	Area-weighted erosion value (mm/yr)	±	1σ SD of dataset
GANGA	Andermann et al., 2012	Upper Karnali	#240	21121			10.4	0.19			
BASIN	Andermann et al., 2012	Karnali	#280	45967			75.9	0.64			
	Lupker et al., 2012	Karnali	-	42890			87.0	0.78			
	Lupker et al., 2012	Karnali	-	45967			210.3	1.76			
	Lupker et al., 2012	Karnali	-	44000			68.6	0.60			
	Andermann et al., 2012	Saradha	#286	808			0.30	0.14			
	Andermann et al., 2012	Upper Rapti	#350	3648			18.3	1.93			
	Andermann et al., 2012	Rapti	#360	5197			13.2	0.98			
			sum area =	**209598**		**sum load =**	**484.1**		**0.89**	**±**	**0.66**
			largest basin=	**45967**		**"Upscaled load"=**	**106.2**				
	Jha et al., 1988	Yamuna	-	**9572**			**18.08**	**0.73**	**0.73**	**±**	**0.73**
	Gabet et al., 2008	Koto	#1	812			2.1	1.00			
	Gabet et al., 2008	Nar Khola	#2	1052			0.27	0.10			
	Gabet et al., 2008	Upper Dharapani	#5	1946			2.0	0.40			
	Gabet et al., 2008	Dudh Khola	#6	491			0.38	0.30			
	Gabet et al., 2008	Lower Dharapani	#8	2605			3.4	0.50			
	Gabet et al., 2008	Bhulbule	#9	3217			4.2	0.50			
	Gabet et al., 2008	Khudi Khola	#10	152			0.79	2.00			
	Andermann et al., 2012	Narayani	#450	32002			97.2	1.17			
	Andermann et al., 2012	Trishuli	#447	4428			2.4	0.21			
	Andermann et al., 2012	Kali Gandaki	#410	7170			31.9	1.71			
	Lupker et al., 2012	Gandak	-	34988			122.8	1.35			
	Sinha & Friend, 1994	Burhi Gandak	-	9580			14.4	0.58			
	Andermann et al., 2012	Bagmati	#589	2849			4.2	0.57			
			sum area =	**101292**		**sum load =**	**286.1**		**1.09**	**±**	**0.60**
			largest basin=	**34988**		**"Upscaled load"=**	**98.8**				
	Andermann et al., 2012	Bhote Koshi	#0	2308			0.3	0.050			
	Andermann et al., 2012	Sapta Koshi	#695	54024			62.7	0.45			
	Lupker et al., 2012	Kosi	-	60400			149.2	0.95			
	Lupker et al., 2012	Kosi	-	62000			166.0	1.03			
	Lupker et al., 2012	Kosi	-	61000			182.4	1.15			
	Lupker et al., 2012	Kosi	-	59280			89.6	0.56			
	Sinha & Friend, 1994	Baghmati	-	12973			10.5	0.31			
	Sinha & Friend, 1994	Kamala-Balan	-	2945			7.7	1.01			
			sum area =	**314930**		**sum load =**	**668.4**		**0.81**	**±**	**0.40**
			largest basin=	**62000**		**"Upscaled load"=**	**131.6**				
	Abbas et al., 1984	Ramganga		32400			10.1	0.12			
	Abbas et al., 1984	Gomti		30400			6.3	0.080			
	Abbas et al., 1984	Ghaghra		12700			11.9	0.36			
			sum area =	**75500**		**sum load =**	**28.3**		**0.14**	**±**	**0.15**
			largest basin=	**32400**		**"Upscaled load"=**	**12.2**				
									Area weighted total erosion rate:		
						sum upscaled=	**370.0**		**0.8**	**±**	**0.55**
					(used this value for conversion)						
Floodplain	Lupker et al., 2012	Ganga	Harding Bridge1	873240	184927		480.0	1.00			
	Lupker et al., 2012	Ganga	Harding Bridge2	873240	184927		448.0	0.93			
	Lupker et al., 2012	Ganga	Harding Bridge3	873240	184927		210.0	0.44			
	Lupker et al., 2012	Ganga	Harding Bridge4	873240	184927		340.0	0.71			
	Lupker et al., 2012	Ganga	Harding Bridge5	873240	184927		200.0	0.42			
	Lupker et al., 2012	Ganga	Harding Bridge6	873240	184927		480.0	1.00			
	Lupker et al., 2012	Ganga	Harding Bridge7	873240	184927		548.0	1.14			
	Lupker et al., 2012	Ganga	Harding Bridge8	873240	184927		390.0	0.81			
									Area weighted total erosion rate:		
						total measured load=	**390.0**		**0.82**		**0.27**

References for supplement:

Aalto, R., Dunne, T. and Guyot, J.L., 2006. Geomorphic controls on Andean denudation rates. Journal of Geology, 114(1): 85-99.

Abbas, N. and Subramanian, V., 1984. Erosion and sediment transport in the Ganges river basin (India). Journal of Hydrology, 69(1-4): 173-182.

Andermann, C., 2011. Climate, topography and erosion in the Nepal Himalayas. Ph.D. Thesis, Université de Rennes 1, Rennes, 173 pp.

Andermann, C., Crave, A., Gloaguen, R., Davy, P. and Bonnet, S., 2012. Connecting source and transport: Suspended sediments in the Nepal Himalayas. Earth and Planetary Science Letters, 351-352(0): 158-170.

Armijos, E., Crave, A., Vauchel, P., Fraizy, P., Santini, W., Moquet, J.-S., Arevalo, N., Carranza, J. and Guyot, J.-L., 2013. Suspended sediment dynamics in the Amazon River of Peru. Journal of South American Earth Sciences, 44(0): 75-84.

Blöthe, J.H. and Korup, O., 2013. Millennial lag times in the Himalayan sediment routing system. Earth and Planetary Science Letters, 382(0): 38-46.

Borchers, B., Marrero, S., Balco, G., Caffee, M., Goehring, B., Lifton, N., Nishiizumi, K., Phillips, F., Schaefer, J. and Stone, J., 2016. Geological calibration of spallation production rates in the CRONUS-Earth project. Quaternary Geochronology, 31: 188-198.

Braucher, R., Merchel, S., Borgomano, J. and Bourlès, D.L., 2011. Production of cosmogenic radionuclides at great depth: A multi element approach. Earth and Planetary Science Letters, 309(1-2): 1-9.

Castelltort, S. and Van Den Driessche, J., 2003. How plausible are high-frequency sediment supply-driven cycles in the stratigraphic record? Sedimentary Geology, 157(1-2): 3-13.

Chmeleff, J., von Blanckenburg, F., Kossert, K. and Jakob, D., 2010. Determination of the ^{10}Be half-life by multicollector ICP-MS and liquid scintillation counting. Nuclear Instruments & Methods in Physics Research Section B- Beam Interactions with Materials and Atoms, 268(2): 192-199.

Dosseto, A., Bourdon, B., Gaillardet, J., Maurice-Bourgoin, L. and Allegre, C.J., 2006. Weathering and transport of sediments in the Bolivian Andes: Time constraints from uranium-series isotopes. Earth and Planetary Science Letters, 248(3-4): 759-771.

Dunai, T.J., 2000. Scaling factors for production rates of in situ produced cosmogenic nuclides: a critical reevaluation. Earth and Planetary Science Letters, 176(1): 157-169.

Dunne, T., Mertes, L.A.K., Meade, R.H., Richey, J.E. and Forsberg, B.R., 1998. Exchanges of sediment between the flood plain and channel of the Amazon River in Brazil. Geological Society of America Bulletin, 110(4): 450-467.

Filizola, N. and Guyot, J.L., 2009. Suspended sediment yields in the Amazon basin: an assessment using the Brazilian national data set. Hydrological Processes, 23: 3207-3215.

Gabet, E.J., Burbank, D.W., Pratt-Sitaula, B., Putkonen, J. and Bookhagen, B., 2008. Modern erosion rates in the High Himalayas of Nepal. Earth and Planetary Science Letters, 267(3-4): 482-494.

Godard, V., Bourlès, D.L., Spinabella, F., Burbank, D.W., Bookhagen, B., Fisher, G.B., Moulin, A. and Léanni, L., 2014. Dominance of tectonics over climate in Himalayan denudation. Geology.

Godard, V., Burbank, D.W., Bourlès, D.L., Bookhagen, B., Braucher, R. and Fisher, G.B., 2012. Impact of glacial erosion on 10Be concentrations in fluvial sediments of the Marsyandi catchment, central Nepal. Journal of Geophysical Research: Earth Surface, 117(F3): F03013.

Granet, M., Chabaux, F., Stille, P., Dosseto, A., France-Lanord, C. and Blaes, E., 2010. U-series disequilibria in suspended river sediments and implication for sediment transfer time in alluvial plains: The case of the Himalayan rivers. Geochimica Et Cosmochimica Acta, 74(10): 2851-2865.

Granet, M., Chabaux, F., Stille, P., France-Lanord, C. and Pelt, E., 2007. Time-scales of sedimentary transfer and weathering processes from U-series nuclides: Clues from the Himalayan rivers. Earth and Planetary Science Letters, 261(3-4): 389-406.

Guyot, J.L., Filizola, N. and Laraque, A., 2005. The suspended sediment flux of the River Amazon at Obidos, Brazil, 1995-2003. In: D.E. Walling and A.J. Horowitz (Editors), Proceedings of symposium S1 held during the Seventh IAHS Scientific Assembly. IAHS Publication, Foz do Iguaco, BRAZIL, pp. 347-354.

Guyot, J.L., Filizola, N., Quintanilla, J. and Cortez, J., 1996. Dissolved solids and suspended sediment yields in the Rio Madeira basin, from the Bolivian Andes to the Amazon, Proceedings of the Exeter Symposium. IAHS Publication, Exeter, UK, pp. 55-63.

Insel, N., Ehlers, T.A., Schaller, M., Barnes, J.B., Tawackoli, S. and Poulsen, C.J., 2010. Spatial and temporal variability in denudation across the Bolivian Andes from multiple geochronometers. Geomorphology, 122(1-2): 65-77.

Jha, P.K., Subramanian, V. and Sitasawad, R., 1988. Chemical and sediment mass transfer in the Yamuna River- tributary of the Ganges system. Journal of Hydrology, 104(1-4): 237-246.

Korschinek, G., Bergmaier, A., Faestermann, T., Gerstmann, U.C., Knie, K., Rugel, G., Wallner, A., Dillmann, I., Dollinger, G., von Gostomski, C.L., Kossert, K., Maiti, M., Poutivtsev, M. and Remmert, A., 2010. A new value for the half-life of ^{10}Be by heavy-ion elastic recoil detection and liquid scintillation counting. Nuclear Instruments & Methods in Physics Research Section B- Beam Interactions with Materials and Atoms, 268(2): 187-191.

Lauer, J.W. and Willenbring, J.K., 2010. Steady-state reach-scale theory for radioactive tracer concentration in a simple channel/floodplain system. J. Geophys. Res. Earth Surface, 115: F04018.

Lupker, M., Blard, P.-H., Lavé, J., France-Lanord, C., Leanni, L., Puchol, N., Charreau, J. and Bourlès, D., 2012. ^{10}Be-derived Himalayan denudation rates and sediment budgets in the Ganga basin. Earth and Planetary Science Letters, 333-334(0): 146-156.

Martinez, J.M., Guyot, J.L., Filizola, N. and Sondag, F., 2009. Increase in suspended sediment discharge of the Amazon River assessed by monitoring network and satellite data. Catena, 79(3): 257-264.

Meade, R.H., 1985. Suspended Sediment in the Amazon River and its tributaries in Brazil during 1982-1984, U.S. Geological Survey, Washington, D.C.

Métivier, F. and Gaudemer, Y., 1999. Stability of output fluxes of large rivers in South and East Asia during the last 2 million years: implications on floodplain processes. Basin Research, 11(4): 293-303.

Nishiizumi, K., Imamura, M., Caffee, M.W., Southon, J.R., Finkel, R.C. and McAninch, J., 2007. Absolute calibration of ^{10}Be AMS standards. Nuclear Instruments & Methods in Physics Research Section B- Beam Interactions with Materials and Atoms, 258(2): 403-413.

Norton, K.P. and Vanacker, V., 2009. Effects of terrain smoothing on topographic shielding correction factors for cosmogenic nuclide-derived estimates of basin-averaged denudation rates. Earth Surface Processes and Landforms, 34(1): 145-154.

Pepin, E., Guyot, J.L., Armijos, E., Bazan, H., Fraizy, P., Moquet, J.S., Noriega, L., Lavado, W., Pombosa, R. and Vauchel, P., 2013. Climatic control on eastern Andean denudation rates (Central Cordillera from Ecuador to Bolivia). Journal of South American Earth Sciences, 44(0): 85-93.

Phillips, F.M., Argento, D.C., Balco, G., Caffee, M.W., Clem, J., Dunai, T.J., Finkel, R., Goehring, B., Gosse, J.C., Hudson, A.M., Jull, A.J.T., Kelly, M.A., Kurz, M., Lal, D., Lifton, N., Marrero, S.M., Nishiizumi, K., Reedy, R.C., Schaefer, J., Stone, J.O.H., Swanson, T. and Zreda, M.G., 2016. The CRONUS-Earth Project: A synthesis. Quaternary Geochronology, 31: 119-154.

Safran, E.B., Bierman, P., Aalto, R., Dunne, T., Whipple, K.X. and Caffee, M., 2005. Erosion rates driven by channel network incision in the Bolivian Andes. Earth Surface Processes and Landforms, 30: 1007-1024.

Santini, W., Martinez, J.M., Espinoza Villar, R., Cochonneau, G., Vauchel, P., Moquet , J.S., Baby, P., Espinoza Villar, J.C., Lavado Casimiro, W.S., Carranza Valle, J.L. and Guyot, J.L., 2014. Sediment budget in the Ucayali River basin, an Andean tributary of the

Amazon River, Sediment Dynamics from the Summit to the Sea. IAHS Publication, New Orleans, USA, pp. 320-325.

Scherler, D., Bookhagen, B. and Strecker, M.R., 2014. Tectonic control on 10Be-derived erosion rates in the Garhwal Himalaya, India. Journal of Geophysical Research: Earth Surface, 119: 1-23.

Sinha, R. and Friend, P.F., 1994. River systems and their sediment flux, Indo-Gangetic plains, Northern Bihar, India. Sedimentology, 41(4): 825-845.

Vance, D., Bickle, M., IvyOchs, S. and Kubik, P., 2003. Erosion and exhumation in the Himalaya from cosmogenic isotope inventories of river sediments. Earth and Planetary Science Letters, 206: 273-288.

Wittmann, H. and von Blanckenburg, F., 2009. Cosmogenic nuclide budgeting of floodplain sediment transfer. Geomorphology, 109(3-4): 246-256.

Wittmann, H., von Blanckenburg, F., Guyot, J.L., Maurice, L. and Kubik, P.W., 2009. From source to sink: Preserving the cosmogenic 10Be-derived denudation rate signal of the Bolivian Andes in sediment of the Beni and Mamoré foreland basins. Earth and Planetary Science Letters, 288(3-4): 463-474.

Wittmann, H., von Blanckenburg, F., Maurice, L., Guyot, J.L., Filizola, N. and Kubik, P.W., 2011. Sediment production and delivery in the Amazon River basin quantified by in situ-produced cosmogenic nuclides and recent river loads. Geological Society of America Bulletin, 123(5-6): 934-950.